

Confidence-Calibrated Adversarial Training: Generalizing to Unseen Attacks

David Stutz¹ Matthias Hein² Bernt Schiele¹

Abstract

Adversarial training yields robust models against a specific threat model, e.g., L_∞ adversarial examples. Typically robustness does *not* generalize to previously unseen threat models, e.g., other L_p norms, or larger perturbations. Our **confidence-calibrated adversarial training (CCAT)** tackles this problem by biasing the model towards low confidence predictions on adversarial examples. By allowing to reject examples with low confidence, robustness generalizes beyond the threat model employed during training. CCAT, trained *only* on L_∞ adversarial examples, increases robustness against larger L_∞ , L_2 , L_1 and L_0 attacks, adversarial frames, distal adversarial examples and corrupted examples and yields better clean accuracy compared to adversarial training. For thorough evaluation we developed novel white- and black-box attacks directly attacking CCAT by maximizing confidence. For each threat model, we use 7 attacks with up to 50 restarts and 5000 iterations and report worst-case robust test error, extended to our confidence-thresholded setting, across *all* attacks.

1. Introduction

Deep networks were shown to be susceptible to adversarial examples (Szegedy et al., 2014): adversarially perturbed examples that cause mis-classification while being nearly “imperceptible”, i.e., close to the original example. Here, “closeness” is commonly enforced by constraining the L_p norm of the perturbation, referred to as threat model. Since then, numerous defenses against adversarial examples have been proposed. However, many were unable to keep up with more advanced attacks (Athalye et al., 2018; Athalye & Carlini, 2018). Moreover, most defenses are tailored to only one specific threat model.

¹Max Planck Institute for Informatics, Saarland Informatics Campus, Saarbrücken ²University of Tübingen, Tübingen. Correspondence to: David Stutz <david.stutz@mpi-inf.mpg.de>.

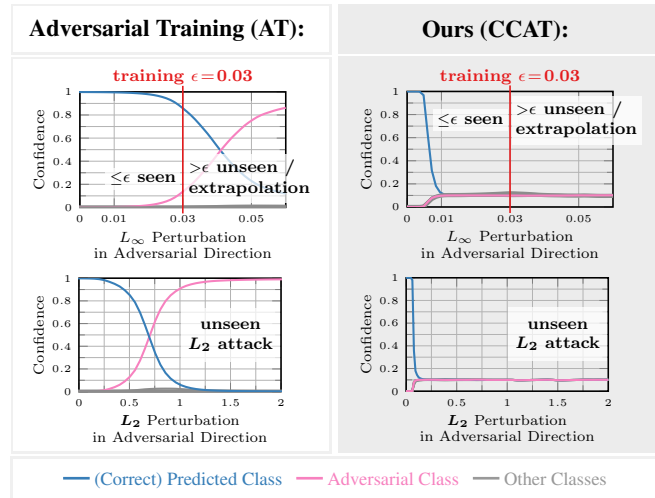


Figure 1: Adversarial Training (AT) versus our CCAT. We plot the confidence in the direction of an adversarial example. AT enforces high confidence predictions for the correct class on the L_∞ -ball of radius ϵ (“seen” attack during training, top left). As AT enforces no particular bias beyond the ϵ -ball, adversarial examples can be found right beyond this ball. In contrast CCAT enforces a decaying confidence in the correct class up to uniform confidence within the ϵ -ball (top right). Thus, CCAT biases the model to extrapolate uniform confidence beyond the ϵ -ball. This behavior also extends to “unseen” attacks during training, e.g., L_2 attacks (bottom), such that adversarial examples can be rejected via confidence-thresholding.

Adversarial training (Goodfellow et al., 2015; Madry et al., 2018), i.e., training on adversarial examples, can be regarded as state-of-the-art. However, following Fig. 1, adversarial training is known to “overfit” to the threat model “seen” during training, e.g., L_∞ adversarial examples. Thus, robustness does not extrapolate to larger L_∞ perturbations, cf. Fig. 1 (top left), or generalize to “unseen” attacks, cf. Fig. 1 (bottom left), e.g., other L_p threat models (Sharma & Chen, 2018; Tramèr & Boneh, 2019; Li et al., 2019; Kang et al., 2019; Maini et al., 2020). We hypothesize this to be a result of enforcing high-confidence predictions on adversarial examples. However, high-confidence predictions are difficult to extrapolate beyond the adversarial examples seen during training. Moreover, it is not meaningful to extrapolate high-confidence predictions to arbitrary regions.

Finally, adversarial training often hurts accuracy, resulting in a robustness-accuracy trade-off (Tsipras et al., 2019; Stutz et al., 2019; Raghunathan et al., 2019; Zhang et al., 2019).

Contributions: We propose **confidence-calibrated adversarial training (CCAT)** which trains the network to predict a convex combination of uniform and (correct) one-hot distribution on adversarial examples that becomes more uniform as the distance to the attacked example increases. This is illustrated in Fig. 1. Thus, CCAT implicitly biases the network to predict a uniform distribution beyond the threat model *seen* during training, cf. Fig. 1 (top right). Robustness is obtained by rejecting low-confidence (adversarial) examples through confidence-thresholding. As a result, having seen *only* L_∞ adversarial examples during training, CCAT improves robustness against previously *unseen* attacks, cf. Fig. 1 (bottom right), e.g., L_2 , L_1 and L_0 adversarial examples or larger L_∞ perturbations. Furthermore, robustness extends to adversarial frames (Zajac et al., 2019), distal adversarial examples (Hein et al., 2019), corrupted examples (e.g., noise, blur, transforms etc.) and accuracy of normal training is preserved better than with adversarial training.

For thorough evaluation, following best practices (Carlini et al., 2019), we adapt several state-of-the-art white- and black-box attacks (Madry et al., 2018; Ilyas et al., 2018; Andriushchenko et al., 2019; Narodytska & Kasiviswanathan, 2017; Khoury & Hadfield-Menell, 2018) to CCAT by explicitly maximizing confidence and improving optimization through a backtracking scheme. In total, we consider 7 different attacks for each threat model (i.e., L_p for $p \in \{\infty, 2, 1, 0\}$), allowing up to 50 random restarts and 5000 iterations each. We report worst-case robust test error, extended to our confidence-thresholded setting, across *all* attacks and restarts, on a *per test example* basis. We demonstrate improved robustness against unseen attacks compared to standard adversarial training (Madry et al., 2018), TRADES (Zhang et al., 2019), adversarial training using multiple threat models (Maini et al., 2020) and two detection methods (Ma et al., 2018; Lee et al., 2018), while training *only* on L_∞ adversarial examples.

We make our code (training and evaluation) and pre-trained models publicly available at davidstutz.de/ccat.

2. Related Work

Adversarial Examples: Adversarial examples can roughly be divided into white-box attacks, i.e., with access to the model gradients, e.g. (Goodfellow et al., 2015; Madry et al., 2018; Carlini & Wagner, 2017b), and black-box attacks, i.e., only with access to the model’s output, e.g. (Ilyas et al., 2018; Narodytska & Kasiviswanathan, 2017; Andriushchenko et al., 2019). Adversarial examples were also found to be transferable between models (Liu et al., 2017;

Xie et al., 2019). In addition to *imperceptible* adversarial examples, adversarial transformations, e.g., (Engstrom et al., 2019; Alaifari et al., 2019), or adversarial patches (Brown et al., 2017) have also been studied. Recently, projected gradient ascent to maximize the cross-entropy loss or surrogate objectives, e.g., (Madry et al., 2018; Dong et al., 2018; Carlini & Wagner, 2017b), has become standard. Instead, we directly maximize the confidence in any but the true class, similar to (Hein et al., 2019; Goodfellow et al., 2019), in order to effectively train and attack CCAT.

Adversarial Training: Numerous defenses have been proposed, of which several were shown to be ineffective (Athalye et al., 2018; Athalye & Carlini, 2018). Currently, adversarial training is standard to obtain robust models. While it was proposed in different variants (Szegedy et al., 2014; Miyato et al., 2016; Huang et al., 2015), the formulation by (Madry et al., 2018) received considerable attention and has been extended in various ways: (Shafahi et al., 2020; Pérolat et al., 2018) train on universal adversarial examples, in (Cai et al., 2018), curriculum learning is used, and in (Tramèr et al., 2018; Grefenstette et al., 2018) ensemble adversarial training is proposed. The increased sample complexity (Schmidt et al., 2018) was addressed in (Lamb et al., 2019; Carmon et al., 2019; Alayrac et al., 2019) by training on interpolated or unlabeled examples. Adversarial training on multiple threat models is also possible (Tramèr & Boneh, 2019; Maini et al., 2020). Finally, the observed robustness-accuracy trade-off has been discussed in (Tsipras et al., 2019; Stutz et al., 2019; Zhang et al., 2019; Raghunathan et al., 2019). Adversarial training has also been combined with self-supervised training (Hendrycks et al., 2019). In contrast to adversarial training, CCAT imposes a target distribution which tends towards a uniform distribution for large perturbations, allowing the model to extrapolate beyond the threat model used at training time. Similar to adversarial training with an additional “abstain” class (Laidlaw & Feizi, 2019), robustness is obtained by rejection. In our case, rejection is based on confidence thresholding.

Detection: Instead of correctly classifying adversarial examples, several works (Gong et al., 2017; Grosse et al., 2017; Feinman et al., 2017; Liao et al., 2018; Ma et al., 2018; Amsaleg et al., 2017; Metzen et al., 2017; Bhagoji et al., 2017; Hendrycks & Gimpel, 2017; Li & Li, 2017; Lee et al., 2018) try to detect adversarial examples. However, several detectors have been shown to be ineffective against adaptive attacks aware of the detection mechanism (Carlini & Wagner, 2017a). Recently, the detection of adversarial examples by confidence, similar to our approach with CCAT, has also been discussed (Pang et al., 2018). Instead, Goodfellow et al. (2019) focus on evaluating confidence-based detection methods using adaptive, targeted attacks maximizing confidence. Our attack, although similar in spirit, is untargeted and hence suited for CCAT.

3. Generalizable Robustness by Confidence Calibration of Adversarial Training

To start, we briefly review adversarial training on L_∞ adversarial examples (Madry et al., 2018), which has become standard to train robust models, cf. Sec. 3.1. However, robustness does not generalize to larger perturbations or unseen attacks. We hypothesize this to be the result of enforcing high-confidence predictions on adversarial examples. CCAT addresses this issue with minimal modifications, cf. Sec. 3.2 and Alg. 1, by encouraging low-confidence predictions on adversarial examples. During testing, adversarial examples can be rejected by confidence thresholding.

Notation: We consider a classifier $f : \mathbb{R}^d \rightarrow \mathbb{R}^K$ with K classes where f_k denotes the confidence for class k . While we use the cross-entropy loss \mathcal{L} for training, our approach also generalizes to other losses. Given $x \in \mathbb{R}^d$ with class $y \in \{1, \dots, K\}$, we let $f(x) := \operatorname{argmax}_k f_k(x)$ denote the predicted class for notational convenience. For $f(x) = y$, an adversarial example $\tilde{x} = x + \delta$ is defined as a ‘‘small’’ perturbation δ such that $f(\tilde{x}) \neq y$, i.e., the classifier changes its decision. The strength of the change δ is measured by some L_p -norm, $p \in \{0, 1, 2, \infty\}$. Here, $p = \infty$ is a popular choice as it leads to the smallest perturbation per pixel.

3.1. Problems of Adversarial Training

Following (Madry et al., 2018), adversarial training is given as the following min-max problem:

$$\min_w \mathbb{E} \left[\max_{\|\delta\|_\infty \leq \epsilon} \mathcal{L}(f(x + \delta; w), y) \right] \quad (1)$$

with w being the classifier’s parameters. During mini-batch training the inner maximization problem,

$$\max_{\|\delta\|_\infty \leq \epsilon} \mathcal{L}(f(x + \delta; w), y), \quad (2)$$

is approximately solved. In addition to the L_∞ -constraint, a box constraint is enforced for images, i.e., $\tilde{x}_i = (x + \delta)_i \in [0, 1]$. Note that maximizing the cross-entropy loss is equivalent to finding the adversarial example with *minimal* confidence in the true class. For neural networks, this is generally a non-convex optimization problem. In (Madry et al., 2018) the problem is tackled using projected gradient descent (PGD), initialized using a random δ with $\|\delta\|_\infty \leq \epsilon$.

In contrast to adversarial training as proposed in (Madry et al., 2018), which computes adversarial examples for the *full* batch in each iteration, others compute adversarial examples only for *half* the examples of each batch (Szegedy et al., 2014). Instead of training *only* on adversarial examples, each batch is divided into 50% clean and 50% adversarial examples. Compared to Eq. (1), 50%/50% adversarial

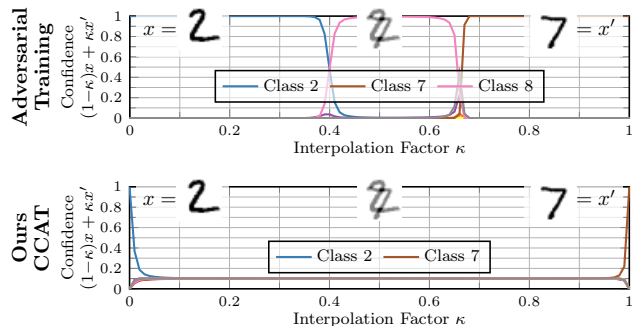


Figure 2: Extrapolation of Uniform Predictions. We plot the confidence in each class along an interpolation between two test examples x and x' , ‘‘2’’ and ‘‘7’’, on MNIST (LeCun et al., 1998): $(1 - \kappa)x + \kappa x'$ where κ is the interpolation factor. CCAT quickly yields low-confidence, uniform predictions in between both examples, extrapolating the behavior enforced within the ϵ -ball during training. Regular adversarial training, in contrast, consistently produces high-confidence predictions, even on unreasonable inputs.

training effectively minimizes

$$\underbrace{\mathbb{E} \left[\max_{\|\delta\|_\infty \leq \epsilon} \mathcal{L}(f(x + \delta; w), y) \right]}_{50\% \text{ adversarial training}} + \underbrace{\mathbb{E} [\mathcal{L}(f(x; w), y)]}_{50\% \text{ ‘‘clean’’ training}}. \quad (3)$$

This improves test accuracy on clean examples compared to 100% adversarial training but typically leads to worse robustness. Intuitively, by balancing both terms in Eq. (3), the trade-off between accuracy and robustness can already be optimized to some extent (Stutz et al., 2019).

Problems: Trained on L_∞ adversarial examples, the robustness of adversarial training does not generalize to previously unseen adversarial examples, including larger perturbations or other L_p adversarial examples. We hypothesize that this is because adversarial training explicitly enforces high-confidence predictions on L_∞ adversarial examples within the ϵ -ball seen during training (‘‘seen’’ in Fig. 1). However, this behavior is difficult to extrapolate to arbitrary regions in a meaningful way. Thus, it is not surprising that adversarial examples can often be found right beyond the ϵ -ball used during training, cf. Fig. 1 (top left). This can be described as ‘‘overfitting’’ to the L_∞ adversarial examples used during training. Also, larger ϵ -balls around training examples might include (clean) examples from other classes. Then, Eq. (2) will focus on these regions and reduce accuracy as considered in our theoretical toy example, see Proposition 2, and related work (Jacobsen et al., 2019b;a).

As suggested in Fig. 1, both problems can be addressed by enforcing low-confidence predictions on adversarial examples in the ϵ -ball. In practice, we found that the low-confidence predictions on adversarial examples within the ϵ -ball are extrapolated beyond the ϵ -ball, i.e., to larger pertur-

Algorithm 1 Confidence-Calibrated Adversarial Training (CCAT). The only changes compared to standard adversarial training are the attack (line 4) and the probability distribution over the classes (lines 6 and 7), which becomes more uniform as distance $\|\delta\|_\infty$ increases. During testing, low-confidence (adversarial) examples are rejected.

```

1: while true do
2:   choose random batch  $(x_1, y_1), \dots, (x_B, y_B)$ .
3:   for  $b = 1, \dots, B/2$  do
4:      $\delta_b := \operatorname{argmax}_{\|\delta\|_\infty \leq \epsilon} \max_{k \neq y_b} f_k(x_b + \delta)$  (Eq. (4))
5:      $\tilde{x}_b := x_b + \delta_b$ 
6:      $\lambda(\delta_b) := (1 - \min(1, \|\delta_b\|_\infty / \epsilon))^\rho$  (Eq. (6))
7:      $\tilde{y}_b := \lambda(\delta_b) \operatorname{one\_hot}(y_b) + (1 - \lambda(\delta_b)) \frac{1}{K}$  (Eq. (5))
8:   end for
9:   update parameters using Eq. (3):
10:   $\sum_{b=1}^{B/2} \mathcal{L}(f(\tilde{x}_b), \tilde{y}_b) + \sum_{b=B/2}^B \mathcal{L}(f(x_b), y_b)$ 
11: end while
    
```

bations, unseen attacks or distal adversarial examples. This allows to reject adversarial examples based on their low confidence. We further enforce this behavior by explicitly encouraging a “steep” transition from high-confidence predictions (on clean examples) to low-confidence predictions (on adversarial examples). As result, the (low-confidence) prediction is almost flat close to the boundary of the ϵ -ball. Additionally, there is no incentive to deviate from the uniform distribution outside of the ϵ -ball. For example, as illustrated in Fig. 2, the confidence stays low in between examples from different classes and only increases if necessary, i.e., close to the examples.

3.2. Confidence-Calibrated Adversarial Training

Confidence-calibrated adversarial training (CCAT) addresses these problems with minimal modifications, as outlined in Alg. 1. During training, we train the network to predict a convex combination of (correct) one-hot distribution on clean examples and uniform distribution on adversarial examples as target distribution within the cross-entropy loss. During testing, adversarial examples can be rejected by confidence thresholding: adversarial examples receive near-uniform confidence while test examples receive high-confidence. By extrapolating the uniform distribution beyond the ϵ -ball used during training, previously unseen adversarial examples such as larger L_∞ perturbations can be rejected, as well. In the following, we first introduce an alternative objective for generating adversarial examples. Then, we specifically define the target distribution, which becomes more uniform with larger perturbations $\|\delta\|_\infty$. In Alg. 1, these changes correspond to lines 4, 6 and 7, requiring only few lines of code in practice.

Given an example x with label y , our adaptive attack during

training maximizes the confidence in any other label $k \neq y$. This results in effective attacks against CCAT, as CCAT will reject low-confidence adversarial examples:

$$\max_{\|\delta\|_\infty \leq \epsilon} \max_{k \neq y} f_k(x + \delta; w) \quad (4)$$

Note that Eq. (2), in contrast, minimizes the confidence in the true label y . Similarly, (Goodfellow et al., 2019) uses targeted attacks in order to maximize confidence, whereas ours is untargeted and, thus, our objective is the maximal confidence over all other classes.

Then, given an adversarial example from Eq. (4) during training, CCAT uses the following combination of uniform and one-hot distribution as target for the cross-entropy loss:

$$\tilde{y} = \lambda(\delta) \operatorname{one_hot}(y) + (1 - \lambda(\delta)) \frac{1}{K}, \quad (5)$$

with $\lambda(\delta) \in [0, 1]$ and $\operatorname{one_hot}(y) \in \{0, 1\}^K$ denoting the one-hot vector corresponding to class y . Thus, we enforce a convex combination of the original label distribution and the uniform distribution which is controlled by the parameter $\lambda = \lambda(\delta)$, computed given the perturbation δ . We choose λ to decrease with the distance $\|\delta\|_\infty$ of the adversarial example to the attacked example x with the intention to enforce uniform predictions when $\|\delta\|_\infty = \epsilon$. Then, the network is encouraged to extrapolate this uniform distribution beyond the used ϵ -ball. Even if extrapolation does not work perfectly, the uniform distribution is much more meaningful for extrapolation to arbitrary regions as well as regions between classes compared to high-confidence predictions as encouraged in standard adversarial training, as demonstrated in Fig. 2. For controlling the trade-off λ between one-hot and uniform distribution, we consider the following “power transition”:

$$\lambda(\delta) := \left(1 - \min\left(1, \frac{\|\delta\|_\infty}{\epsilon}\right)\right)^\rho \quad (6)$$

This ensures that for $\delta = 0$ we impose the original (one-hot) label. For growing δ , however, the influence of the original label decays proportional to $\|\delta\|_\infty$. The speed of decay is controlled by the parameter ρ . For $\rho = 10$, Fig. 1 (top right) shows the transition as approximated by the network. The power transition ensures that for $\|\delta\|_\infty \geq \epsilon$, i.e., perturbations larger than encountered during training, a uniform distribution is enforced as λ is 0. We train on 50% clean and 50% adversarial examples in each batch, as in Eq. (3), such that the network has an incentive to predict correct labels.

The convex combination of uniform and one-hot distribution in Eq. (5) resembles the label smoothing regularizer introduced in (Szegedy et al., 2016). In concurrent work, label smoothing has also been used as regularizer for adversarial training (Cheng et al., 2020). However, in our case,

$\lambda = \lambda(\delta)$ from Eq. (6) is not a fixed hyper-parameter as in (Szegedy et al., 2016; Cheng et al., 2020). Instead, λ depends on the perturbation δ and reaches zero for $\|\delta\|_\infty = \epsilon$ to encourage low-confidence predictions beyond the ϵ -ball used during training. Thereby, λ explicitly models the transition from one-hot to uniform distribution.

3.3. Confidence-Calibrated Adversarial Training Results in Accurate Models

Proposition 2 discusses a problem where standard adversarial training is unable to reconcile robustness and accuracy while CCAT is able to obtain *both* robustness and accuracy:

Proposition 1. *We consider a classification problem with two points $x = 0$ and $x = \epsilon$ in \mathbb{R} with deterministic labels, i.e., $p(y = 2|x = 0) = 1$ and $p(y = 1|x = \epsilon) = 1$, such that the problem is fully determined by the probability $p_0 = p(x = 0)$. The Bayes error of this classification problem is zero. Let the predicted probability distribution over classes be $\tilde{p}(y|x) = \frac{e^{g_1 y(x)}}{e^{g_1(x)} + e^{g_2(x)}}$, where $g : \mathbb{R}^d \rightarrow \mathbb{R}^2$ is the classifier and we assume that the function $\lambda : \mathbb{R}_+ \rightarrow [0, 1]$ used in CCAT is monotonically decreasing and $\lambda(0) = 1$. Then, the error of the Bayes optimal classifier (with cross-entropy loss) for*

- *adversarial training on 100% adversarial examples, cf. Eq. (1), is $\min\{p_0, 1 - p_0\}$.*
- *adversarial training on 50%/50% adversarial/clean examples per batch, cf. Eq. (3), is $\min\{p_0, 1 - p_0\}$.*
- *CCAT on 50% clean and 50% adversarial examples, cf. Alg. 1, is zero if $\lambda(\epsilon) < \min\{p_0/1-p_0, 1-p_0/p_0\}$.*

Here, 100% and 50%/50% standard adversarial training are unable to obtain *both* robustness and accuracy: The ϵ -ball used during training contains examples of different classes such that adversarial training enforces high-confidence predictions in contradicting classes. CCAT addresses this problem by encouraging low-confidence predictions on adversarial examples within the ϵ -ball. Thus, CCAT is able to improve accuracy while preserving robustness.

4. Detection and Robustness Evaluation with Adaptive Attack

CCAT allows to reject (adversarial) inputs by confidence-thresholding before classifying them. As we will see, this “reject option”, is also beneficial for standard adversarial training (AT). Thus, evaluation also requires two stages: First, we fix the confidence threshold at 99% true positive rate (TPR), where correctly classified clean examples are positives such that at most 1% (correctly classified) clean examples are rejected. Second, on the non-rejected examples, we evaluate accuracy and robustness using *confidence-thresholded* (robust) test error.

4.1. Adaptive Attack

As CCAT encourages low confidence on adversarial examples, we use PGD to maximize the confidence of adversarial examples, cf. Eq. (4), as effective adaptive attack against CCAT. In order to effectively optimize our objective, we introduce a simple but crucial improvement: after each iteration, the computed update is only applied if the objective is improved; otherwise the learning rate is reduced. Additionally, we use momentum (Dong et al., 2018) and run the attack for exactly T iterations, choosing the perturbation corresponding to the best objective across all iterations. In addition to random initialization, we found that $\delta = 0$ is an effective initialization against CCAT. We applied the same principles for (Ilyas et al., 2018), i.e., PGD with approximated gradients, Eq. (4) as objective, momentum and backtracking; we also use Eq. (4) as objective for the black-box attacks of (Andriushchenko et al., 2019; Narodytska & Kasiviswanathan, 2017; Khoury & Hadfield-Menell, 2018).

4.2. Detection Evaluation

In the first stage, we consider a detection setting: adversarial example are *negatives* and correctly classified clean examples are *positives*. The confidence threshold τ is chosen extremely conservatively by requiring a **99% true positive rate (TPR)**: at most 1% of correctly classified clean examples can be rejected. As result, the confidence threshold is determined *only* by correctly classified clean examples, independent of adversarial examples. Incorrectly rejecting a significant fraction of correctly classified clean examples is unacceptable. This is also the reason why we do not report the area under the receiver operating characteristic (ROC) curve as related work (Lee et al., 2018; Ma et al., 2018). Instead, we consider the **false positive rate (FPR)**. The supplementary material includes a detailed discussion.

4.3. Robustness Evaluation

In the second stage, after confidence-thresholding, we consider the widely used robust test error (RErr) (Madry et al., 2018). It quantifies the model’s test error in the case where all test examples are allowed to be attacked, i.e., modified within the chosen threat model, e.g., for L_p :

$$\text{“Standard” RErr} = \frac{1}{N} \sum_{n=1}^N \max_{\|\delta\|_p \leq \epsilon} \mathbb{1}_{f(x_n + \delta) \neq y_n} \quad (7)$$

where $\{(x_n, y_n)\}_{n=1}^N$ are test examples and labels. In practice, RErr is computed empirically using adversarial attacks. Unfortunately, standard RErr does not take into account the option of rejecting (adversarial) examples.

We propose a generalized definition adapted to our confidence-thresholded setting where the model can reject examples. For fixed confidence threshold τ at 99%TPR, the

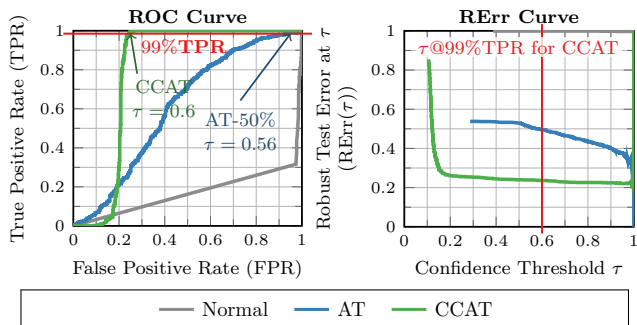


Figure 3: ROC and RErr Curves. On SVHN, we show ROC curves when distinguishing *correctly classified* test examples from adversarial examples by confidence (left) and (confidence-thresholded) RErr against confidence threshold τ (right) for worst-case adversarial examples across L_∞ attacks with $\epsilon = 0.03$. The confidence threshold τ is chosen exclusively on correctly classified clean examples to obtain 99%TPR. For CCAT, this results in $\tau \approx 0.6$. Note that RErr subsumes both Err and FPR.

confidence-thresholded RErr is defined as

$$\text{RErr}(\tau) = \frac{\sum_{n=1}^N \max_{\|\delta\|_p \leq \epsilon, c(x_n + \delta) \geq \tau} \mathbb{1}_{f(x_n + \delta) \neq y_n}}{\sum_{n=1}^N \max_{\|\delta\|_p \leq \epsilon} \mathbb{1}_{c(x_n + \delta) \geq \tau}} \quad (8)$$

with $c(x) = \max_k f_k(x)$ and $f(x)$ being the model’s confidence and predicted class on example x , respectively. Essentially, this is the **test error on test examples that can be modified within the chosen threat model and pass confidence thresholding**. For $\tau = 0$ (i.e., all examples pass confidence thresholding) this reduces to the standard RErr, comparable to related work. We stress that our adaptive attack in Eq. (4) directly maximizes the numerator of Eq. (8) by maximizing the confidence of classes not equal y . A (clean) **confidence-thresholded test error (Err(τ))** is obtained similarly. In the following, if not stated otherwise, we report *confidence-thresholded* RErr and Err as default and omit the confidence threshold τ for brevity.

FPR and RErr: FPR quantifies how well an adversary can perturb (correctly classified) examples while not being rejected. The confidence-thresholded RErr is more conservative as it measures *any* non-rejected error (adversarial or not). As result, RErr implicitly includes FPR *and* Err. Therefore, we report only RErr and include FPRs for all our experiments in the supplementary material.

Per-Example Worst-Case Evaluation: Instead of reporting average or per-attack results, we use a per-example *worst-case* evaluation scheme: For each individual test example, all adversarial examples from all attacks (and restarts) are accumulated. Subsequently, *per test example*,

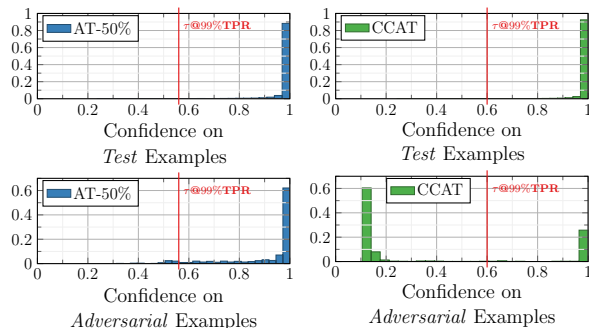


Figure 4: Confidence Histograms. On SVHN, for AT (50%/50% adversarial training, left) and CCAT (right), we show confidence histograms corresponding to *correctly classified* test examples (top) and adversarial examples (bottom). We consider the worst-case adversarial examples across all L_∞ attacks for $\epsilon = 0.03$. While the confidence of adversarial examples is reduced slightly for AT, CCAT is able to distinguish the majority of adversarial examples from (clean) test examples by confidence thresholding (in red).

only the adversarial example with highest confidence is considered, resulting in a significantly stronger robustness evaluation compared to related work.

5. Experiments

We evaluate CCAT in comparison with AT (Madry et al., 2018) and related work (Maini et al., 2020; Zhang et al., 2019) on MNIST (LeCun et al., 1998), SVHN (Netzer et al., 2011) and Cifar10 (Krizhevsky, 2009) as well as MNIST-C (Mu & Gilmer, 2019) and Cifar10-C (Hendrycks & Dietterich, 2019b) with corrupted examples (e.g., blur, noise, compression, transforms etc.). We report **confidence-thresholded test error (Err; ↓ lower is better)** and **confidence-thresholded robust test error (RErr; ↓ lower is better)** for a confidence-threshold τ corresponding to 99% true positive rate (TPR); we omit τ for brevity. We note that normal and standard adversarial training (AT) are also allowed to reject examples by confidence thresholding. Err is computed on 9000 test examples. RErr is computed on 1000 test examples. The confidence threshold τ depends *only* on correctly classified clean examples and is fixed at 99%TPR on the held-out *last* 1000 test examples.

Attacks: For thorough evaluation, we consider 7 different L_p attacks for $p \in \{\infty, 2, 1, 0\}$. As white-box attacks, we use PGD to maximize the objectives Eq. (2) and (4), referred to as PGD-CE and PGD-Conf. We use $T = 1000$ iterations and 10 random restarts with random initialization plus one restart with zero initialization for PGD-Conf, and $T = 200$ with 50 random restarts for PGD-CE. For L_∞ , L_2 , L_1 and L_0 attacks, we set ϵ to **0.3, 3, 18, 15 (MNIST) or 0.03, 2, 24, 10 (SVHN/Cifar10)**.

SVHN: RErr @99%TPR, L_∞ , $\epsilon = 0.03$						
	worst case	top-5 attacks/restarts out of 7 attacks with 84 restarts				
AT-50%	56.0	52.1	52.0	51.9	51.6	51.4
CCAT	39.1	23.6	13.7	13.6	12.6	12.5

Table 1: Per-Example Worst-Case Evaluation. We compare confidence-thresholded RErr with $\tau@99\%$ TPR for the per-example worst-case and the top-5 individual attacks/restarts among 7 attacks with 84 restarts in total. Multiple restarts are *necessary* to effectively attack CCAT, while a single attack and restart is nearly sufficient against AT-50%. This demonstrates that CCAT is more difficult to “crack”.

As black-box attacks, we additionally use the Query Limited (QL) attack (Ilyas et al., 2018) adapted with momentum and backtracking for $T = 1000$ iterations with 10 restarts, the Simple attack (Narodytska & Kasiviswanathan, 2017) for $T = 1000$ iterations and 10 restarts, and the Square attack (L_∞ and L_2) (Andriushchenko et al., 2019) with $T = 5000$ iterations. In the case of L_0 we also use Corner Search (CS) (Croce & Hein, 2019). For all L_p , $p \in \{\infty, 2, 1, 0\}$, we consider 5000 (uniform) random samples from the L_p -ball and the Geometry attack (Khoury & Hadfield-Menell, 2018). Except for CS, all black-box attacks use Eq. (4) as objective:

Attack	Objective	T	Restarts
PGD-CE	Eq. (2), random init.	200	50
PGD-Conf	Eq. (4), zero + random init.	1000	11
QL [†]	Eq. (4), zero + random init.	1000	11
Simple [†]	Eq. (4)	1000	10
Square [†]	Eq. (4), L_∞ , L_2 only	5000	1
CS [†]	Eq. (2), L_0 only	200	1
Geometry [†]	Eq. (4)	1000	1
Random [†]	Eq. (4)	–	5000

[†] Black-box attacks.

Additionally, we consider adversarial frames and distal adversarial examples: Adversarial frames (Zajac et al., 2019) allow a 2 (MNIST) or 3 (SVHN/Cifar10) pixel border to be manipulated arbitrarily within $[0, 1]$ to maximize Eq. (4) using PGD. Distal adversarial examples start with a (uniform) random image and use PGD to maximize (4) within a L_∞ -ball of size $\epsilon = 0.3$ (MNIST) or $\epsilon = 0.03$ (SVHN/Cifar10).

Training: We train 50%/50% AT (AT-50%) and CCAT as well as 100% AT (AT-100%) with L_∞ attacks using $T = 40$ iterations for PGD-CE and PGD-Conf, respectively, and $\epsilon = 0.3$ (MNIST) or $\epsilon = 0.03$ (SVHN/Cifar10). We use ResNet-20 (He et al., 2016), implemented in PyTorch (Paszke et al., 2017), trained using stochastic gradient descent. For CCAT, we use $\rho = 10$.

Baselines: We compare to multi-steepest descent (MSD) adversarial training (Maini et al., 2020) using the pre-trained LeNet on MNIST and pre-activation ResNet-18 on Cifar10 trained with L_∞ , L_2 and L_1 adversarial examples and ϵ set

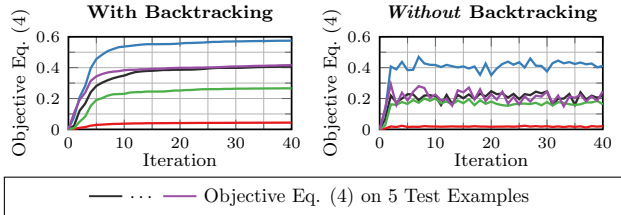


Figure 5: Backtracking. Our L_∞ PGD-Conf attack, i.e., PGD maximizing Eq. (4), using 40 iterations with momentum and our developed backtracking scheme (left) and without both (right) on SVHN. We plot Eq. (4) over iterations for the first 5 test examples corresponding to different colors. Backtracking avoids oscillation and obtains higher overall objective values within the same number of iterations.

to 0.3, 1.5, 12 and 0.03, 0.5, 12, respectively. The L_2 and L_1 attacks in Tab. 2 (larger ϵ) are unseen. For TRADES (Zhang et al., 2019), we use the pre-trained convolutional network (Carlini & Wagner, 2017b) on MNIST and WRN-10-28 (Zagoruyko & Komodakis, 2016) on Cifar10, trained on L_∞ adversarial examples with $\epsilon = 0.3$ and $\epsilon = 0.03$, respectively. On Cifar10, we further consider the pre-trained ResNet-50 of (Madry et al., 2018) (AT-Madry, L_∞ adversarial examples with $\epsilon = 0.03$). We also consider the Mahalanobis (MAHA) (Lee et al., 2018) and local intrinsic dimensionality (LID) detectors (Ma et al., 2018) using the provided pre-trained ResNet-34 on SVHN/Cifar10.

5.1. Ablation Study

Evaluation Metrics: Fig. 3 shows ROC curves, i.e., how well adversarial examples can be rejected by confidence. As marked in red, we are only interested in the FPR for the conservative choice of 99%TPR, yielding the confidence threshold τ . The RErr curves highlight how robustness is influenced by the threshold: AT also benefits from a reject option, however, not as much as CCAT which has been explicitly designed for rejecting adversarial examples.

Worst-Case Evaluation: Tab. 1 illustrates the importance of worst-case evaluation on SVHN, showing that CCAT is significantly “harder” to attack than AT. We show the worst-case RErr over all L_∞ attacks as well as the top-5 individual attacks (each restart treated as separate attack). For AT-50%, a single restart of PGD-Conf with $T = 1000$ iterations is highly successful, with 52.1% RErr close to the overall worst-case of 56%. For CCAT, in contrast, multiple restarts are crucial as the best individual attack, PGD-Conf with $T = 1000$ iterations and zero initialization obtains only 23.6% RErr compared to the overall worst-case of 39.1%.

Backtracking: Fig. 5 illustrates the advantage of backtracking for PGD-Conf with $T=40$ iterations on 5 test examples of SVHN. Backtracking results in better objective values and avoids oscillation, i.e., a stronger attack for training and

Confidence-Calibrated Adversarial Training

MNIST:	Err ↓ in %		confidence-thresholded RErr ↓ for $\tau@99\%$ TPR						FPR ↓ distal	Err ↓ corrupted MNIST-C
	(clean) $\tau = 0$	(clean) 99%TPR	L_∞ $\epsilon = 0.3$	L_∞ $\epsilon = 0.4$	L_2 $\epsilon = 3$	L_1 $\epsilon = 18$	L_0 $\epsilon = 15$	adv. frames		
	(seen)	(seen)	seen	unseen	unseen	unseen	unseen	unseen		
Normal	0.4	0.1	100.0	100.0	100.0	100.0	92.3	87.7	100.0	32.8
AT-50%	0.5	0.0	1.7	100.0	81.5	24.6	23.9	73.7	100.0	12.6
AT-100%	0.5	0.0	1.7	100.0	84.8	21.3	13.9	62.3	100.0	17.6
CCAT	0.3	0.1	7.4	11.9	0.3	1.8	14.8	0.2	0.0	5.7
* MSD	1.8	0.9	34.3	98.9	59.2	55.9	66.4	8.8	100.0	6.0
* TRADES	0.5	0.1	4.0	99.9	44.3	9.0	35.5	0.2	100.0	7.9
SVHN:	Err ↓ in %		confidence-thresholded RErr ↓ for $\tau@99\%$ TPR						FPR ↓ distal	Err ↓ corrupted CIFAR10-C
	(clean) $\tau = 0$	(clean) 99%TPR	L_∞ $\epsilon = 0.03$	L_∞ $\epsilon = 0.06$	L_2 $\epsilon = 2$	L_1 $\epsilon = 24$	L_0 $\epsilon = 10$	adv. frames		
	(seen)	(seen)	seen	unseen	unseen	unseen	unseen	unseen		
Normal	3.6	2.6	99.9	100.0	100.0	100.0	83.7	78.7	87.1	
AT-50%	3.4	2.5	56.0	88.4	99.4	99.5	73.6	33.6	86.3	
AT-100%	5.9	4.6	48.3	87.1	99.5	99.8	89.4	26.0	81.0	
CCAT	2.9	2.1	39.1	53.1	29.0	31.7	3.5	3.7	0.0	
* LID	3.3	2.2	91.0	93.1	92.2	90.0	41.6	89.8	8.6	
* MAHA	3.3	2.2	73.0	79.5	78.1	67.5	41.5	9.9	0.0	
CIFAR10:	Err ↓ in %		confidence-thresholded RErr ↓ for $\tau@99\%$ TPR						FPR ↓ distal	Err ↓ corrupted CIFAR10-C
	(clean) $\tau = 0$	(clean) 99%TPR	L_∞ $\epsilon = 0.03$	L_∞ $\epsilon = 0.06$	L_2 $\epsilon = 2$	L_1 $\epsilon = 24$	L_0 $\epsilon = 10$	adv. frames		
	(seen)	(seen)	seen	unseen	unseen	unseen	unseen	unseen		
Normal	8.3	7.4	100.0	100.0	100.0	100.0	84.7	96.7	83.3	12.3
AT-50%	16.6	15.5	62.7	93.7	98.4	98.4	74.4	78.7	75.0	16.2
AT-100%	19.4	18.3	59.9	90.3	98.3	98.0	72.3	79.6	72.5	19.6
CCAT	10.1	<u>6.7</u>	68.4	92.4	52.2	58.8	23.0	66.1	0.0	8.5
* MSD	18.4	17.6	53.2	89.4	88.5	68.6	39.2	82.6	76.7	19.3
* TRADES	15.2	13.2	43.5	81.0	70.9	96.9	36.9	72.1	76.2	15.0
* AT-Madry	13.0	11.7	45.1	84.5	98.7	97.8	42.3	73.3	78.5	12.9
* LID	6.4	4.9	99.0	99.2	70.6	89.4	47.0	66.1	0.1	11.59
* MAHA	6.4	4.9	94.1	95.3	90.6	97.6	49.8	70.0	2.4	12.4

Table 2: Main Results: Generalizing Robustness. For L_∞, L_2, L_1, L_0 attacks and adversarial frames, we report per-example worst-case (confidence-thresholded) Err and RErr at 99%TPR across all attacks; ϵ is reported in the corresponding columns. For distal adversarial examples and corrupted examples, we report FPR and Err, respectively. L_∞ attacks with $\epsilon=0.3$ on MNIST and $\epsilon = 0.03$ on SVHN/Cifar10 were used for training (seen). The remaining attacks were not encountered during training (unseen). CCAT outperforms AT and the other baselines regarding robustness against unseen attacks. FPRs included in the supplementary material. * Pre-trained models with different architecture, LID/MAHA use the same model.

testing. In addition, while $T=200$ iterations are sufficient against AT, we needed up to $T=1000$ iterations for CCAT.

5.2. Main Results (Table 2)

Robustness Against seen L_∞ Attacks: Considering Tab. 2 and L_∞ adversarial examples as seen during training, CCAT exhibits comparable robustness to AT. With 7.4%/67.9% RErr on MNIST/Cifar10, CCAT lacks behind AT-50% (1.7%/62.7%) only slightly. On SVHN, in contrast CCAT outperforms AT-50% and AT-100% significantly with 39.1% vs. 56.0% and 48.3%. We note that CCAT and AT-50% are trained on 50% clean / 50% adversarial examples. This is in contrast to AT-100% trained on 100%

adversarial examples, which improves robustness slightly, e.g., from 56%/62.7% to 48.3%/59.9% on SVHN/Cifar10.

Robustness Against unseen L_p Attacks: Regarding unseen attacks, AT’s robustness deteriorates quickly while CCAT is able to generalize robustness to novel threat models. On SVHN, for example, RErr of AT-50% goes up to 88.4%, 99.4%, 99.5% and 73.6% for larger L_∞, L_2, L_1 and L_0 attacks. In contrast, CCAT’s robustness generalizes to these unseen attacks significantly better, with 53.1%, 29%, 31.7% and 3.5%, respectively. The results on MNIST and Cifar10 or for AT-100% tell a similar story. However, AT generalizes better to L_1 and L_0 attacks on MNIST, possibly due to the large L_∞ -ball used during training ($\epsilon = 0.3$).

Here, training purely on adversarial examples, i.e., AT-100% is beneficial. On Cifar10, CCAT has more difficulties with large L_∞ attacks ($\epsilon = 0.06$) with 92% RErr. As detailed in the supplementary material, these observations are supported by considering FPR. AT benefits from considering FPR as clean Err is not taken into account. On Cifar10, for example, 47.6% FPR compared to 62.7% RErr for AT-50%. This is less pronounced for CCAT due to the improved Err compared to AT. Overall, CCAT improves robustness against arbitrary (unseen) L_p attacks, demonstrating that CCAT indeed extrapolates near-uniform predictions beyond the L_∞ ϵ -ball used during training.

Comparison to MSD and TRADES: TRADES is able to outperform CCAT alongside AT (including AT-Madry) on Cifar10 with respect to the L_∞ adversarial examples *seen* during training: 43.5% RErr compared to 68.4% for CCAT. This might be a result of training on 100% adversarial examples and using more complex models: TRADES uses a WRN-10-28 with roughly 46.1M weights, in contrast to our ResNet-18 with 4.3M (and ResNet-20 with 11.1M for MSD). However, regarding *unseen* L_2 , L_1 and L_0 attacks, CCAT outperforms TRADES with 52.2%, 58.8% and 23% compared to 70.9%, 96.9% and 36.9% in terms of RErr. Similarly, CCAT outperforms MSD. This is surprising, as MSD trains on both L_2 and L_1 attacks with smaller ϵ , while CCAT does not. Only against larger L_∞ adversarial examples with $\epsilon = 0.06$, TRADES reduces RErr from 92.4% (CCAT) to 81%. Similar to AT, TRADES also generalizes better to L_2 , L_1 or L_0 on MNIST, while MSD is not able to compete. Overall, compared to MSD and TRADES, the robustness obtained by CCAT generalizes better to previously unseen attacks. We also note that, on MNIST, CCAT outperforms the robust Analysis-by-Synthesis (ABS) approach of (Schott et al., 2019) wrt. L_∞ , L_2 , and L_0 attacks.

Detection Baselines: The detection methods LID and MAHA are outperformed by CCAT across all datasets and threat models. On SVHN, for example, MAHA obtains 73% RErr against the seen L_∞ attacks and 79.5%, 78.1%, 67.5% and 41.5% RErr for the unseen L_∞ , L_2 , L_1 and L_0 attacks. LID is consistently outperformed by MAHA on SVHN. This is striking, as we *only* used PGD-CE and PGD-Conf to attack these approaches and emphasizes the importance of training *adversarially* against an adaptive attack to successfully reject adversarial examples.

Robustness Against Unconventional Attacks: Against adversarial frames, robustness of AT reduces to 73.7% /62.3% RErr (AT-50%/100%), even on MNIST, while CCAT achieves 0.2%. MSD, in contrast, is able to preserve robustness better with 8.8% RErr, which might be due to the L_2 and L_1 attacks seen during training. CCAT outperforms both approaches with 0.2% RErr, as does TRADES. On SVHN and Cifar10, however, CCAT outperforms all

approaches, including TRADES, considering adversarial frames. Against distal adversarial examples, CCAT outperforms all approaches significantly, with 0% FPR, compared to the second-best of 72.5% for AT-100% on Cifar10. Only the detection baselines LID and MAHA are competitive, reaching close to 0% FPR. This means that CCAT is able to extrapolate low-confidence distributions to far-away regions of the input space. Finally, we consider corrupted examples (e.g., blur, noise, transforms etc.) where CCAT also improves results, i.e., mean Err across all corruptions. On Cifar10-C, for example, CCAT achieves 8.5% compared 12.9% for AT-Madry and 12.3% for normal training. On MNIST-C, only MSD yields a comparably low Err: 6% vs. 5.7% for CCAT.

Improved Test Error: CCAT also outperforms AT regarding Err, coming close to that of normal training. On all datasets, *confidence-thresholded* Err for CCAT is better or equal than that of normal training. On Cifar10, only LID/MAHA achieve a better standard and confidence-thresholded Err using a ResNet-34 compared to our ResNet-20 for CCAT (21.2M vs. 4.3M weights). In total the performance of CCAT shows that the robustness-generalization trade-off can be improved significantly.

Our **supplementary material** includes detailed descriptions of our PGD-Conf attack (including pseudo-code), a discussion of our confidence-thresholded RErr, and more details regarding baselines. We also include results for confidence thresholds at 98% and 95%TPR, which improves results only slightly, at the cost of “throwing away” significantly more clean examples. Furthermore, we provide ablation studies, qualitative examples and per-attack results.

6. Conclusion

Adversarial training results in robust models against the threat model *seen* during training, e.g., L_∞ adversarial examples. However, generalization to *unseen* attacks such as other L_p adversarial examples or larger L_∞ perturbations is insufficient. We propose **confidence-calibrated adversarial training (CCAT)** which biases the model towards low confidence predictions on adversarial examples and beyond. Then, adversarial examples can easily be rejected based on their confidence. Trained exclusively on L_∞ adversarial examples, CCAT improves robustness against unseen threat models such as larger L_∞ , L_2 , L_1 and L_0 adversarial examples, adversarial frames, distal adversarial examples and corrupted examples. Additionally, accuracy is improved in comparison to adversarial training. We thoroughly evaluated CCAT using 7 different white-and black-box attacks with up to 50 random restarts and 5000 iterations. These attacks were adapted to CCAT by directly maximizing confidence. We reported worst-case robust test error, extended to our confidence-thresholded setting, across *all* attacks.

References

- Alaifari, R., Alberti, G. S., and Gauksson, T. Adef: an iterative algorithm to construct adversarial deformations. In *ICLR*, 2019.
- Alayrac, J., Uesato, J., Huang, P., Fawzi, A., Stanforth, R., and Kohli, P. Are labels required for improving adversarial robustness? In *NeurIPS*, 2019.
- Amsaleg, L., Bailey, J., Barbe, D., Erfani, S. M., Houle, M. E., Nguyen, V., and Radovanovic, M. The vulnerability of learning to adversarial perturbation increases with intrinsic dimensionality. In *WIFS*, 2017.
- Andriushchenko, M., Croce, F., Flammarion, N., and Hein, M. Square attack: a query-efficient black-box adversarial attack via random search. *arXiv.org*, abs/1912.00049, 2019.
- Athalye, A. and Carlini, N. On the robustness of the CVPR 2018 white-box adversarial example defenses. *arXiv.org*, abs/1804.03286, 2018.
- Athalye, A., Carlini, N., and Wagner, D. A. Obfuscated gradients give a false sense of security: Circumventing defenses to adversarial examples. In *ICML*, 2018.
- Bhagoji, A. N., Cullina, D., and Mittal, P. Dimensionality reduction as a defense against evasion attacks on machine learning classifiers. *arXiv.org*, abs/1704.02654, 2017.
- Brown, T. B., Mané, D., Roy, A., Abadi, M., and Gilmer, J. Adversarial patch. *arXiv.org*, abs/1712.09665, 2017.
- Cai, Q., Liu, C., and Song, D. Curriculum adversarial training. In *IJCAI*, 2018.
- Carlini, N. and Wagner, D. Adversarial examples are not easily detected: Bypassing ten detection methods. In *AISec*, 2017a.
- Carlini, N. and Wagner, D. Towards evaluating the robustness of neural networks. In *SP*, 2017b.
- Carlini, N., Athalye, A., Brendel, N. P. W., Rauber, J., Tsipras, D., Goodfellow, I., Madry, A., and Kurakin, A. On evaluating adversarial robustness. *arXiv.org*, abs/1902.06705, 2019.
- Carmon, Y., Raghunathan, A., Schmidt, L., Duchi, J. C., and Liang, P. Unlabeled data improves adversarial robustness. In *NeurIPS*, 2019.
- Cheng, M., Lei, Q., Chen, P., Dhillon, I. S., and Hsieh, C. CAT: customized adversarial training for improved robustness. *arXiv.org*, abs/2002.06789, 2020.
- Croce, F. and Hein, M. Sparse and imperceivable adversarial attacks. In *ICCV*, 2019.
- Dong, Y., Liao, F., Pang, T., Su, H., Zhu, J., Hu, X., and Li, J. Boosting adversarial attacks with momentum. In *CVPR*, 2018.
- Duchi, J. C., Shalev-Shwartz, S., Singer, Y., and Chandra, T. Efficient projections onto the l_1 -ball for learning in high dimensions. In *ICML*, 2008.
- Engstrom, L., Tran, B., Tsipras, D., Schmidt, L., and Madry, A. Exploring the landscape of spatial robustness. In *ICML*, 2019.
- Feinman, R., Curtin, R. R., Shintre, S., and Gardner, A. B. Detecting adversarial samples from artifacts. *arXiv.org*, abs/1703.00410, 2017.
- Gong, Z., Wang, W., and Ku, W. Adversarial and clean data are not twins. *arXiv.org*, abs/1704.04960, 2017.
- Goodfellow, I., Qin, Y., and Berthelot, D. Evaluation methodology for attacks against confidence thresholding models, 2019. URL <https://openreview.net/forum?id=Hlg0piA9tQ>.
- Goodfellow, I. J., Shlens, J., and Szegedy, C. Explaining and harnessing adversarial examples. In *ICLR*, 2015.
- Grefenstette, E., Stanforth, R., O’Donoghue, B., Uesato, J., Swirszcz, G., and Kohli, P. Strength in numbers: Trading-off robustness and computation via adversarially-trained ensembles. *arXiv.org*, abs/1811.09300, 2018.
- Grosse, K., Manoharan, P., Papernot, N., Backes, M., and McDaniel, P. On the (statistical) detection of adversarial examples. *arXiv.org*, abs/1702.06280, 2017.
- He, K., Zhang, X., Ren, S., and Sun, J. Deep residual learning for image recognition. In *CVPR*, 2016.
- Hein, M., Andriushchenko, M., and Bitterwolf, J. Why relu networks yield high-confidence predictions far away from the training data and how to mitigate the problem. *CVPR*, 2019.
- Hendrycks, D. and Dietterich, T. G. Benchmarking neural network robustness to common corruptions and perturbations. *arXiv.org*, abs/1903.12261, 2019a.
- Hendrycks, D. and Dietterich, T. G. Benchmarking neural network robustness to common corruptions and perturbations. In *ICLR*, 2019b.
- Hendrycks, D. and Gimpel, K. Early methods for detecting adversarial images. In *ICLR*, 2017.
- Hendrycks, D., Mazeika, M., Kadavath, S., and Song, D. Using self-supervised learning can improve model robustness and uncertainty. In *NeurIPS*, 2019.

- Huang, R., Xu, B., Schuurmans, D., and Szepesvári, C. Learning with a strong adversary. *arXiv.org*, abs/1511.03034, 2015.
- Ilyas, A., Engstrom, L., Athalye, A., and Lin, J. Black-box adversarial attacks with limited queries and information. In *ICML*, 2018.
- Ioffe, S. and Szegedy, C. Batch normalization: Accelerating deep network training by reducing internal covariate shift. In *ICML*, 2015.
- Jacobsen, J., Behrmann, J., Carlini, N., Tramèr, F., and Papernot, N. Exploiting excessive invariance caused by norm-bounded adversarial robustness. *arXiv.org*, abs/1903.10484, 2019a.
- Jacobsen, J., Behrmann, J., Zemel, R. S., and Bethge, M. Excessive invariance causes adversarial vulnerability. In *ICLR*, 2019b.
- Kang, D., Sun, Y., Hendrycks, D., Brown, T., and Steinhardt, J. Testing robustness against unforeseen adversaries. *arXiv.org*, abs/1908.08016, 2019.
- Khoury, M. and Hadfield-Menell, D. On the geometry of adversarial examples. *arXiv.org*, abs/1811.00525, 2018.
- Krizhevsky, A. Learning multiple layers of features from tiny images. Technical report, 2009.
- Laidlaw, C. and Feizi, S. Playing it safe: Adversarial robustness with an abstain option. *arXiv.org*, abs/1911.11253, 2019.
- Lamb, A., Verma, V., Kannala, J., and Bengio, Y. Interpolated adversarial training: Achieving robust neural networks without sacrificing too much accuracy. In *AISec*, 2019.
- LeCun, Y., Bottou, L., Bengio, Y., and Haffner, P. Gradient-based learning applied to document recognition. *Proc. of the IEEE*, 86(11), 1998.
- Lee, K., Lee, K., Lee, H., and Shin, J. A simple unified framework for detecting out-of-distribution samples and adversarial attacks. In *NeurIPS*, 2018.
- Li, B., Chen, C., Wang, W., and Carin, L. On norm-agnostic robustness of adversarial training. *arXiv.org*, abs/1905.06455, 2019.
- Li, X. and Li, F. Adversarial examples detection in deep networks with convolutional filter statistics. In *ICCV*, 2017.
- Liao, F., Liang, M., Dong, Y., Pang, T., Hu, X., and Zhu, J. Defense against adversarial attacks using high-level representation guided denoiser. In *CVPR*, 2018.
- Liu, Y., Chen, X., Liu, C., and Song, D. Delving into transferable adversarial examples and black-box attacks. *ICLR*, 2017.
- Ma, X., Li, B., Wang, Y., Erfani, S. M., Wijewickrema, S. N. R., Schoenebeck, G., Song, D., Houle, M. E., and Bailey, J. Characterizing adversarial subspaces using local intrinsic dimensionality. In *ICLR*, 2018.
- Madry, A., Makelov, A., Schmidt, L., Tsipras, D., and Vladu, A. Towards deep learning models resistant to adversarial attacks. *ICLR*, 2018.
- Maini, P., Wong, E., and Kolter, J. Z. Adversarial robustness against the union of multiple perturbation models. *ICML*, 2020.
- Metzen, J. H., Genewein, T., Fischer, V., and Bischoff, B. On detecting adversarial perturbations. In *ICLR*, 2017.
- Miyato, T., Maeda, S.-i., Koyama, M., Nakae, K., and Ishii, S. Distributional smoothing with virtual adversarial training. *ICLR*, 2016.
- Mu, N. and Gilmer, J. Mnist-c: A robustness benchmark for computer vision. *ICML Workshops*, 2019.
- Narodytska, N. and Kasiviswanathan, S. P. Simple black-box adversarial attacks on deep neural networks. In *CVPR Workshops*, 2017.
- Netzer, Y., Wang, T., Coates, A., Bissacco, A., Wu, B., and Ng, A. Y. Reading digits in natural images with unsupervised feature learning. In *NeurIPS*, 2011.
- Pang, T., Du, C., Dong, Y., and Zhu, J. Towards robust detection of adversarial examples. In *NeurIPS*, 2018.
- Paszke, A., Gross, S., Chintala, S., Chanan, G., Yang, E., DeVito, Z., Lin, Z., Desmaison, A., Antiga, L., and Lerer, A. Automatic differentiation in pytorch. In *NeurIPS Workshops*, 2017.
- Pedregosa, F., Varoquaux, G., Gramfort, A., Michel, V., Thirion, B., Grisel, O., Blondel, M., Prettenhofer, P., Weiss, R., Dubourg, V., Vanderplas, J., Passos, A., Cournapeau, D., Brucher, M., Perrot, M., and Duchesnay, E. Scikit-learn: Machine learning in Python. *JMLR*, 12: 2825–2830, 2011.
- Pérolat, J., Malinowski, M., Piot, B., and Pietquin, O. Playing the game of universal adversarial perturbations. *CoRR*, abs/1809.07802, 2018.
- Raghunathan, A., Xie, S. M., Yang, F., Duchi, J. C., and Liang, P. Adversarial training can hurt generalization. *arXiv.org*, abs/1906.06032, 2019.

- Schmidt, L., Santurkar, S., Tsipras, D., Talwar, K., and Madry, A. Adversarially robust generalization requires more data. In *NeurIPS*, 2018.
- Schott, L., Rauber, J., Bethge, M., and Brendel, W. Towards the first adversarially robust neural network model on MNIST. In *ICLR*, 2019.
- Shafahi, A., Najibi, M., Xu, Z., Dickerson, J. P., Davis, L. S., and Goldstein, T. Universal adversarial training. In *AAAI*, 2020.
- Sharma, Y. and Chen, P. Attacking the madry defense model with ℓ_1 -based adversarial examples. In *ICLR Workshops*, 2018.
- Stutz, D., Hein, M., and Schiele, B. Disentangling adversarial robustness and generalization. *CVPR*, 2019.
- Szegedy, C., Zaremba, W., Sutskever, I., Bruna, J., Erhan, D., Goodfellow, I. J., and Fergus, R. Intriguing properties of neural networks. In *ICLR*, 2014.
- Szegedy, C., Vanhoucke, V., Ioffe, S., Shlens, J., and Wojna, Z. Rethinking the inception architecture for computer vision. In *CVPR*, 2016.
- Tramèr, F. and Boneh, D. Adversarial training and robustness for multiple perturbations. In *NeurIPS*, 2019.
- Tramèr, F., Kurakin, A., Papernot, N., Boneh, D., and McDaniel, P. D. Ensemble adversarial training: Attacks and defenses. *ICLR*, 2018.
- Tsipras, D., Santurkar, S., Engstrom, L., Turner, A., and Madry, A. Robustness may be at odds with accuracy. *arXiv.org*, abs/1805.12152, 2018.
- Tsipras, D., Santurkar, S., Engstrom, L., Turner, A., and Madry, A. Robustness may be at odds with accuracy. In *ICLR*, 2019.
- Xie, C., Zhang, Z., Zhou, Y., Bai, S., Wang, J., Ren, Z., and Yuille, A. L. Improving transferability of adversarial examples with input diversity. In *CVPR*, 2019.
- Zagoruyko, S. and Komodakis, N. Wide residual networks. In *BMVC*, 2016.
- Zajac, M., Zolna, K., Rostamzadeh, N., and Pinheiro, P. O. Adversarial framing for image and video classification. In *AAAI Workshops*, 2019.
- Zhang, H., Yu, Y., Jiao, J., Xing, E. P., Ghaoui, L. E., and Jordan, M. I. Theoretically principled trade-off between robustness and accuracy. In *ICML*, 2019.

Supplementary Material for Confidence-Calibrated Adversarial Training: Generalizing to Unseen Attacks

Abstract

This document provides supplementary material for **confidence-calibrated adversarial training (CCAT)**. First, in Sec. B, we provide the proof of Proposition 1, showing that there exist problems where standard adversarial training (AT) is unable to reconcile robustness and accuracy, while CCAT is able to obtain *both* robustness *and* accuracy. In Sec. C, to promote reproducibility and emphasize our thorough evaluation, we discuss details regarding the used attacks, training procedure, baselines and evaluation metrics. Furthermore, Sec. C includes additional experimental results in support of the observations in the main paper. For example, we present results for confidence threshold at 95% and 98% true positive rate (TPR), results for the evaluated detection baselines as well as per-attack and per-corruption results for in-depth analysis. We also include qualitative results highlighting how CCAT obtains robustness through confidence thresholding. Code and pre-trained models are available at davidstutz.de/ccat.

A. Introduction

Confidence-calibrated adversarial training (CCAT) biases the network towards low-confidence predictions on adversarial examples. This is achieved by training the network to predict a uniform distribution between (correct) one-hot and uniform distribution which becomes more uniform as the distance to the attacked example increases. In the main paper, we show that CCAT addresses two problems of standard adversarial training (AT) as, e.g., proposed in (Madry et al., 2018): the poor generalization of robustness to attacks not employed during training, e.g., other L_p attacks or larger perturbations, and the reduced accuracy. We show that CCAT, trained only on L_∞ adversarial examples, improves robustness against previously unseen attacks through confidence thresholding, i.e., rejecting low-confidence (adversarial) examples. Furthermore, we demonstrate that CCAT is able to improve accuracy compared to adversarial training. In this document, Sec. B provides the proof of Proposition 1. Then, Sec. C includes details on our experimental setup, emphasizing our efforts to thoroughly evaluate CCAT, and additional experimental results allowing an in-depth analysis of the robustness obtained through CCAT.

In Sec. B, corresponding to the proof of Proposition 1, we show that there exist problems where standard adversarial training is indeed unable to reconcile robustness and accuracy. CCAT, in contrast, is able to obtain *both* robustness and accuracy, given that the “transition” between one-hot and uniform distribution used during training is chosen appropriately.

In Sec. C, we discuss our thorough experimental setup to facilitate reproducibility and present additional experimental results in support of the conclusions of the main paper. In the first part of Sec. C, starting with Sec. C.1, we provide a detailed description of the employed projected gradient descent (PGD) attack with momentum and backtracking, including pseudo-code and used hyper-parameters. Similarly, we discuss details of the used black-box attacks. In Sec. C.2, we include details on our training procedure, especially for CCAT. In Sec. C.3, we discuss the evaluated baselines, i.e., (Maini et al., 2020; Madry et al., 2018; Zhang et al., 2019; Lee et al., 2018; Ma et al., 2018). Then, in Sec. C.4, we discuss the employed evaluation metrics, focusing on our *confidence-thresholded* robust test error (RErr). In the second part of Sec. C, starting with Sec. C.5, we perform ablation studies considering our attack and CCAT. Regarding the attack, we demonstrate the importance of enough iterations, backtracking and appropriate initialization to successfully attack CCAT. Regarding CCAT, we consider various values for the hyper-parameter ρ which controls the transition from one-hot to uniform distribution during training. In Sec. C.6, we analyze how CCAT achieves robustness by considering its behavior in adversarial directions as well as in between clean examples. Finally, we provide additional experimental results in Sec. C.7: our main results, i.e., robustness against seen and unseen adversarial examples, for a confidence threshold at 95% and 98% true positive rate (TPR), per-attack results on all datasets and per-corruption results on MNIST-C (Mu & Gilmer, 2019) and Cifar10-C (Hendrycks & Dietterich, 2019a).

B. Proof of Proposition 1

Adversarial training usually results in reduced accuracy on clean examples. In practice, training on 50% clean and 50% adversarial examples instead of training *only* on adversarial examples allows to control the robustness-accuracy trade-off to some extent, i.e., increase accuracy while sacrificing robustness. The following proposition shows that there exist problems where adversarial training is unable to reconcile robustness and accuracy, while CCAT is able to obtain *both*:

Proposition 2. *We consider a classification problem with two points $x = 0$ and $x = \epsilon$ in \mathbb{R} with deterministic labels, i.e., $p(y = 2|x = 0) = 1$ and $p(y = 1|x = \epsilon) = 1$, such that the problem is fully determined by the probability $p_0 = p(x = 0)$. The Bayes error of this classification problem is zero. Let the predicted probability distribution over classes be $\tilde{p}(y|x) = \frac{e^{g_y(x)}}{e^{g_1(x)} + e^{g_2(x)}}$, where $g : \mathbb{R}^d \rightarrow \mathbb{R}^2$ is the classifier and we assume that the function $\lambda : \mathbb{R}_+ \rightarrow [0, 1]$ used in CCAT is monotonically decreasing and $\lambda(0) = 1$. Then, the error of the Bayes optimal classifier (with cross-entropy loss) for*

- *adversarial training on 100% adversarial examples is $\min\{p_0, 1 - p_0\}$.*
- *adversarial training on 50%/50% adversarial/clean examples per batch is $\min\{p_0, 1 - p_0\}$.*
- *CCAT on 50% clean and 50% adversarial examples is zero if $\lambda(\epsilon) < \min\{p_0/1-p_0, 1-p_0/p_0\}$.*

Proof. First, we stress that we are dealing with three different probability distributions over the labels: the true one $p(y|x)$, the imposed one during training $\hat{p}(y|x)$ and the predicted one $\tilde{p}(y|x)$. We also note that \hat{p} depends on λ as follows:

$$\hat{p}(k) = \lambda p_y(k) + (1 - \lambda)u(k) \quad (9)$$

where $p_y(k)$ is the original one-hot distribution, i.e., $p_y(k) = 1$ iff $k = y$ and $p_y(k) = 0$ otherwise with y being the true label, and $u(k) = 1/K$ is the uniform distribution. We note that this is merely an alternative formulation to the target distribution as outlined in the main paper. Also note that λ itself is a function of the norm $\|\delta\|$; here, this dependence is made explicit by writing $\hat{p}(\lambda)(y|x)$. This makes the expressions for the expected loss of CCAT slightly more complicated. We first derive the Bayes optimal classifier and its loss for CCAT. We introduce

$$a = g_1(0) - g_2(0), \quad b = g_1(\epsilon) - g_2(\epsilon). \quad (10)$$

and express the logarithm of the predicted probabilities (confidences) of class 1 and 2 in terms of these quantities.

$$\begin{aligned} -\log \tilde{p}(y = 2|x = x) &= -\log \left(\frac{e^{g_2(x)}}{e^{g_1(x)} + e^{g_2(x)}} \right) = \log \left(1 + e^{g_1(x) - g_2(x)} \right) = \begin{cases} \log(1 + e^a) & \text{if } x = 0 \\ \log(1 + e^b) & \text{if } x = \epsilon \end{cases} \\ -\log \tilde{p}(y = 1|x = x) &= -\log \left(\frac{e^{g_1(x)}}{e^{g_1(x)} + e^{g_2(x)}} \right) = \log \left(1 + e^{g_2(x) - g_1(x)} \right) = \begin{cases} \log(1 + e^{-a}) & \text{if } x = 0 \\ \log(1 + e^{-b}) & \text{if } x = \epsilon \end{cases} \end{aligned}$$

We consider the approach by (Madry et al., 2018) with 100% adversarial training. The expected loss can be written as

$$\begin{aligned} &\mathbb{E} \left[\max_{\|\delta\|_\infty \leq \epsilon} L(y, g(x + \delta)) \right] = \mathbb{E} \left[\mathbb{E} \left[\max_{\|\delta\|_\infty \leq \epsilon} L(y, g(x + \delta)) | x \right] \right] \\ &= p(x = 0) p(y = 2|x = 0) \max \left\{ -\log(\tilde{p}(y = 2|x = 0)), -\log(\tilde{p}(y = 2|x = \epsilon)) \right\} \\ &\quad + (1 - p(x = 0)) p(y = 1|x = \epsilon) \max \left\{ -\log(\tilde{p}(y = 1|x = 0)), -\log(\tilde{p}(y = 1|x = \epsilon)) \right\} \\ &= p(x = 0) \max \left\{ -\log(\tilde{p}(y = 2|x = 0)), -\log(\tilde{p}(y = 2|x = \epsilon)) \right\} \\ &\quad + (1 - p(x = 0)) \max \left\{ -\log(\tilde{p}(y = 1|x = 0)), -\log(\tilde{p}(y = 1|x = \epsilon)) \right\} \end{aligned}$$

This yields in terms of the parameters a, b the expected loss:

$$L(a, b) = \max \left\{ \log(1 + e^a), \log(1 + e^b) \right\} p_0 + \max \left\{ \log(1 + e^{-a}), \log(1 + e^{-b}) \right\} (1 - p_0)$$

The expected loss is minimized if $a = b$ as then both maxima are minimal. This results in the expected loss

$$L(a) = \log(1 + e^a) p_0 + \log(1 + e^{-a}) (1 - p_0).$$

The critical point is attained at $a^* = b^* = \log\left(\frac{1-p_0}{p_0}\right)$. Thus

$$a^* = b^* = \begin{cases} > 0 & \text{if } p_0 < \frac{1}{2}, \\ < 0 & \text{if } p_0 > \frac{1}{2}. \end{cases}$$

Thus, we classify $x = 0$ correctly, if $p_0 > \frac{1}{2}$ and $x = \epsilon$ correctly if $p_0 < \frac{1}{2}$. As result, the error of 100% adversarial training is given by $\min\{p_0, 1 - p_0\}$ whereas the Bayes optimal error is zero as the problem is deterministic.

Next we consider 50% adversarial plus 50% clean training. The expected loss

$$\mathbb{E}\left[\max_{\|\delta\|_\infty \leq \epsilon} L(y, g(x + \delta))\right] + \mathbb{E}\left[L(y, g(x + \delta))\right],$$

can be written as

$$\begin{aligned} L(a, b) &= \max\left\{\log(1 + e^a), \log(1 + e^b)\right\}p_0 \\ &\quad + \max\left\{\log(1 + e^{-a}), \log(1 + e^{-b})\right\}(1 - p_0) \\ &\quad + \log(1 + e^a)p_0 + \log(1 + e^{-b})(1 - p_0) \end{aligned}$$

We make a case distinction. If $a \geq b$, then the loss reduces to

$$\begin{aligned} L(a, b) &= \log(1 + e^a)p_0 + \log(1 + e^{-b})(1 - p_0) \\ &\quad + \log(1 + e^a)p_0 + \log(1 + e^{-b})(1 - p_0) \\ &\geq L(a, a) \\ &= 2\log(1 + e^a)p_0 + 2\log(1 + e^{-a})(1 - p_0) \end{aligned}$$

Solving for the critical point yields $a^* = \log\left(\frac{1-p_0}{p_0}\right) = b^*$. Next we consider the set $a \leq b$. This yields the loss

$$\begin{aligned} L(a, b) &= \log(1 + e^b)p_0 + \log(1 + e^{-a})(1 - p_0) \\ &\quad + \log(1 + e^a)p_0 + \log(1 + e^{-b})(1 - p_0) \end{aligned}$$

Solving for the critical point yields $a^* = \log\left(\frac{1-p_0}{p_0}\right) = b^*$ which fulfills $a \leq b$. Actually, it coincides with the solution found already for 100% adversarial training and thus resulting error of 50% adversarial, 50% clean training is again $\min\{p_0, 1 - p_0\}$ which is not equal to the Bayes optimal error.

For our confidence-calibrated adversarial training one first has to solve

$$\delta_x^*(j) = \operatorname{argmax}_{\|\delta\|_\infty \leq \epsilon} \max_{k \neq j} \tilde{p}(y = k | x + \delta).$$

We get with the expressions above (note that we have a binary classification problem):

$$\begin{aligned} \delta_0^*(1) &= \operatorname{argmax}_{\|\delta\|_\infty \leq \epsilon} \tilde{p}(y = 2|0 + \delta) = \begin{cases} 0 & \text{if } a < b \\ \epsilon & \text{else.} \end{cases} \\ \delta_0^*(2) &= \operatorname{argmax}_{\|\delta\|_\infty \leq \epsilon} \tilde{p}(y = 1|0 + \delta) = \begin{cases} \epsilon & \text{if } a < b \\ 0 & \text{else.} \end{cases} \\ \delta_\epsilon^*(1) &= \operatorname{argmax}_{\|\delta\|_\infty \leq \epsilon} \tilde{p}(y = 2|\epsilon + \delta) = \begin{cases} -\epsilon & \text{if } a < b \\ 0 & \text{else.} \end{cases} \\ \delta_\epsilon^*(2) &= \operatorname{argmax}_{\|\delta\|_\infty \leq \epsilon} \tilde{p}(y = 1|\epsilon + \delta) = \begin{cases} 0 & \text{if } a < b \\ -\epsilon & \text{else.} \end{cases} \end{aligned}$$

Note that the imposed distribution \hat{p} over the classes depends on the true label y of x and $\delta_x^*(y)$ and then $\lambda(\|\delta_x^*(y)\|_\infty)$. Due to the simple structure of the problem it holds that $\|\delta_x^*(y)\|_\infty$ is either 0 or ϵ .

In CCAT we use for 50% of the batch the standard cross-entropy loss and for the other 50% we use the following loss:

$$L(\hat{p}_y(\lambda(\|\delta_x^*(y)\|))(x), \tilde{p}(x)) = - \sum_{j=1}^2 \hat{p}_y(\lambda(\|\delta_x^*(y)\|))(y = j | x = x) \log(\tilde{p}(y = j | x = x + \delta_x^*(j))).$$

The corresponding expected loss is then given by

$$\begin{aligned} \mathbb{E}\left[L(\hat{p}_y(\lambda(\|\delta_x^*(y)\|))(x), \tilde{p}(x))\right] &= \mathbb{E}\left[\mathbb{E}\left[L(\hat{p}_y(\lambda(\|\delta_x^*(y)\|))(x), \tilde{p}(x)) \middle| x\right]\right] \\ &= p(x = 0) \mathbb{E}\left[L(\hat{p}_y(\lambda(\|\delta_0^*(y)\|))(0), \tilde{p}(0)) \middle| x = 0\right] + p(x = \epsilon) \mathbb{E}\left[L(\hat{p}_y(\lambda(\|\delta_\epsilon^*(y)\|))(\epsilon), \tilde{p}(\epsilon)) \middle| x = \epsilon\right], \end{aligned}$$

where $p(x = 0) = p_0$ and $p(x = \epsilon) = 1 - p(x = 0) = 1 - p_0$. With the true conditional probabilities $p(y = s | x)$ we get

$$\begin{aligned} \mathbb{E}\left[L(\hat{p}_y(\lambda(\delta))(x), \tilde{p}(x)) \middle| x\right] &= \sum_{s=1}^2 p(y = s | x) L(\hat{p}_s(\lambda(\|\delta_x^*(s)\|))(x), \tilde{p}(x)) \\ &= - \sum_{s=1}^2 p(y = s | x) \sum_{j=1}^2 \hat{p}_s(\lambda(\|\delta_x^*(s)\|))(y = j | x) \log(\tilde{p}(y = j | x = x + \delta_x^*(s))) \end{aligned}$$

For our problem it holds with $p(y = 2 | x = 0) = p(y = 1 | x = \epsilon) = 1$ (by assumption). Thus,

$$\begin{aligned} \mathbb{E}\left[L(\hat{p}_y(\lambda(\delta))(x), \tilde{p}(x)) \middle| x = 0\right] &= - \sum_{j=1}^2 \hat{p}_2(\lambda(\|\delta_0^*(2)\|))(y = j | x = 0) \log(\tilde{p}(y = j | x = x + \delta_0^*(2))) \\ \mathbb{E}\left[L(\hat{p}_y(\lambda(\delta))(x), \tilde{p}(x)) \middle| x = \epsilon\right] &= - \sum_{j=1}^2 \hat{p}_1(\lambda(\|\delta_\epsilon^*(1)\|))(y = j | x = \epsilon) \log(\tilde{p}(y = j | x = x + \delta_\epsilon^*(1))) \end{aligned}$$

As $\|\delta_x^*(y)\|_\infty$ is either 0 or ϵ and $\lambda(0) = 1$ we use in the following for simplicity the notation $\lambda = \lambda(\|\epsilon\|_\infty)$. Moreover, note that

$$\hat{p}_y(\lambda)(y = j | x = x) = \begin{cases} \lambda + \frac{(1-\lambda)}{K} & \text{if } y = j, \\ \frac{(1-\lambda)}{K} & \text{else} \end{cases},$$

where K is the number of classes. Thus, $K = 2$ in our example and we note that $\lambda + \frac{(1-\lambda)}{2} = \frac{1+\lambda}{2}$.

With this we can write the total loss (remember that we have half normal cross-entropy loss and half the loss for the adversarial part with the modified ‘‘labels’’) as

$$\begin{aligned} L(a, b) &= p_0 \left[\log(1 + e^a) \mathbb{1}_{a \geq b} + \mathbb{1}_{a < b} \left(\frac{(1+\lambda)}{2} \log(1 + e^b) + \frac{(1-\lambda)}{2} \log(1 + e^{-b}) \right) \right] \\ &\quad + (1 - p_0) \left[\log(1 + e^{-b}) \mathbb{1}_{a \geq b} + \mathbb{1}_{a < b} \left(\frac{(1+\lambda)}{2} \log(1 + e^{-a}) + \frac{(1-\lambda)}{2} \log(1 + e^a) \right) \right] \\ &\quad + \log(1 + e^a) p_0 + \log(1 + e^{-b}) (1 - p_0), \end{aligned}$$

where we have omitted a global factor $\frac{1}{2}$ for better readability (the last row is the cross-entropy loss). We distinguish two sets in the optimization. First we consider the case $a \geq b$. Then it is easy to see that in order to minimize the loss we have $a = b$.

$$\partial_a L = 2 \frac{e^a}{1 + e^a} p_0 - \frac{e^{-a}}{1 + e^{-a}} (1 - p_0)$$

This yields $e^a = \frac{1-p_0}{p_0}$ or $a = \log\left(\frac{1-p_0}{p_0}\right)$ and the minimum for $a \geq b$ is attained on the boundary of the domain of $a \leq b$. The other case is $a \leq b$. We get

$$\begin{aligned} \partial_a L &= \left[\frac{(1+\lambda)}{2} \frac{-e^{-a}}{1 + e^{-a}} + \frac{(1-\lambda)}{2} \frac{e^a}{1 + e^a} \right] (1 - p_0) + p_0 \frac{e^a}{1 + e^a} \\ \partial_b L &= \left[\frac{(1+\lambda)}{2} \frac{e^b}{1 + e^b} + \frac{(1-\lambda)}{2} \frac{-e^{-b}}{1 + e^{-b}} \right] p_0 + (1 - p_0) \frac{-e^{-b}}{1 + e^{-b}} \end{aligned}$$

This yields the solution

$$a^* = \log \left(\frac{\frac{1+\lambda}{2}(1-p_0)}{p_0 + \frac{1-\lambda}{2}(1-p_0)} \right), \quad b^* = \log \left(\frac{\frac{1-\lambda}{2}p_0 + (1-p_0)}{\frac{1+\lambda}{2}p_0} \right)$$

It is straightforward to check that $a^* < b^*$ for all $0 < p_0 < 1$, indeed we have

$$\frac{\frac{1+\lambda}{2}(1-p_0)}{p_0 + \frac{1-\lambda}{2}(1-p_0)} = \frac{\frac{1+\lambda}{2}(1-p_0)}{p_0 \frac{1+\lambda}{2} + \frac{1-\lambda}{2}} = \frac{1-p_0 - \frac{(1-\lambda)}{2}(1-p_0)}{p_0 \frac{1+\lambda}{2} + \frac{1-\lambda}{2}} < \frac{\frac{1-\lambda}{2}p_0 + (1-p_0)}{\frac{1+\lambda}{2}p_0}$$

if $0 < p_0 < 1$ and note that $\lambda < 1$ by assumption. We have $a^* < 0$ and thus $g_2(0) > g_1(0)$ (Bayes optimal decision for $x = 0$) if

$$1 > \frac{1-p_0}{p_0} \lambda,$$

and $b^* > 0$ and thus $g_1(\epsilon) > g_2(\epsilon)$ (Bayes optimal decision for $x = \epsilon$) if

$$1 > \frac{p_0}{1-p_0} \lambda.$$

Thus we recover the Bayes classifier if

$$\lambda < \min \left\{ \frac{1-p_0}{p_0}, \frac{p_0}{1-p_0} \right\}.$$

□

C. Experiments

In the following, we provide additional details on our experimental setup regarding (a) the used attacks, especially our PGD-Conf attack including pseudo-code in Sec. C.1, (b) training of AT and CCAT in Sec. C.2, (c) the evaluated baselines in Sec. C.3 and (d) the used evaluation metrics in Sec. C.4. Afterwards, we include additional experimental results, including ablation studies in Sec. C.5, qualitative results for analysis in Sec. C.6, and further results for 95% and 98% true positive rate (TPR), results per attack and results per corruption on MNIST-C (Mu & Gilmer, 2019) and Cifar10-C (Hendrycks & Dietterich, 2019a) in Sec. C.7.

C.1. Attacks

Projected Gradient Descent (PGD): Complementary to the description of the projected gradient descent (PGD) attack by (Madry et al., 2018) and our adapted attack, we provide a detailed algorithm in Alg. 2. We note that the objective maximized in (Madry et al., 2018) is

$$\mathcal{F}(x + \delta, y) = \mathcal{L}(f(x + \delta; w), y) \quad (11)$$

where \mathcal{L} denotes the cross-entropy loss, $f(\cdot; w)$ denotes the model and (x, y) is an input-label pair from the test set. Our adapted attack, in contrast, maximizes

$$\mathcal{F}(x + \delta, y) = \max_{k \neq y} f_k(x + \delta; w) \quad (12)$$

where f_k denotes the confidence of f in class k . Note that the maximum over labels, i.e., $\max_{k \neq y}$, is explicitly computed during optimization; this means that in contrast to (Goodfellow et al., 2019), we do not run $(K - 1)$ targeted attacks and subsequently take the maximum-confidence one, where K is the number of classes. We denote these two variants as PGD-CE and PGD-Conf, respectively. Deviating from (Madry et al., 2018), we initialize δ uniformly over directions and norm (instead of uniform initialization over the volume of the ϵ -ball):

$$\delta = u \epsilon \frac{\delta'}{\|\delta'\|_\infty}, \quad \delta' \sim \mathcal{N}(0, I), u \sim U(0, 1) \quad (13)$$

Algorithm 2 Projected Gradient Descent (PGD) with Backtracking. Pseudo-code for the used PGD procedure to maximize Eq. (11) or Eq. (12) using momentum and backtracking subject to the constraints $\tilde{x}_i = x_i + \delta_i \in [0, 1]$ and $\|\delta\|_\infty \leq \epsilon$; in practice, the procedure is applied on batches of inputs. The algorithm is easily adapted to work with arbitrary L_p -norm; only the projections on Line 6 and 24 as well as the normalized gradient in Line 10 need to be adapted.

```

input: example  $x$  with label  $y$ 
input: number of iterations  $T$ 
input: learning rate  $\gamma$ , momentum  $\beta$ , learning rate factor  $\alpha$ 
input: initial  $\delta^{(0)}$ , e.g., Eq. (13) or  $\delta^{(0)} = 0$ 
1:  $v := 0$  {saves the best objective achieved}
2:  $\tilde{x} := x + \delta^{(0)}$  {best adversarial example obtained}
3:  $g^{(-1)} := 0$  {accumulated gradients}
4: for  $t = 0, \dots, T$  do
5:   {projection onto  $L_\infty$   $\epsilon$ -ball and on  $[0, 1]$ :}
6:   clip  $\delta_i^{(t)}$  to  $[-\epsilon, \epsilon]$ 
7:   clip  $x_i + \delta_i^{(t)}$  to  $[0, 1]$ 
8:   {forward and backward pass to get objective and gradient:}
9:    $v^{(t)} := \mathcal{F}(x + \delta^{(t)}, y)$  {see Eq. (11) or Eq. (12)}
10:   $g^{(t)} := \text{sign}(\nabla_{\delta^{(t)}} \mathcal{F}(x + \delta^{(t)}, y))$ 
11:  {keep track of adversarial example resulting in best objective:}
12:  if  $v^{(t)} > v$  then
13:     $v := v^{(t)}$ 
14:     $\tilde{x} := x + \delta^{(t)}$ 
15:  end if
16:  {iteration  $T$  is only meant to check whether last update improved objective:}
17:  if  $t = T$  then
18:    break
19:  end if
20:  {integrate momentum term:}
21:   $g^{(t)} := \beta g^{(t-1)} + (1 - \beta)g^{(t)}$ 
22:  {"try" the update step and see if objective increases:}
23:   $\hat{\delta}^{(t)} := \delta^{(t)} + \gamma g^{(t)}$ 
24:  clip  $\hat{\delta}_i^{(t)}$  to  $[-\epsilon, \epsilon]$ 
25:  clip  $x_i + \hat{\delta}_i^{(t)}$  to  $[0, 1]$ 
26:   $\hat{v}^{(t)} := \mathcal{F}(x + \hat{\delta}^{(t)}, y)$ 
27:  {only keep the update if the objective increased; otherwise decrease learning rate:}
28:  if  $\hat{v}^{(t)} \geq v^{(t)}$  then
29:     $\delta^{(t+1)} := \hat{\delta}^{(t)}$ 
30:  else
31:     $\gamma := \gamma/\alpha$ 
32:  end if
33: end for
34: return  $\tilde{x}, \tilde{v}$ 

```

where δ' is sampled from a standard Gaussian and $u \in [0, 1]$ from a uniform distribution. We also consider zero initialization, i.e., $\delta = 0$. For random initialization we always consider multiple restarts, 10 for PGD-Conf and 50 for PGD-CE; for zero initialization, we use 1 restart. Finally, in contrast to (Madry et al., 2018), we run PGD for exactly T iterations, taking the perturbation corresponding to the best objective value obtained throughout the optimization.

PGD for L_p , $p \in \{0, 1, 2\}$: Both PGD-CE and PGD-Conf can also be applied using the L_2 , L_1 and L_0 norms following the description above. Then, gradient normalization in Line 10 of Alg. 2, the projection in Line 6, and the initialization in Eq. (13) need to be adapted. For the L_2 norm, the gradient is normalized by dividing by the L_2 norm; for the L_1 norm only the 1% largest values (in absolute terms) of the gradient are kept and normalized by their L_1 norm; and for the L_0 norm, the gradient is normalized by dividing by the L_1 norm. We follow the algorithm of (Duchi et al., 2008) for the L_1 projection; for the L_0 projection (onto the ϵ -ball for $\epsilon \in \mathbb{N}_0$), only the ϵ largest values are kept. Similarly, initialization for L_2 and L_1 are simple by randomly choosing a direction (as in Eq. (13)) and then normalizing by their norm. For L_0 , we randomly choose pixels with probability $(\frac{2}{3}\epsilon)/(HWD)$ and set them to a uniformly random values $u \in [0, 1]$, where $H \times W \times D$ is the image size. In experiments, we found that tuning the learning rate for PGD with L_1 and L_0 constraints (independent of

Confidence-Calibrated Adversarial Training

MNIST: Attack Ablation with confidence-thresholded RErr in % for $\tau@99\%$ TPR (L_∞ attack with $\epsilon = 0.3$ for training and testing)									
Optimization	momentum+backtrack					mom		-	
Initialization	zero				rand	zero		zero	
Iterations	40	200	1000	2000	2000	60	300	60	300
AT	0.4	0.4	0.4	0.3	0.6	0.4	0.6	0.4	0.4
AT Conf (AT trained with PGD-Conf)	0.8	0.8	0.8	0.8	1.1	1.0	1.1	1.0	1.0
CCAT	0.2	1.4	4.6	4.6	3.7	0.7	0.7	0.2	0.2

SVHN: Attack Ablation with confidence-thresholded RErr in % for $\tau@99\%$ TPR (L_∞ attack with $\epsilon = 0.03$ for training and testing)									
Optimization	momentum+backtrack					mom		-	
Initialization	zero				rand	zero		zero	
Iterations	40	200	1000	2000	2000	60	300	60	300
AT	38.4	46.2	49.9	50.1	51.8	37.7	38.1	29.9	30.8
AT Conf (AT trained with PGD-Conf)	27.4	40.5	46.9	47.3	48.1	27.1	28.5	21.1	23.8
CCAT	4.0	5.0	22.8	23.3	5.2	2.6	2.6	2.6	2.6

CIFAR10: Attack Ablation with confidence-thresholded RErr in % for $\tau@99\%$ TPR (L_∞ attack with $\epsilon = 0.03$ for training and testing)									
Optimization	momentum+backtrack					mom		-	
Initialization	zero				rand	zero		zero	
Iterations	40	200	1000	2000	2000	60	300	60	300
AT	60.9	60.8	60.8	60.8	60.9	60.9	60.9	57.4	57.6
AT Conf (AT trained with PGD-Conf)	60.4	60.6	60.5	60.5	60.9	60.4	60.6	56.2	56.6
CCAT	14.8	16.2	40.2	41.3	34.9	7.2	7.2	7.2	7.2

Table 3: Detailed Attack Ablation Studies. We compare our L_∞ PGD-Conf attack with T iterations and different combinations of momentum, backtracking and initialization on all three datasets. We consider AT, AT trained with PGD-Conf (AT Conf), and CCAT; we report RErr for confidence threshold $\tau@99\%$ TPR. As backtracking requires an additional forward pass per iteration, we use $T = 60$ and $T = 300$ for attacks without backtracking to be comparable to attacks with $T = 40$ and $T = 200$ with backtracking. Against CCAT, $T = 1000$ iterations or more are required and backtracking is essential to achieve high RErr. AT, in contrast, is “easier” to attack, requiring less iterations and less sophisticated optimization (i.e., without momentum and/or backtracking).

the objective, i.e., Eq. (11) or Eq. (12)) is much more difficult. Additionally, PGD using the L_0 norm seems to get easily stuck in sub-optimal local optima.

Backtracking: Alg. 2 also gives more details on the employed momentum and backtracking scheme. These two “tricks” add two additional hyper-parameters to the number of iterations T and the learning rate γ , namely the momentum parameter β and the learning rate factor α . After each iteration, the computed update, already including the momentum term, is only applied if this improves the objective. This is checked through an additional forward pass. If not, the learning rate is divided by α , and the update is rejected. Alg. 2 includes this scheme as an algorithm for an individual test example x with label y for brevity; however, extending it to work on batches is straight-forward. However, it is important to note that the learning rate is updated per test example individually. In practice, for PGD-CE, with $T = 200$ iterations, we use $\gamma = 0.05$, $\beta = 0.9$ and $\alpha = 1.25$; for PGD-Conf, with $T = 1000$ iterations, we use $\gamma = 0.001$, $\beta = 0.9$ and $\alpha = 1.1$.

Black-Box Attacks: We also give more details on the used black-box attacks. For random sampling, we apply Eq. (13) $T = 5000$ times. We also implemented the Query-Limited (QL) black-box attack of (Ilyas et al., 2018) using a population of 50 and variance of 0.1 for estimating the gradient in Line 10 of Alg. 2; a detailed algorithm is provided in (Ilyas et al., 2018). We use a learning rate of 0.001 (note that the gradient is signed, as in (Madry et al., 2018)) and also integrated a momentum with $\beta = 0.9$ and backtracking with $\alpha = 1.1$ and $T = 1000$ iterations. We use zero and random initialization; in the latter case we allow 10 random restarts. For the Simple black-box attack we follow the algorithmic description in (Narodytska & Kasiviswanathan, 2017) considering only axis-aligned perturbations of size ϵ per pixel. We run the attack for $T = 1000$ iterations and allow 10 random restarts. Following, (Khoury & Hadfield-Menell, 2018), we further use the Geometry attack for $T = 1000$ iterations. Random sampling, QL, Simple and Geometry attacks are run for arbitrary L_p , $p \in \{\infty, 2, 1, 0\}$. For L_∞ , we also use the Square attack proposed in (Andriushchenko et al., 2019) with $T = 5000$

Confidence-Calibrated Adversarial Training

SVHN: Training Ablation for Detection ($\tau@99\%$ TPR) and Standard Settings ($\tau = 0$) (L_∞ attack with $\epsilon = 0.03$ during training and testing)					
	Detection Setting $\tau@99\%$ TPR			Standard Setting $\tau = 0$	
	ROC AUC	Err in %	RErr in %	Err in %	RErr in %
Normal	0.17	2.6	99.9	3.6	99.9
AT	0.55	2.5	54.9	3.4	56.9
AT Conf (AT trained with PGD-Conf)	0.61	2.8	52.5	3.7	58.7
CCAT, $\rho = 1$	0.74	2.2	43.0	2.7	82.4
CCAT, $\rho = 2$	0.68	2.1	44.2	2.9	79.6
CCAT, $\rho = 4$	0.68	1.8	35.8	2.7	80.4
CCAT, $\rho = 6$	0.64	1.8	32.8	2.9	72.1
CCAT, $\rho = 8$	0.63	2.2	42.3	2.9	84.6
CCAT, $\rho = 10$	0.67	2.1	38.5	2.9	91.0
CCAT, $\rho = 12$	0.67	1.9	36.3	2.8	81.8

CIFAR10: Training Ablation for Detection ($\tau@99\%$ TPR) and Standard Settings ($\tau = 0$) (L_∞ attack with $\epsilon = 0.03$ during training and testing)					
	Detection Setting $\tau@99\%$ TPR			Standard Setting $\tau = 0$	
	ROC AUC	Err in %	RErr in %	Err in %	RErr in %
Normal	0.20	7.4	100.0	8.3	100.0
AT	0.65	15.1	60.9	16.6	61.3
AT Conf (AT trained with PGD-Conf)	0.63	15.1	61.5	16.1	61.7
CCAT, $\rho = 1$	0.63	8.7	72.4	9.7	95.3
CCAT, $\rho = 2$	0.60	8.4	70.6	9.7	95.1
CCAT, $\rho = 4$	0.61	8.6	66.3	9.8	93.5
CCAT, $\rho = 6$	0.54	8.0	69.8	9.2	94.1
CCAT, $\rho = 8$	0.58	8.5	65.3	9.4	93.2
CCAT, $\rho = 10$	0.60	8.7	63.0	10.1	95.0
CCAT, $\rho = 12$	0.62	9.4	63.0	10.1	96.6

Table 4: Training Ablation Studies. We report unthresholded RErr and Err, i.e., $\tau = 0$ (“Standard Setting”), and $\tau@99\%$ TPR as well as ROC AUC (“Detection Setting”) for CCAT with various values for ρ . The models are tested against our L_∞ PGD-Conf attack with $T = 1000$ iterations and zero as well as random initialization. On Cifar10, $\rho = 10$ works best and performance stagnates for $\rho > 10$. On SVHN, we also use $\rho = 10$, although $\rho = 6$ shows better results.

iterations with a probability of change of 0.05. For all attacks, we use Eq. (12) as objective. Finally, for L_0 , we also use Corner Search (Croce & Hein, 2019) with the cross-entropy loss as objective, for $T = 200$ iterations. We emphasize that, except for QL, these attacks are not gradient-based and do not approximate the gradient. Furthermore, we note that all attacks except Corner Search are adapted to explicitly attack CCAT by maximizing Eq. (12).

C.2. Training

We follow the ResNet-20 architecture by (He et al., 2016) implemented in PyTorch (Paszke et al., 2017). For training we use a batch size of 100 and train for 100 and 200 epochs on MNIST and SVHN/Cifar10, respectively: this holds for normal training, adversarial training (AT) and confidence-calibrated adversarial training (CCAT). For the latter two, we use PGD-CE and PGD Conf, respectively, for $T = 40$ iterations including momentum and backtracking ($\beta = 0.9$, $\alpha = 1.5$). For PGD-CE we use a learning rate of 0.05, 0.01 and 0.005 on MNIST, SVHN and Cifar10. For PGD-Conf we use a learning rate of 0.005. For CCAT, we randomly switch between the initialization in Eq. (13) and zero initialization. For training, we use standard stochastic gradient descent, starting with a learning rate of 0.1 on MNIST/SVHN and 0.075 on Cifar10. The learning rate is multiplied by 0.95 after each epoch. We do not use weight decay; but the network includes batch normalization (Ioffe & Szegedy, 2015). On SVHN and Cifar10, we use random cropping, random flipping (only Cifar10) and contrast augmentation during training. We always train on 50% clean and 50% adversarial examples per batch, i.e., each batch contains both clean and adversarial examples which is important when using batch normalization.

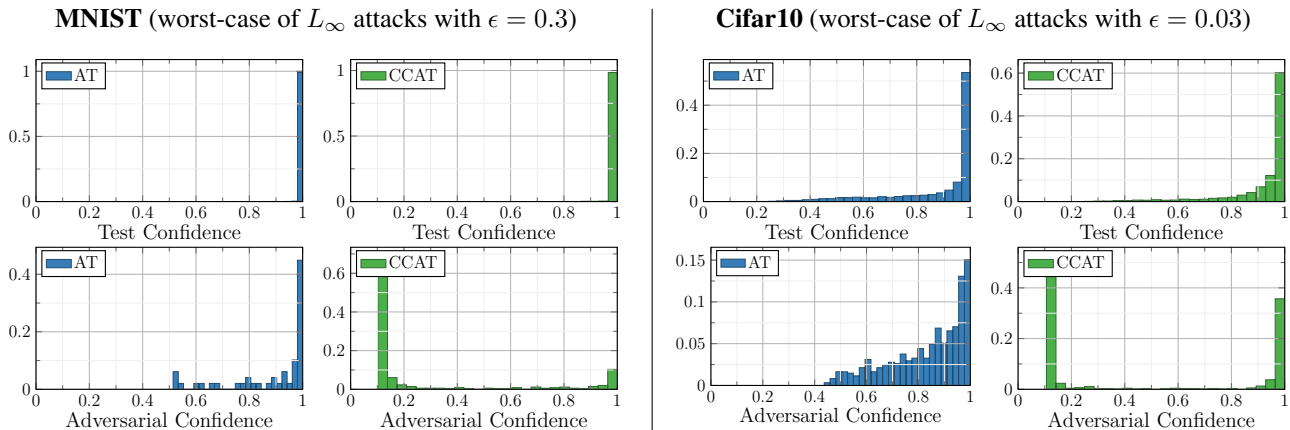


Figure 6: Confidence Histograms. We show histograms of confidences on correctly classified test examples (top) and on adversarial examples (bottom) for both AT and CCAT. Note that for AT, the number of successful adversarial examples is usually lower than for CCAT. For CCAT in contrast, nearly all adversarial examples are successful, while only a part has high confidence. Histograms obtained for the worst-case adversarial examples across all tested L_∞ attacks with $\epsilon = 0.3$ and $\epsilon = 0.03$ on MNIST and Cifar10, respectively.

C.3. Baselines

As baseline, we use the multi-steepest descent (MSD) adversarial training of (Maini et al., 2020), using the code and models provided in the official repository¹. The models correspond to a LeNet-like (LeCun et al., 1998) architecture on MNIST, and the pre-activation version of ResNet-18 (He et al., 2016) on Cifar10. The models were trained with L_∞ , L_2 and L_1 adversarial examples and ϵ set to 0.3, 1.5, 12 and 0.03, 0.5, 12, respectively. We attacked these models using the same setup as used for standard AT and our CCAT.

Additionally, we compare to TRADES (Zhang et al., 2019) using the code and pre-trained models from the official repository². The models correspond to a convolutional architecture with four convolutional and three fully-connected layers (Carlini & Wagner, 2017b) on MNIST, and a wide ResNet, specifically WRN-10-28 (Zagoruyko & Komodakis, 2016), on Cifar10. Both are trained using *only* L_∞ adversarial examples with $\epsilon = 0.3$ and $\epsilon = 0.03$, respectively. The evaluation protocol follows the same setup as used for standard AT and CCAT.

On Cifar10, we also use the pre-trained ResNet-50 from (Madry et al., 2018) obtained from the official repository³. The model was trained on L_∞ adversarial examples with $\epsilon = 0.03$. The same evaluation as for CCAT applies.

Furthermore, we evaluate two detection baseline: the Mahalanobis detector (MAHA) of (Ma et al., 2018) and the local intrinsic dimensionality (LID) detector of (Lee et al., 2018). We used the code provided by (Lee et al., 2018) from the official repository⁴. For evaluation, we used the provided setup, adding *only* PGD-CE and PGD-Conf with $T = 1000$, $T = 200$ and $T = 40$. For $T = 1000$, we used 5 random restarts, for $T = 200$, we used 25 restarts, and for $T = 40$, we used one restart. These were run for L_∞ , L_2 , L_1 and L_0 . We also evaluated distal adversarial examples as in the main paper. While the hyper-parameters were chosen considering our L_∞ PGD-CE attack ($T = 40$, one restart) and kept fixed for other threat models, the logistic regression classifier trained on the computed statistics (e.g., the Mahalanobis statistics) is trained for each threat model individually, resulting in an advantage over AT and CCAT. For worst-case evaluation, where we keep the highest-confidence adversarial example per test example for CCAT, we use the obtained detection score instead. This means, for each test example individually, we consider the adversarial example with worst detection score for evaluation.

¹https://github.com/locuslab/robust_union

²<https://github.com/yaodongyu/TRADES>

³<https://github.com/MadryLab/robustness>

⁴https://github.com/pokaxpoka/deep_Mahalanobis_detector

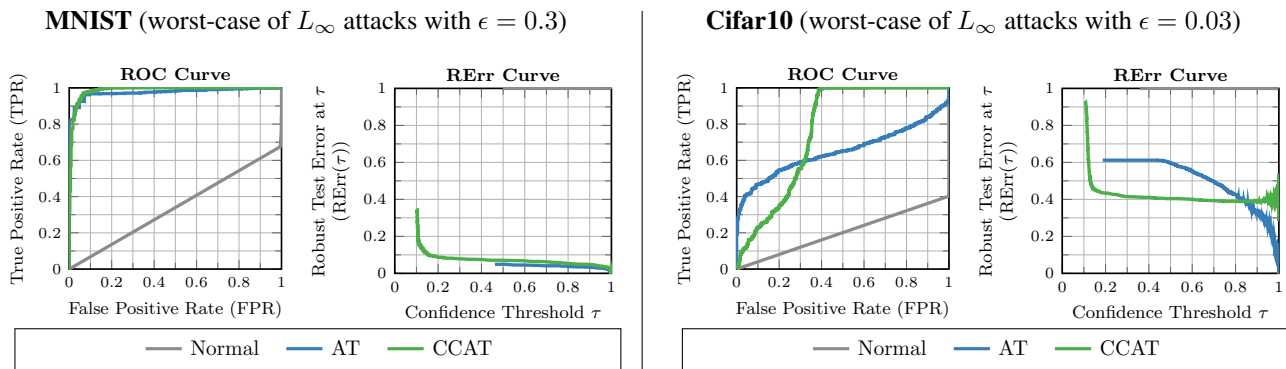


Figure 7: ROC and RErr curves. ROC curves, i.e. FPR plotted against TPR for all possible confidence thresholds τ , and (confidence-thresholded) RErr curves, i.e., RErr over confidence threshold τ for AT and CCAT, including different ρ parameters. Worst-case adversarial examples across all L_∞ attacks with $\epsilon = 0.3$ (MNIST) and $\epsilon = 0.03$ (Cifar10) were tested. For evaluation, the confidence threshold τ is fixed at 99%TPR, allowing to reject at most 1% correctly classified clean examples. Thus, we also do not report the area under the ROC curve in the main paper.

C.4. Evaluation Metrics

Complementing the discussion in the main paper, we describe the used evaluation metrics and evaluation procedure in more detail. Adversarial examples are computed on the first 1000 examples of the test set; the used confidence threshold is computed on the last 1000 examples of the test set; test errors are computed on all test examples minus the last 1000. As we consider multiple attacks, and some attacks allow multiple random restarts, we always consider the worst case adversarial example per test example and across all attacks/restarts; the worst-case is selected based on confidence.

FPR and ROC AUC: To compute receiver operating characteristic (ROC) curves, and the area under the curve, i.e., ROC AUC, we define negatives as *successful* adversarial examples (corresponding to correctly classified test examples) and positives as the corresponding *correctly classified* test examples. The ROC AUC as well as the curve itself can easily be calculated using scikit-learn (Pedregosa et al., 2011). Practically, the generated curve could be used to directly estimate a threshold corresponding to a pre-determined true positive rate (TPR). However, this requires interpolation; after trying several interpolation schemes, we concluded that the results are distorted significantly, especially for TPRs close to 100%. Thus, we follow a simpler scheme: on a held out validation set of size 1000 (the last 1000 samples of the test set), we sorted the corresponding confidences, and picked the confidence threshold in order to obtain (at least) the desired TPR, e.g., 99%.

In the main paper, instead of reporting ROC AUC, we reported only confidence-thresholded robust test error (RErr), which implicitly subsumes the false positive rate (FPR), at a confidence threshold of 99%TPR. Again, we note that this is an extremely conservative choice, allowing to reject at most 1% correctly classified clean examples. In addition, comparison to other approaches is fair as the corresponding confidence threshold only depends on correctly classified clean examples, not on adversarial examples. As also seen in Fig. 7, ROC AUC is not a practical metric to evaluate the detection/rejection of adversarial examples. This is because rejecting a significant part of correctly classified clean examples is not acceptable. In this sense, ROC AUC measures how well positives and negatives can be distinguished in general, while we are only interested in the performance for very high TPR, e.g., 99%TPR as in the main paper. In this document, we also report FPR to complement our evaluation using (confidence-thresholded) RErr.

Robust Test Error: The standard robust test error (Madry et al., 2018) is the model’s test error in the case where all test examples are allowed to be attacked, i.e., modified within the chosen threat model, e.g., for L_p :

$$\text{“Standard” RErr} = \frac{1}{N} \sum_{n=1}^N \max_{\|\delta\|_p \leq \epsilon} \mathbb{1}_{f(x_n + \delta) \neq y_n} \quad (14)$$

where $\{(x_n, y_n)\}_{n=1}^N$ are test examples and labels. In practice, RErr is computed empirically using several adversarial attacks, potentially with multiple restarts as the inner maximization problem is generally non-convex.

As standard RErr does not account for a reject option, we propose a generalized definition adapted to our confidence-

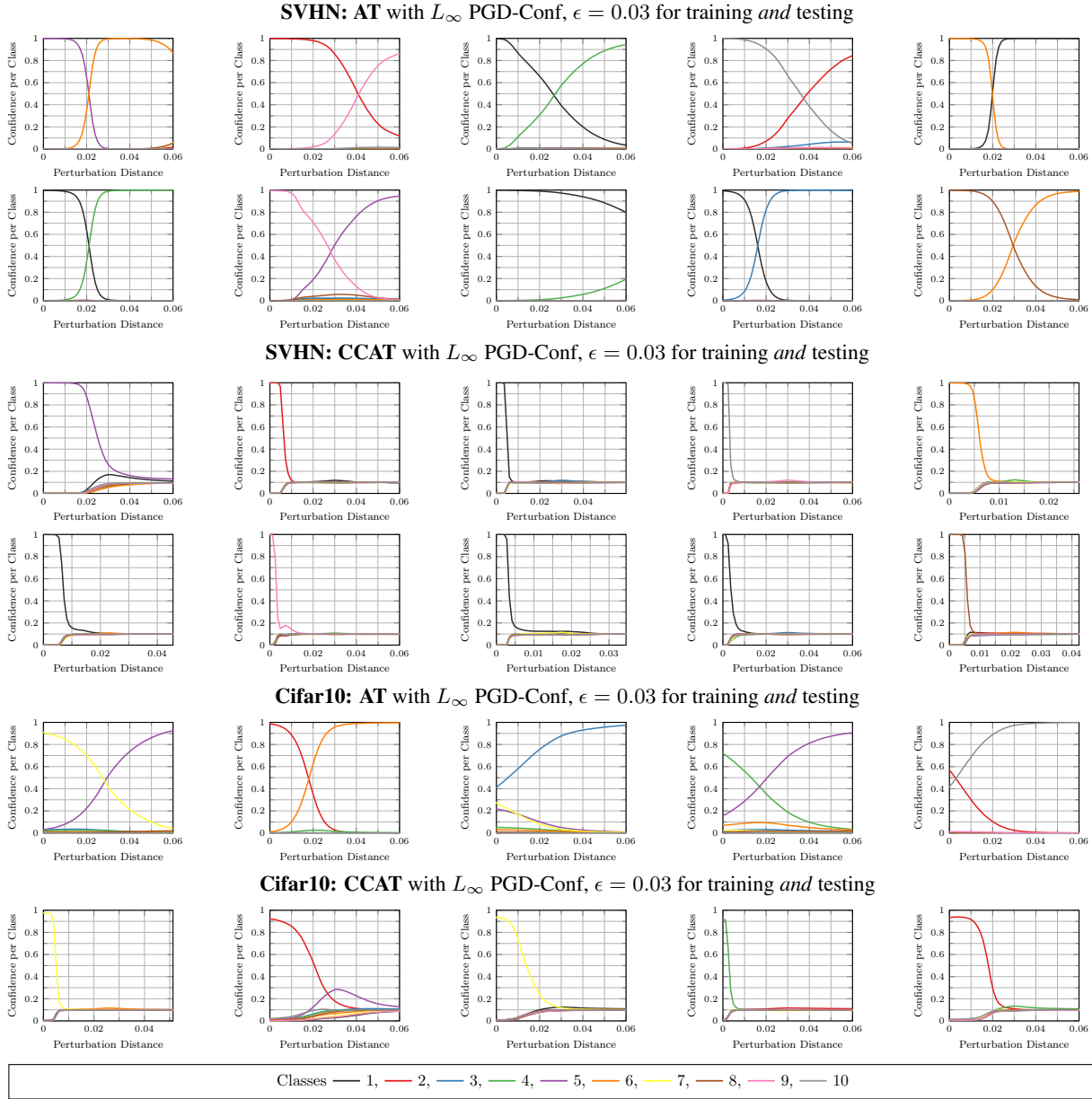


Figure 8: Effect of Confidence Calibration. Confidences for classes along adversarial directions for AT and CCAT. Adversarial examples were computed using PGD-Conf with $T = 1000$ iterations and zero initialization. For both AT and CCAT, we show the first ten examples of the test set on SVHN, and the first five examples of the test set on Cifar10. As can be seen, CCAT biases the network to predict uniform distributions beyond the ϵ -ball used during training ($\epsilon = 0.03$). For AT, in contrast, adversarial examples can usually be found right beyond the ϵ -ball.

thresholded setting. For fixed confidence threshold τ , e.g., at 99%TPR, the confidence-thresholded RErr is defined as

$$\text{RErr}(\tau) = \frac{\sum_{n=1}^N \max_{\|\delta\|_p \leq \epsilon, c(x_n + \delta) \geq \tau} \mathbb{1}_{f(x_n + \delta) \neq y_n}}{\sum_{n=1}^N \max_{\|\delta\|_p \leq \epsilon} \mathbb{1}_{c(x_n + \delta) \geq \tau}} \quad (15)$$

with $c(x) = \max_k f_k(x)$ and $f(x)$ being the model's confidence and predicted class on example x , respectively. This is the test error on test examples that can be modified within the chosen threat model *and* pass confidence thresholding. It reduces

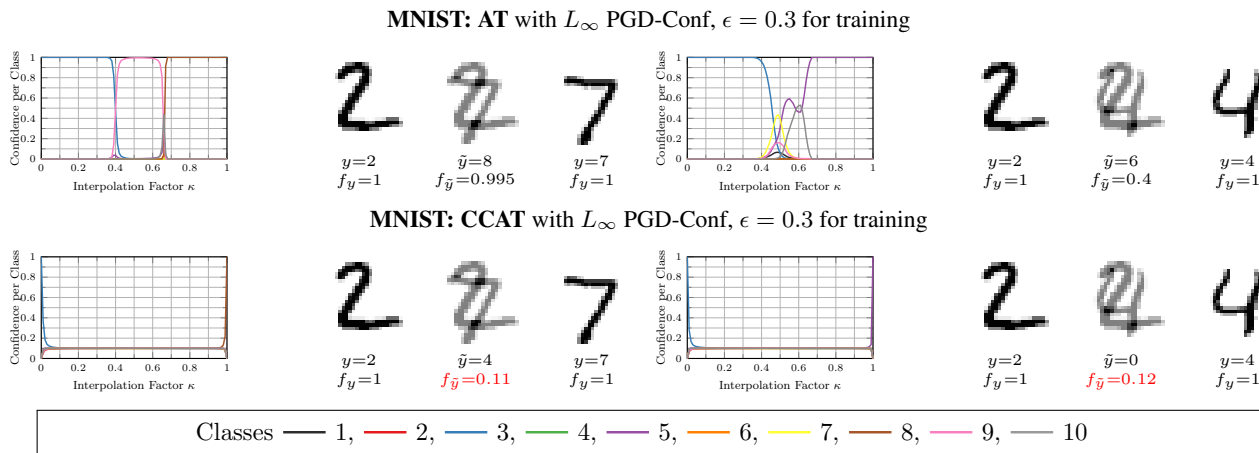


Figure 9: Confidence Calibration Between Test Examples. We plot the confidence for all classes when interpolating linearly between test examples: $(1 - \kappa)x_1 + \kappa x_2$ for two test examples x_1 and x_2 with $\kappa \in [0, 1]$; x_1 is fixed and we show two examples corresponding to different x_2 . Additionally, we show the corresponding images for $\kappa = 0$, i.e., x_1 , $\kappa = 0.5$, i.e., the mean image, and $\kappa = 1$, i.e., x_2 , with the corresponding labels and confidences. As can be seen, CCAT is able to perfectly predict a uniform distribution between test examples. AT, in contrast, enforces high-confidence predictions, resulting in conflicts if x_1 and x_2 are too close together (i.e., within one ϵ -ball) or in sudden changes of the predicted class in between, as seen above.

to standard RErr for $\tau = 0$, is in $[0, 1]$ and, thus, fully comparable to related work.

As both Eq. (14) and Eq. (15) cannot be computed exactly, we compute

$$\frac{\sum_{n=1}^N \max\{\mathbb{1}_{f(x_n) \neq y_n} \mathbb{1}_{c(x_n) \geq \tau}, \mathbb{1}_{f(\tilde{x}_n) \neq y_n} \mathbb{1}_{c(\tilde{x}_n) \geq \tau}\}}{\sum_{n=1}^N \max\{\mathbb{1}_{c(x_n) \geq \tau}, \mathbb{1}_{c(\tilde{x}_n) \geq \tau}\}} \quad (16)$$

which is an upper bound assuming that our attack is perfect. Essentially, this counts the test examples x_n that are either classified incorrectly with confidence $c(x_n) \geq \tau$ or that can be attacked successfully $\tilde{x}_n = x_n + \delta$ with confidence $c(\tilde{x}_n) \geq \tau$. This is normalized by the total number of test examples x_n that have $c(x_n) \geq \tau$ or where the corresponding adversarial example \tilde{x}_n has $c(\tilde{x}_n) \geq \tau$. It can easily be seen that $\tau = 0$ reduces Eq. (16) to its unthresholded variant, i.e., standard RErr, ensuring full comparability to related work.

In the following, we also highlight two special cases that are (correctly) taken into account by Eq. (16): (a) if a correctly classified test example x_n , i.e., $f(x_n) = y_n$, has confidence $c(x_n) < \tau$, i.e., is rejected, but the corresponding adversarial example \tilde{x}_n with $f(\tilde{x}_n) \neq y$ has $c(\tilde{x}_n) \geq \tau$, i.e., is *not* rejected, this is counted both in the numerator and denominator; (b) if an incorrectly classified test example x_n , i.e., $f(x_n) \neq y$, with $c(x_n) < \tau$, i.e., rejected, has a corresponding adversarial example \tilde{x}_n , i.e., also $f(\tilde{x}_n) \neq y$, but with $c(\tilde{x}_n) \geq \tau$, i.e., *not* rejected, this is also counted in the numerator as well as denominator. Note that these cases are handled differently in our detection evaluation following related work (Ma et al., 2018; Lee et al., 2018): negatives are adversarial examples corresponding to correctly classified clean examples that are successful, i.e., change the label. For example, case (b) would not contribute towards the FPR since the original test example is already mis-classified. Thus, while RErr implicitly includes FPR as well as Err, it is even more conservative than just considering ‘‘FPR + Err’’.

C.5. Ablation Study

In the following, we include ablation studies for our attack PGD-Conf, in Tab. 3, and for CCAT, in Tab. 4.

Attack. Regarding the proposed attack PGD-Conf using momentum and backtracking, Tab. 3 shows that backtracking and sufficient iterations are essential to attack CCAT. On SVHN, for AT, the difference in RErr between $T = 200$ and $T = 1000$ iterations is only 3.7%, specifically, 46.2% and 49.9%. For CCAT, in contrast, using $T = 200$ iterations is not sufficient, with merely 5% RErr. However, $T = 1000$ iterations with zero initialization increases RErr to 22.8%. For more iterations, i.e., $T = 2000$, RErr stagnates with 23.3%. When using random initialization (one restart), RErr drops to 5.2%,

Confidence-Calibrated Adversarial Training

MNIST: FPR and RErr in % for $\tau@99\%$ TPR												
	L_∞ $\epsilon = 0.3$		L_∞ $\epsilon = 0.4$		L_2 $\epsilon = 3$		L_1 $\epsilon = 18$		L_0 $\epsilon = 15$		adv. frames	
	seen		unseen		unseen		unseen		unseen		unseen	
	FPR↓	RErr↓	FPR↓	RErr↓	FPR↓	RErr↓	FPR↓	RErr↓	FPR↓	RErr↓	FPR↓	RErr↓
Normal	99.3	100.0	99.3	100.0	99.3	100.0	99.3	100.0	91.6	92.3	87.0	87.7
AT-50%	1.0	1.7	99.3	100.0	80.7	81.5	23.8	24.6	23.0	23.9	72.9	73.7
AT-100%	1.0	1.7	99.2	100.0	83.9	84.8	20.2	21.3	12.9	13.9	61.3	62.3
CCAT	6.9	7.4	11.4	11.9	0.0	0.3	1.3	1.8	14.2	14.8	0.0	0.2
* MSD	32.1	34.3	96.7	98.9	57.0	59.2	53.7	55.9	64.2	66.4	6.6	8.8
* TRADES	3.4	4.0	99.3	99.9	43.6	44.3	8.2	9.0	34.6	35.5	0.0	0.2
SVHN: FPR and RErr in % for $\tau@99\%$ TPR												
	L_∞ $\epsilon = 0.03$		L_∞ $\epsilon = 0.06$		L_2 $\epsilon = 2$		L_1 $\epsilon = 24$		L_0 $\epsilon = 10$		adv. frames	
	seen		unseen		unseen		unseen		unseen		unseen	
	FPR↓	RErr↓	FPR↓	RErr↓	FPR↓	RErr↓	FPR↓	RErr↓	FPR↓	RErr↓	FPR↓	RErr↓
Normal	95.8	99.9	95.9	100.0	95.9	100.0	95.9	100.0	79.6	83.7	74.6	78.7
AT-50%	52.3	56.0	84.7	88.4	95.7	99.4	95.8	99.5	70.0	73.6	30.0	33.6
AT-100%	42.1	48.3	80.9	87.1	93.3	99.5	93.6	99.8	83.1	89.4	19.9	26.0
CCAT	35.5	39.1	49.5	53.1	25.4	29.0	28.1	31.7	0.4	3.5	1.0	3.7
* LID	87.1	91	89.2	93.1	96.1	92.2	85.7	90	37.6	41.6	85.1	89.8
* MAHA	68.6	73	75.2	79.5	73.2	78.1	63.2	67.5	36.9	41.5	6.3	9.9
CIFAR10: FPR and RErr in % for $\tau@99\%$ TPR												
	L_∞ $\epsilon = 0.03$		L_∞ $\epsilon = 0.06$		L_2 $\epsilon = 2$		L_1 $\epsilon = 24$		L_0 $\epsilon = 10$		adv. frames	
	seen		unseen		unseen		unseen		unseen		unseen	
	FPR↓	RErr↓	FPR↓	RErr↓	FPR↓	RErr↓	FPR↓	RErr↓	FPR↓	RErr↓	FPR↓	RErr↓
Normal	93.0	100.0	93.0	100.0	93.0	100.0	93.0	100.0	77.7	84.7	89.7	96.7
AT-50%	47.6	62.7	78.6	93.7	83.3	98.4	83.3	98.4	59.3	74.4	63.6	78.7
AT-100%	42.3	59.9	72.7	90.3	80.7	98.3	80.4	98.0	54.7	72.3	62.0	79.6
CCAT	59.9	68.4	83.9	92.4	43.7	52.2	50.3	58.8	14.4	23.0	57.4	66.1
* MSD	35.3	53.2	71.5	89.4	70.6	88.5	50.7	68.6	21.4	39.2	64.7	82.6
* TRADES	28.9	43.5	66.4	81.0	56.3	70.9	82.3	96.9	22.3	36.9	57.5	72.1
* AT-Madry	33.8	45.1	73.2	84.5	87.4	98.7	86.5	97.8	31.0	42.3	62.0	73.3
* LID	92.7	99	92.9	99.2	64	70.6	82.9	89.4	40.6	47	59.9	66.1
* MAHA	87.7	94.1	89	95.3	84.2	90.6	91.3	97.6	43.5	49.8	64.1	70

Table 5: Main Results: FPR for 99%TPR. For 99%TPR, we report confidence-thresholded RErr and FPR for the results from the main paper. We emphasize that only PGD-CE and PGD-Conf were used against LID and MAHA. In general, the observations of the main paper can be confirmed considering FPR. Due to the poor Err of AT, MSD or TRADES on Cifar10, these methods benefit most from considering FPR instead of (confidence-thresholded) RErr. * Pre-trained models with different architectures.

even when using $T = 2000$ iterations. Similar significant drops are observed without backtracking. These observations generalize to MNIST and Cifar10.

Training: Tab. 4 reports results for CCAT with different values for ρ . We note that ρ controls the (speed of the) transition from (correct) one-hot distribution to uniform distribution depending on the distance of adversarial example to the corresponding original training example. Here, higher ρ results in a sharper (i.e., faster) transition from one-hot to uniform distribution. It is also important to note that the power transition does not preserve a bias towards the true label, i.e., for the maximum possible perturbation ($\|\delta\|_\infty = \epsilon$), the network is forced to predict a purely uniform distribution. As can be seen, both on SVHN and Cifar10, higher ρ usually results in better robustness. Thus, for the main paper, we chose $\rho = 10$. Only on SVHN, $\rho = 6$ of $\rho = 12$ perform slightly better. However, we found that $\rho = 10$ generalizes better to previously unseen attacks.

Confidence-Calibrated Adversarial Training

MNIST: FPR and confidence-thresholded RErr in % for $\tau@98\%$TPR															
	L_∞ $\epsilon = 0.3$		L_∞ $\epsilon = 0.4$		L_2 $\epsilon = 3$		L_1 $\epsilon = 18$		L_0 $\epsilon = 15$		adv. frames		distal	corr. MNIST-C	
	seen		unseen		unseen		unseen		unseen		unseen		unseen	unseen	
	FPR↓	RErr↓	FPR↓	RErr↓	FPR↓	RErr↓	FPR↓	RErr↓	FPR↓	RErr↓	FPR↓	RErr↓	FPR↓	Err↓	
Normal	99.3	100.0	99.3	100.0	99.3	100.0	99.3	100.0	87.3	88.1	79.8	80.5	100.0	31.0	
AT-50%	0.5	0.8	99.3	100.0	66.7	67.9	16.3	17.5	16.1	17.2	61.3	62.5	100.0	12.3	
AT-100%	0.6	1.3	99.2	100.0	77.3	78.3	16.9	18.0	9.2	10.2	52.6	53.7	100.0	15.4	
CCAT	5.2	5.7	8.8	9.3	0.0	0.2	0.6	0.9	7.6	8.1	0.0	0.1	0.0	5.3	
* MSD	28.8	31.0	96.6	98.8	53.9	56.2	51.3	53.5	61.5	63.7	4.4	6.6	100.0	5.6	
* TRADES	1.2	1.9	99.1	99.7	31.6	32.6	4.3	5.1	28.0	29.7	0.0	0.1	100.0	5.7	

SVHN: FPR and confidence-thresholded RErr in % for $\tau@98\%$TPR															
	L_∞ $\epsilon = 0.03$		L_∞ $\epsilon = 0.06$		L_2 $\epsilon = 2$		L_1 $\epsilon = 24$		L_0 $\epsilon = 10$		adv. frames		distal		
	seen		unseen		unseen		unseen		unseen		unseen		unseen		
	FPR↓	RErr↓	FPR↓	RErr↓	FPR↓	RErr↓	FPR↓	RErr↓	FPR↓	RErr↓	FPR↓	RErr↓	FPR↓	Err↓	
Normal	95.7	99.8	95.9	100.0	95.9	100.0	95.9	100.0	72.7	76.8	72.4	76.5	87.1		
AT-50%	50.0	53.7	83.4	87.1	95.5	99.2	95.7	99.4	54.0	57.9	26.8	30.6	86.3		
AT-100%	42.1	48.3	80.9	87.1	93.3	99.5	93.6	99.8	82.2	88.8	19.3	25.1	81.0		
CCAT	34.0	37.6	40.5	44.1	20.3	23.9	25.0	28.6	0.2	2.6	0.1	2.2	0.0		

CIFAR10: FPR and confidence-thresholded RErr in % for $\tau@98\%$TPR															
	L_∞ $\epsilon = 0.03$		L_∞ $\epsilon = 0.06$		L_2 $\epsilon = 2$		L_1 $\epsilon = 24$		L_0 $\epsilon = 10$		adv. frames		corr.	corr. CIFAR10-C	
	seen		unseen		unseen		unseen		unseen		unseen		unseen	unseen	
	FPR↓	RErr↓	FPR↓	RErr↓	FPR↓	RErr↓	FPR↓	RErr↓	FPR↓	RErr↓	FPR↓	RErr↓	FPR↓	Err↓	
Normal	93.0	100.0	93.0	100.0	93.0	100.0	93.0	100.0	70.1	77.1	89.6	96.6	83.3	11.4	
AT-50%	47.6	62.7	78.6	93.7	83.3	98.4	83.3	98.4	57.2	72.4	63.6	78.7	75.0	15.1	
AT-100%	42.1	59.7	72.7	90.3	80.7	98.3	80.4	98.0	52.1	70.0	62.0	79.6	72.5	17.8	
CCAT	59.4	67.9	83.5	92.0	43.3	51.8	50.0	58.5	11.7	20.3	56.4	65.1	0.0	8.1	
* MSD	35.1	53.0	71.5	89.4	69.9	87.8	50.6	68.5	17.8	35.8	64.7	82.6	76.7	17.1	
* TRADES	28.9	43.5	66.4	81.0	56.2	70.8	82.3	96.9	21.9	36.4	57.4	72.0	76.2	14.1	
* AT-Madry	33.6	44.9	73.2	84.5	87.4	98.7	86.5	97.8	30.8	42.0	61.9	73.2	78.5	11.4	

Table 6: Main Results: Generalizable Robustness for 98%TPR. While reporting results for 99%TPR in the main paper, reducing the TPR requirement for confidence-thresholding to 98%TPR generally improves results, but only slightly. We report FPR and confidence-thresholded RErr for 98%TPR. For MNIST-C and Cifar10-C, we report mean Err across all corruptions. L_∞ attacks with $\epsilon=0.3$ on MNIST and $\epsilon = 0.03$ on SVHN/Cifar10 were used for training (seen). All other attacks were not used during training (unseen). * Pre-trained models with different architectures.

C.6. Analysis

Confidence Histograms: For further analysis, Fig. 6 shows confidence histograms for AT and CCAT on MNIST and Cifar10. The confidence histograms for CCAT reflect the expected behavior: adversarial examples are mostly successful in changing the label, which is supported by high RErr values for confidence threshold $\tau = 0$, but their confidence is pushed towards uniform distributions. For AT, in contrast, successful adversarial examples – fewer in total – generally obtain high confidence. As a result, while confidence thresholding generally benefits AT, the improvement is not as significant as for CCAT.

Confidence Along Adversarial Directions: In Fig. 8, we plot the probabilities for all ten classes along an adversarial direction. We note that these directions do not necessarily correspond to successful or high-confidence adversarial examples. Instead, we chose the first 10 test examples on SVHN and Cifar10. The adversarial examples were obtained using our L_∞ PGD-Conf attack with $T = 1000$ iterations and zero initialization for $\epsilon = 0.03$. For AT, we usually observe a change in predictions along these directions; some occur within $\|\delta\|_\infty \leq \epsilon$, corresponding to successful adversarial examples (within ϵ), some occur for $\|\delta\|_\infty > \epsilon$, corresponding to unsuccessful adversarial examples (within ϵ). However, AT always assigns high confidence. Thus, when allowing larger adversarial perturbations at test time, robustness of AT reduces significantly. For CCAT, in contrast, there are only few such cases; more often, the model achieves a near uniform prediction for small

Confidence-Calibrated Adversarial Training

MNIST: FPR and confidence-thresholded RErr in % for $\tau@95\%TPR$														
	L_∞ $\epsilon = 0.3$		L_∞ $\epsilon = 0.4$		L_2 $\epsilon = 3$		L_1 $\epsilon = 18$		L_0 $\epsilon = 15$		adv. frames		distal	corr. MNIST-C
	seen		unseen		unseen		unseen		unseen		unseen		unseen	unseen
	FPR↓	RErr↓	FPR↓	RErr↓	FPR↓	RErr↓	FPR↓	RErr↓	FPR↓	RErr↓	FPR↓	RErr↓	FPR↓	Err↓
Normal	99.3	100.0	99.3	100.0	99.3	100.0	99.0	99.7	75.6	76.7	65.9	67.0	100.0	27.5
AT-50%	0.2	0.4	99.3	100.0	54.6	56.7	12.3	13.7	11.1	12.3	47.3	49.2	100.0	8.6
AT-100%	0.2	0.9	99.2	100.0	63.9	65.6	10.7	12.4	3.6	4.4	35.0	37.2	100.0	10.5
CCAT	3.1	3.7	5.7	6.3	0.0	0.1	0.0	0.1	2.0	2.2	0.0	0.1	0.0	5.5
* MSD	22.0	24.6	95.0	97.2	44.0	46.8	42.1	44.6	54.5	57.3	2.3	4.4	100.0	4.4
* TRADES	0.6	1.0	98.1	98.8	16.5	18.3	2.1	2.7	21.4	24.0	0.0	0.0	100.0	3.2

SVHN: FPR and confidence-thresholded RErr in % for $\tau@95\%TPR$														
	L_∞ $\epsilon = 0.03$		L_∞ $\epsilon = 0.06$		L_2 $\epsilon = 2$		L_1 $\epsilon = 24$		L_0 $\epsilon = 10$		adv. frames		distal	
	seen		unseen		unseen		unseen		unseen		unseen		unseen	
	FPR↓	RErr↓	FPR↓	RErr↓	FPR↓	RErr↓	FPR↓	RErr↓	FPR↓	RErr↓	FPR↓	RErr↓	FPR↓	
Normal	95.6	99.7	95.9	100.0	95.9	100.0	95.9	100.0	65.3	69.5	66.8	71.1	87.1	
AT-50%	45.5	49.2	79.7	83.4	95.4	99.1	95.5	99.2	34.8	38.9	21.5	25.5	59.3	
AT-100%	40.5	46.9	80.9	87.1	93.3	99.5	93.6	99.8	78.5	85.5	15.9	21.7	75.1	
CCAT	32.8	36.5	38.6	42.2	16.5	20.3	21.1	24.9	0.0	1.2	0.0	1.2	0.0	

CIFAR10: FPR and confidence-thresholded RErr in % for $\tau@95\%TPR$														
	L_∞ $\epsilon = 0.03$		L_∞ $\epsilon = 0.06$		L_2 $\epsilon = 2$		L_1 $\epsilon = 24$		L_0 $\epsilon = 10$		adv. frames		corr.	corr. CIFAR10-C
	seen		unseen		unseen		unseen		unseen		unseen		unseen	unseen
	FPR↓	RErr↓	FPR↓	RErr↓	FPR↓	RErr↓	FPR↓	RErr↓	FPR↓	RErr↓	FPR↓	RErr↓	FPR↓	Err↓
Normal	93.0	100.0	93.0	100.0	93.0	100.0	93.0	100.0	52.0	59.0	88.8	95.9	83.3	7.7
AT-50%	46.6	61.7	78.6	93.7	83.3	98.4	83.3	98.4	43.9	59.6	62.8	77.9	75.0	12.1
AT-100%	41.3	59.1	72.7	90.3	80.6	98.2	80.4	98.0	47.2	65.3	62.0	79.7	72.5	15.6
CCAT	57.4	66.0	80.8	89.3	39.7	48.2	48.9	57.4	3.6	11.1	50.8	59.7	0.0	6.0
* MSD	32.8	50.9	71.5	89.4	67.7	85.6	49.1	67.3	11.4	28.4	64.2	82.2	76.7	13.7
* TRADES	26.5	41.3	66.1	80.7	53.9	68.5	82.3	96.9	17.6	32.0	56.4	71.1	76.2	10.7
* AT-Madry	32.4	43.9	73.2	84.5	87.4	98.7	86.5	97.8	28.6	40.1	61.5	72.8	78.5	9.1

Table 7: Main Results: Generalizable Robustness for 95%TPR. We report FPR and RErr for 95%TPR, in comparison with 98% in Tab. 6 and 99% in the main paper. For MNIST-C and Cifar10-C, we report mean Err across all corruptions. L_∞ attacks with $\epsilon=0.3$ on MNIST and $\epsilon = 0.03$ on SVHN/Cifar10 **seen** during training; all other attacks **unseen** during training. Results improve slightly in comparison with 98%TPR. However, the improvements are rather small and do not justify the significantly increased fraction of “thrown away” (correctly classified) clean examples. * Pre-trained models with different architectures.

$\|\delta\|_\infty$ and extrapolates this behavior beyond the ϵ -ball used for training. On SVHN, this behavior successfully allows to generalize the robustness to larger adversarial perturbations. Furthermore, these plots illustrate why using more iterations at test time, and using techniques such as momentum and backtracking, are necessary to find adversarial examples as the objective becomes more complex compared to AT.

Confidence Along Interpolation: In Fig. 9, on MNIST, we additionally illustrate the advantage of CCAT with respect to the toy example in Proposition 2. Here, we consider the case where the ϵ -balls of two training or test examples (in different classes) overlap. As we show in Proposition 2, adversarial training is not able to handle such cases, resulting in the trade-off between accuracy in robustness reported in the literature (Tsipras et al., 2018; Stutz et al., 2019; Raghunathan et al., 2019; Zhang et al., 2019). This is because adversarial training enforces high-confidence predictions on both ϵ -balls (corresponding to different classes), resulting in an obvious conflict. CCAT, in contrast, enforces uniform predictions throughout the largest parts of both ϵ -balls, resolving the conflict.

	MNIST:		SVHN:		CIFAR10:		CIFAR10:	
	all unseen		all unseen		all unseen		unseen except L_∞ with $\epsilon=0.06$	
	FPR↓	RErr ↓	FPR↓	RErr ↓	FPR↓	RErr ↓	FPR↓	RErr ↓
Normal	99.3	100.0	95.9	100.0	93.0	100.0	93.0	100.0
AT-50%	99.3	100.0	96.2	99.9	84.1	99.2	84.1	99.2
AT-100%	99.2	100.0	93.7	99.9	81.0	98.6	81.1	98.7
CCAT	23.4	23.9	57.5	61.1	86.3	94.8	69.1	77.6
* MSD	97.0	99.2	–	–	76.2	94.1	75.6	93.5
* TRADES	99.3	99.9	–	–	82.8	97.4	82.7	97.3
* AT-Madry	–	–	–	–	87.6	98.9	87.6	98.9

Table 8: Worst-Case Results Across Unseen Attacks. We report the (per-example) worst-case, confidence-thresholded RErr and FPR across **all** unseen attacks on MNIST, SVHN and Cifar10. On Cifar10, we additionally present results for all attacks except L_∞ adversarial examples with larger $\epsilon = 0.06$ (indicated in blue). CCAT is able to outperform all baselines, including MSD and TRADES, significantly on MNIST and SVHN. On Cifar10, CCAT performs poorly on L_∞ adversarial examples with larger $\epsilon = 0.06$. However, excluding these adversarial examples, CCAT also outperforms all baselines on Cifar10. * Pre-trained models with different architectures.

C.7. Results

Main Results for 98% and 95% TPR: Tab. 6 reports our main results requiring only 98%TPR; Tab. 7 shows results for 95%TPR. This implies, that compared to 99%TPR, up to 1% (or 4%) more correctly classified test examples can be rejected, increasing the confidence threshold and potentially improving robustness. For relatively simple tasks such as MNIST and SVHN, where Err is low, this is a significant “sacrifice”. However, as can be seen, robustness in terms of RErr only improves slightly. We found that the same holds for 95%TPR, however, rejecting more than 2% of correctly classified examples seems prohibitive large for the considered datasets.

Worst-Case Across Unseen Attacks: Tab. 8 reports *per-example* worst-case RErr and FPR for 99%TPR considering **all** **unseen** attacks. On MNIST and SVHN, RErr increases to nearly 100% for AT, both AT-50% and AT-100%. CCAT, in contrast, is able to achieve considerably lower RErr: 23.9% on MNIST and 61.1% on SVHN. Only on Cifar10, CCAT does not result in a significant improvement; all methods, including related work such as MSD and TRADES yield RErr of 94% or higher. However, this is mainly due to the poor performance of CCAT against large L_∞ adversarial examples with $\epsilon = 0.06$. Excluding these adversarial examples (right most table, indicated in blue) shows that RErr improves to 77.6% for CCAT, while RErr for the remaining methods remains nearly unchanged. Overall, these experiments emphasize that CCAT is able to generalize robustness to previously unseen attacks.

Per-Attack Results: In Tab. 9 to 19, we break down our main results regarding all used L_p attacks for $p \in \{\infty, 2, 1, 0\}$. For simplicity we focus on PGD-CE and PGD-Conf while reporting the used black-box attacks together, i.e., taking the per-example worst-case adversarial examples across all black-box attacks. For comparison, we also include the area under the ROC curve (ROC AUC), non-thresholded Err and non-thresholded RErr. On MNIST, where AT performs very well in practice, it is striking that for $4/3\epsilon = 0.4$ even black-box attacks are able to reduce robustness completely, resulting in high RErr. This observation also transfers to SVHN and Cifar10. For CCAT, black-box attacks are only effective on Cifar10, where they result in roughly 87% RErr with $\tau@99\%$ TPR. For the L_2 , L_1 and L_0 attacks we can make similar observations. Across all L_p norms, it can also be seen that PGD-CE performs significantly worse against our CCAT compared to AT, which shows that it is essential to optimize the right objective to evaluate the robustness of defenses and adversarially trained models, i.e., maximize confidence against CCAT.

Results on Corrupted MNIST/Cifar10: We also conducted experiments on MNIST-C (Mu & Gilmer, 2019) and Cifar10-C (Hendrycks & Dietterich, 2019a). These datasets are variants of MNIST and Cifar10 that contain common perturbations of the original images obtained from various types of noise, blur or transformations; examples include zoom or motion blur, Gaussian and shot noise, rotations, translations and shear. Tab. 20 to 23 presents the per-corruption results on MNIST-C and Cifar10-C, respectively. Here, **all** includes all corruptions and **mean** reports the average results across all corruptions. We

Confidence-Calibrated Adversarial Training

MNIST: Supplementary Results for L_∞ Adversarial Examples								
Attack	Training	Detection Setting					Standard Setting	
		ROC AUC	FPR in %	Err in %	RErr in %	τ	Err in %	RErr in %
Worst-Case ($L_\infty, \epsilon = 0.30$)	Normal	0.34	99.3	0.1	100.0	0.98	0.4	100.0
	AT-50%	0.97	1.0	0.0	1.0	1.00	0.5	7.2
	AT-100%	0.98	1.0	0.0	1.0	1.00	0.5	7.1
	CCAT	0.99	6.9	0.2	7.1	0.85	0.4	48.9
	MSD	0.86	32.1	0.9	33.9	0.51	1.8	38.0
	TRADES	0.96	3.4	0.1	3.5	0.92	0.5	9.5
PGD Conf ($L_\infty, \epsilon = 0.30$)	Normal	0.34	99.3	0.1	100.0	0.98	0.4	100.0
	AT-50%	0.97	0.4	0.0	0.4	1.00	0.5	5.6
	AT-100%	0.98	0.6	0.0	0.6	1.00	0.5	5.4
	CCAT	0.98	6.9	0.2	7.1	0.85	0.4	45.9
	MSD	0.87	28.7	0.9	30.5	0.51	1.8	34.6
	TRADES	0.96	1.6	0.1	1.6	0.92	0.5	7.0
PGD CE ($L_\infty, \epsilon = 0.30$)	Normal	0.34	99.3	0.1	100.0	0.98	0.4	100.0
	AT-50%	0.97	0.8	0.0	0.8	1.00	0.5	6.7
	AT-100%	0.98	0.7	0.0	0.7	1.00	0.5	6.3
	CCAT	1.00	0.0	0.2	0.2	0.85	0.4	100.0
	MSD	0.88	28.0	0.9	29.8	0.51	1.8	37.6
	TRADES	0.96	2.8	0.1	2.9	0.92	0.5	8.6
Black-Box ($L_\infty, \epsilon = 0.30$)	Normal	0.34	99.3	0.1	100.0	0.98	0.4	100.0
	AT-50%	0.98	1.0	0.0	1.0	1.00	0.5	7.2
	AT-100%	0.98	1.0	0.0	1.0	1.00	0.5	6.9
	CCAT	1.00	0.1	0.2	0.3	0.85	0.4	82.4
	MSD	0.88	27.7	0.9	29.5	0.51	1.8	35.9
	TRADES	0.96	3.2	0.1	3.3	0.92	0.5	9.1
Worst-Case ($L_\infty, \epsilon = 0.40$)	Normal	0.34	99.3	0.1	100.0	0.98	0.4	100.0
	AT-50%	0.20	99.3	0.0	100.0	1.00	0.5	100.0
	AT-100%	0.27	99.2	0.0	100.0	1.00	0.5	100.0
	CCAT	0.97	11.4	0.2	11.6	0.85	0.4	69.3
	MSD	0.66	96.7	0.9	98.9	0.51	1.8	99.8
	TRADES	0.56	99.3	0.1	99.9	0.92	0.5	100.0
PGD Conf ($L_\infty, \epsilon = 0.40$)	Normal	0.34	99.3	0.1	100.0	0.98	0.4	100.0
	AT-50%	0.36	97.1	0.0	97.8	1.00	0.5	99.8
	AT-100%	0.81	46.5	0.0	46.9	1.00	0.5	77.0
	CCAT	0.97	11.4	0.2	11.6	0.85	0.4	58.9
	MSD	0.73	89.3	0.9	91.4	0.51	1.8	93.3
	TRADES	0.76	87.0	0.1	87.5	0.92	0.5	96.9
PGD CE ($L_\infty, \epsilon = 0.40$)	Normal	0.34	99.3	0.1	100.0	0.98	0.4	100.0
	AT-50%	0.20	99.3	0.0	100.0	1.00	0.5	100.0
	AT-100%	0.27	99.2	0.0	100.0	1.00	0.5	100.0
	CCAT	1.00	0.0	0.2	0.2	0.85	0.4	100.0
	MSD	0.69	95.6	0.9	97.8	0.51	1.8	99.7
	TRADES	0.58	99.3	0.1	99.9	0.92	0.5	100.0
Black-Box ($L_\infty, \epsilon = 0.40$)	Normal	0.34	99.3	0.1	100.0	0.98	0.4	100.0
	AT-50%	0.23	99.3	0.0	100.0	1.00	0.5	100.0
	AT-100%	0.27	99.2	0.0	100.0	1.00	0.5	100.0
	CCAT	1.00	0.2	0.2	0.4	0.85	0.4	91.2
	MSD	0.76	92.5	0.9	94.7	0.51	1.8	99.3
	TRADES	0.78	95.4	0.1	96.0	0.92	0.5	99.8

Table 9: Per-Attack Results on MNIST, Part I (L_∞). Per-attack results considering PGD-CE, as in (Madry et al., 2018), our PGD-Conf and the remaining black-box attacks for the L_∞ threat model. The used ϵ values are reported in the left-most column. For the black-box attacks, we report the per-example worst-case across all black-box attacks. In addition to FPR and RErr, we include ROC AUC, Err as well as Err and RErr in the standard, non-thresholded setting, as reference.

note that, due to the thresholding, different numbers of corrupted examples are left after detection for different corruptions. Thus, the distinction between `all` and `mean` is meaningful. Striking is the performance of CCAT on noise corruptions such as `gaussian_noise` or `shot_noise`. Here, CCAT is able to reject 100% of the corrupted examples, resulting in a thresholded Err of 0%. This is in stark contrast to AT, exhibiting a Err of roughly 15% after rejection on `Cifar10-C`. On the remaining corruptions, CCAT is able to perform slightly better than AT, which is often due to higher detection rate, i.e., higher ROC AUC. On, `Cifar10`, the generally lower Err of CCAT also contributes to the results. Overall, this illustrates that CCAT is able to preserve the inductive bias of predicting near-uniform distribution on noise similar to L_∞ adversarial examples as seen during training.

Confidence-Calibrated Adversarial Training

MNIST: Supplementary Results for L_2 Adversarial Examples									
Attack	Training	Detection Setting $\tau@99\%TPR$					Standard Setting $\tau=0$		
		ROC AUC	FPR in %	Err in %	RErr in %	τ	Err in %	RErr in %	
Worst-Case ($L_2, \epsilon = 1.5$)	Normal	0.39	98.9	0.1	99.6	0.98	0.4	100.0	
	AT-50%	0.96	2.3	0.0	2.4	1.00	0.5	13.6	
	AT-100%	0.96	2.6	0.0	2.7	1.00	0.5	12.0	
	CCAT	1.00	0.0	0.2	0.2	0.85	0.4	6.7	
	MSD	0.94	7.9	0.9	9.6	0.51	1.8	15.2	
	TRADES	0.96	2.2	0.1	2.3	0.92	0.5	8.5	
PGD Conf ($L_2, \epsilon = 1.5$)	Normal	0.56	83.3	0.1	83.9	0.98	0.4	91.6	
	AT-50%	0.99	0.2	0.0	0.2	1.00	0.5	3.2	
	AT-100%	0.99	0.1	0.0	0.1	1.00	0.5	2.5	
	CCAT	1.00	0.0	0.2	0.2	0.85	0.4	5.5	
	MSD	0.96	2.0	0.9	3.7	0.51	1.8	6.5	
	TRADES	0.99	0.2	0.1	0.2	0.92	0.5	3.6	
PGD CE ($L_2, \epsilon = 1.5$)	Normal	0.39	98.8	0.1	99.5	0.98	0.4	99.9	
	AT-50%	0.96	1.9	0.0	2.0	1.00	0.5	10.2	
	AT-100%	0.96	1.9	0.0	2.0	1.00	0.5	10.0	
	CCAT	1.00	0.0	0.2	0.2	0.85	0.4	100.0	
	MSD	0.94	7.5	0.9	9.2	0.51	1.8	15.8	
	TRADES	0.96	2.2	0.1	2.3	0.92	0.5	8.2	
Black-Box ($L_2, \epsilon = 1.5$)	Normal	0.55	91.0	0.1	91.7	0.98	0.4	97.4	
	AT-50%	0.97	0.8	0.0	0.8	1.00	0.5	8.1	
	AT-100%	0.98	0.9	0.0	0.9	1.00	0.5	6.8	
	CCAT	1.00	0.0	0.2	0.2	0.85	0.4	84.8	
	MSD	0.95	3.6	0.9	5.3	0.51	1.8	8.6	
	TRADES	0.99	0.3	0.1	0.3	0.92	0.5	4.4	
Worst-Case ($L_2, \epsilon = 3$)	Normal	0.34	99.3	0.1	100.0	0.98	0.4	100.0	
	AT-50%	0.73	80.7	0.0	81.4	1.00	0.5	98.8	
	AT-100%	0.66	83.9	0.0	84.7	1.00	0.5	98.5	
	CCAT	1.00	0.0	0.2	0.2	0.85	0.4	15.5	
	MSD	0.81	57.0	0.9	59.0	0.51	1.8	67.6	
	TRADES	0.90	43.6	0.1	44.0	0.92	0.5	69.9	
PGD Conf ($L_2, \epsilon = 3$)	Normal	0.41	93.2	0.1	93.9	0.98	0.4	96.9	
	AT-50%	0.98	0.2	0.0	0.2	1.00	0.5	3.4	
	AT-100%	0.99	0.1	0.0	0.1	1.00	0.5	2.7	
	CCAT	1.00	0.0	0.2	0.2	0.85	0.4	4.9	
	MSD	0.96	2.3	0.9	4.0	0.51	1.8	7.3	
	TRADES	0.98	0.4	0.1	0.4	0.92	0.5	3.8	
PGD CE ($L_2, \epsilon = 3$)	Normal	0.34	99.3	0.1	100.0	0.98	0.4	100.0	
	AT-50%	0.93	11.3	0.0	11.5	1.00	0.5	29.2	
	AT-100%	0.92	9.3	0.0	9.5	1.00	0.5	24.5	
	CCAT	1.00	0.0	0.2	0.2	0.85	0.4	100.0	
	MSD	0.82	55.7	0.9	57.8	0.51	1.8	67.7	
	TRADES	0.95	5.3	0.1	5.4	0.92	0.5	15.9	
Black-Box ($L_2, \epsilon = 3$)	Normal	0.35	99.3	0.1	100.0	0.98	0.4	100.0	
	AT-50%	0.73	79.5	0.0	80.1	1.00	0.5	98.7	
	AT-100%	0.67	83.0	0.0	83.8	1.00	0.5	98.1	
	CCAT	1.00	0.0	0.2	0.2	0.85	0.4	88.4	
	MSD	0.88	28.6	0.9	30.4	0.51	1.8	37.4	
	TRADES	0.91	42.6	0.1	43.0	0.92	0.5	69.1	

Table 10: Per-Attack Results on MNIST, Part II (L_2). Per-attack results considering PGD-CE, as in (Madry et al., 2018), our PGD-Conf and the remaining black-box attacks for the L_2 threat model. The used ϵ values are reported in the left-most column. For the black-box attacks, we report the per-example worst-case across all black-box attacks. In addition to FPR and RErr we include ROC AUC, Err as well as Err and RErr in the standard, non-thresholded setting, as reference.

Confidence-Calibrated Adversarial Training

MNIST: Supplementary Results for L_1 Adversarial Examples									
Attack	Training	Detection Setting $\tau@99\%TPR$					Standard Setting $\tau=0$		
		ROC AUC	FPR in %	Err in %	RErr in %	τ	Err in %	RErr in %	
Worst-Case ($L_1, \epsilon = 12$)	Normal	0.44	98.9	0.1	99.6	0.98	0.4	100.0	
	AT-50%	0.93	8.6	0.0	8.8	1.00	0.5	26.3	
	AT-100%	0.91	8.2	0.0	8.4	1.00	0.5	23.6	
	CCAT	1.00	0.8	0.2	1.0	0.85	0.4	16.5	
	MSD	0.87	25.5	0.9	27.3	0.51	1.8	32.3	
	TRADES	0.96	2.7	0.1	2.8	0.92	0.5	9.5	
PGD Conf ($L_1, \epsilon = 12$)	Normal	0.45	98.9	0.1	99.6	0.98	0.4	100.0	
	AT-50%	0.92	6.3	0.0	6.4	1.00	0.5	19.3	
	AT-100%	0.90	5.8	0.0	6.0	1.00	0.5	16.7	
	CCAT	1.00	0.7	0.2	0.9	0.85	0.4	14.2	
	MSD	0.87	24.8	0.9	26.6	0.51	1.8	31.7	
	TRADES	0.96	1.8	0.1	1.9	0.92	0.5	6.7	
PGD CE ($L_1, \epsilon = 12$)	Normal	0.58	92.4	0.1	93.1	0.98	0.4	96.5	
	AT-50%	0.94	6.4	0.0	6.6	1.00	0.5	20.2	
	AT-100%	0.92	5.9	0.0	6.1	1.00	0.5	17.3	
	CCAT	1.00	0.0	0.2	0.2	0.85	0.4	100.0	
	MSD	0.92	12.5	0.9	14.3	0.51	1.8	21.8	
	TRADES	0.96	2.4	0.1	2.5	0.92	0.5	8.8	
Black-Box ($L_1, \epsilon = 12$)	Normal	0.98	3.3	0.1	3.5	0.98	0.4	10.8	
	AT-50%	0.96	0.7	0.0	0.7	1.00	0.5	4.4	
	AT-100%	0.97	0.8	0.0	0.8	1.00	0.5	5.3	
	CCAT	1.00	0.1	0.2	0.3	0.85	0.4	8.8	
	MSD	0.96	0.4	0.9	2.1	0.51	1.8	3.2	
	TRADES	0.98	0.1	0.1	0.1	0.92	0.5	1.4	
Worst-Case ($L_1, \epsilon = 18$)	Normal	0.36	99.3	0.1	100.0	0.98	0.4	100.0	
	AT-50%	0.88	23.8	0.0	24.1	1.00	0.5	50.4	
	AT-100%	0.88	20.2	0.0	20.7	1.00	0.5	43.8	
	CCAT	1.00	1.3	0.2	1.5	0.85	0.4	22.0	
	MSD	0.81	53.7	0.9	55.6	0.51	1.8	60.8	
	TRADES	0.95	8.2	0.1	8.4	0.92	0.5	21.4	
PGD Conf ($L_1, \epsilon = 18$)	Normal	0.36	99.3	0.1	100.0	0.98	0.4	100.0	
	AT-50%	0.88	15.5	0.0	15.7	1.00	0.5	33.8	
	AT-100%	0.87	12.7	0.0	13.0	1.00	0.5	27.6	
	CCAT	1.00	0.8	0.2	1.0	0.85	0.4	15.5	
	MSD	0.81	53.1	0.9	55.0	0.51	1.8	60.3	
	TRADES	0.95	2.9	0.1	3.0	0.92	0.5	8.9	
PGD CE ($L_1, \epsilon = 18$)	Normal	0.45	97.7	0.1	98.4	0.98	0.4	98.8	
	AT-50%	0.90	17.0	0.0	17.3	1.00	0.5	37.6	
	AT-100%	0.90	11.7	0.0	12.0	1.00	0.5	29.8	
	CCAT	1.00	0.0	0.2	0.2	0.85	0.4	100.0	
	MSD	0.88	27.0	0.9	28.9	0.51	1.8	36.3	
	TRADES	0.95	4.8	0.1	4.9	0.92	0.5	13.6	
Black-Box ($L_1, \epsilon = 18$)	Normal	0.98	3.3	0.1	3.5	0.98	0.4	10.8	
	AT-50%	0.96	0.7	0.0	0.7	1.00	0.5	4.4	
	AT-100%	0.97	0.8	0.0	0.8	1.00	0.5	5.3	
	CCAT	1.00	0.1	0.2	0.3	0.85	0.4	8.8	
	MSD	0.96	0.4	0.9	2.1	0.51	1.8	3.2	
	TRADES	0.98	0.1	0.1	0.1	0.92	0.5	1.4	

Table 11: Per-Attack Results on MNIST, Part III (L_1). Per-attack results considering PGD-CE, as in (Madry et al., 2018), our PGD-Conf and the remaining black-box attacks for the L_1 threat model. The used ϵ values are reported in the left-most column. For the black-box attacks, we report the per-example worst-case across all black-box attacks. In addition to FPR and RErr we include ROC AUC, Err as well as Err and RErr in the standard, non-thresholded setting, as reference.

MNIST: Supplementary Results for L_0 Adversarial Examples and Adversarial Frames								
Attack	Training	Detection Setting $\tau@99\%TPR$					Standard Setting $\tau=0$	
		ROC AUC	FPR in %	Err in %	RErr in %	τ	Err in %	RErr in %
Worst-Case ($L_0, \epsilon = 15$)	Normal	0.63	91.6	0.1	92.3	0.98	0.4	99.1
	AT-50%	0.94	23.0	0.0	23.5	1.00	0.5	95.3
	AT-100%	0.98	12.9	0.0	13.3	1.00	0.5	94.3
	CCAT	0.99	14.2	0.2	14.5	0.85	0.4	83.5
	MSD	0.75	64.2	0.9	66.2	0.51	1.8	74.2
	TRADES	0.87	34.6	0.1	35.1	0.92	0.5	86.7
PGD Conf ($L_0, \epsilon = 15$)	Normal	0.69	84.4	0.1	85.0	0.98	0.4	92.7
	AT-50%	0.98	0.5	0.0	0.5	1.00	0.5	5.2
	AT-100%	0.98	0.3	0.0	0.3	1.00	0.5	3.6
	CCAT	0.99	3.1	0.2	3.3	0.85	0.4	13.7
	MSD	0.88	26.7	0.9	28.5	0.51	1.8	35.4
	TRADES	0.97	3.0	0.1	3.1	0.92	0.5	12.6
PGD CE ($L_0, \epsilon = 15$)	Normal	0.63	90.3	0.1	90.9	0.98	0.4	95.2
	AT-50%	0.98	2.3	0.0	2.4	1.00	0.5	17.7
	AT-100%	0.99	0.5	0.0	0.5	1.00	0.5	11.1
	CCAT	1.00	0.9	0.2	1.1	0.85	0.4	10.3
	MSD	0.88	30.5	0.9	32.3	0.51	1.8	41.5
	TRADES	0.95	10.7	0.1	11.0	0.92	0.5	27.9
Black-Box ($L_0, \epsilon = 15$)	Normal	0.97	18.3	0.1	18.5	0.98	0.4	98.6
	AT-50%	0.94	21.7	0.0	22.3	1.00	0.5	95.3
	AT-100%	0.98	12.9	0.0	13.3	1.00	0.5	94.3
	CCAT	0.99	12.5	0.2	12.8	0.85	0.4	84.4
	MSD	0.78	51.8	0.9	54.0	0.51	1.8	70.8
	TRADES	0.88	31.7	0.1	32.4	0.92	0.5	86.7
Adversarial Frames	Normal	0.69	87.0	0.1	87.6	0.98	0.4	94.6
	AT-50%	0.82	72.9	0.0	73.6	1.00	0.5	95.4
	AT-100%	0.86	61.3	0.0	62.0	1.00	0.5	93.9
	CCAT	1.00	0.0	0.2	0.2	0.85	0.4	95.4
	MSD	0.96	6.6	0.9	8.3	0.51	1.8	17.3
	TRADES	0.99	0.0	0.1	0.0	0.92	0.5	1.9

Table 12: Per-Attack Results on MNIST, Part IV (L_0 , Adversarial Frames). Per-attack results considering PGD-CE, as in (Madry et al., 2018), our PGD-Conf and the remaining black-box attacks for L_0 threat models and adversarial frames. The used ϵ values are reported in the left-most column. For the black-box attacks, we report the per-example worst-case across all black-box attacks. In addition to FPR and RErr we include ROC AUC, Err as well as Err and RErr in the standard, non-thresholded setting, as reference.

Confidence-Calibrated Adversarial Training

SVHN: Supplementary Results for L_∞ Adversarial Examples								
Attack	Training	Detection Setting $\tau@99\%TPR$					Standard Setting $\tau=0$	
		ROC AUC	FPR in %	Err in %	RErr in %	τ	Err in %	RErr in %
Worst-Case ($L_\infty, \epsilon = 0.03$)	Normal	0.17	95.8	2.6	99.9	0.78	3.6	100.0
	AT-50%	0.55	52.3	2.5	55.6	0.56	3.4	57.3
	AT-100%	0.73	42.1	4.6	47.5	0.27	5.9	48.4
	CCAT	0.70	35.5	2.1	38.5	0.60	2.9	97.8
PGD Conf ($L_\infty, \epsilon = 0.03$)	Normal	0.17	95.8	2.6	99.9	0.78	3.6	99.9
	AT-50%	0.55	51.6	2.5	54.9	0.56	3.4	56.9
	AT-100%	0.73	40.9	4.6	46.2	0.27	5.9	47.1
	CCAT	0.67	35.5	2.1	38.5	0.60	2.9	91.0
PGD CE ($L_\infty, \epsilon = 0.03$)	Normal	0.17	95.8	2.6	99.9	0.78	3.6	100.0
	AT-50%	0.68	40.0	2.5	43.2	0.56	3.4	50.7
	AT-100%	0.81	34.6	4.6	39.9	0.27	5.9	45.3
	CCAT	1.00	0.0	2.1	2.6	0.60	2.9	94.9
Black-Box ($L_\infty, \epsilon = 0.03$)	Normal	0.23	95.6	2.6	99.7	0.78	3.6	99.7
	AT-50%	0.95	27.7	2.5	30.8	0.56	3.4	46.2
	AT-100%	0.78	38.5	4.6	43.8	0.27	5.9	45.5
	CCAT	1.00	3.7	2.1	6.4	0.60	2.9	79.6
Worst-Case ($L_\infty, \epsilon = 0.06$)	Normal	0.16	95.9	2.6	100.0	0.78	3.6	100.0
	AT-50%	0.32	84.7	2.5	88.3	0.56	3.4	89.0
	AT-100%	0.38	80.9	4.6	86.9	0.27	5.9	87.1
	CCAT	0.64	49.5	2.1	52.6	0.60	2.9	99.9
PGD Conf ($L_\infty, \epsilon = 0.06$)	Normal	0.16	95.9	2.6	100.0	0.78	3.6	100.0
	AT-50%	0.31	81.1	2.5	84.7	0.56	3.4	86.1
	AT-100%	0.40	77.4	4.6	83.3	0.27	5.9	83.6
	CCAT	0.64	42.1	2.1	45.2	0.60	2.9	98.1
PGD CE ($L_\infty, \epsilon = 0.06$)	Normal	0.16	95.9	2.6	100.0	0.78	3.6	100.0
	AT-50%	0.61	84.4	2.5	88.0	0.56	3.4	88.9
	AT-100%	0.43	80.9	4.6	86.9	0.27	5.9	87.1
	CCAT	0.99	14.3	2.1	17.2	0.60	2.9	100.0
Black-Box ($L_\infty, \epsilon = 0.06$)	Normal	0.17	95.9	2.6	100.0	0.78	3.6	100.0
	AT-50%	0.78	78.9	2.5	82.4	0.56	3.4	84.0
	AT-100%	0.51	76.5	4.6	82.4	0.27	5.9	82.7
	CCAT	1.00	4.5	2.1	7.2	0.60	2.9	83.7

Table 13: Per-Attack Results on SVHN, Part I (L_∞). Per-attack results considering PGD-CE, as in (Madry et al., 2018), our PGD-Conf and the remaining black-box attacks for the L_∞ threat model. The used ϵ values are reported in the left-most column. For the black-box attacks, we report the per-example worst-case across all black-box attacks. In addition to FPR and RErr we include ROC AUC, Err as well as Err and RErr in the standard, non-thresholded setting, as reference.

Confidence-Calibrated Adversarial Training

SVHN: Supplementary Results for L_2 Adversarial Examples								
Attack	Training	Detection Setting $\tau@99\%TPR$					Standard Setting $\tau=0$	
		ROC AUC	FPR in %	Err in %	RErr in %	τ	Err in %	RErr in %
Worst-Case ($L_2, \epsilon = 0.5$)	Normal	0.27	93.3	2.6	97.4	0.78	3.6	97.7
	AT-50%	0.53	65.2	2.5	68.6	0.56	3.4	70.7
	AT-100%	0.67	60.1	4.6	65.8	0.27	5.9	66.3
	CCAT	0.87	17.2	2.1	20.0	0.60	2.9	63.3
PGD Conf ($L_2, \epsilon = 0.5$)	Normal	0.32	91.1	2.6	95.1	0.78	3.6	96.4
	AT-50%	0.56	57.5	2.5	60.8	0.56	3.4	62.9
	AT-100%	0.68	54.0	4.6	59.6	0.27	5.9	60.2
	CCAT	0.85	16.9	2.1	19.7	0.60	2.9	54.5
PGD CE ($L_2, \epsilon = 0.5$)	Normal	0.28	93.3	2.6	97.4	0.78	3.6	97.7
	AT-50%	0.57	63.1	2.5	66.5	0.56	3.4	70.1
	AT-100%	0.72	57.7	4.6	63.5	0.27	5.9	66.5
	CCAT	0.99	1.8	2.1	4.5	0.60	2.9	100.0
Black-Box ($L_2, \epsilon = 0.5$)	Normal	0.67	53.8	2.6	57.3	0.78	3.6	63.7
	AT-50%	0.99	3.0	2.5	5.9	0.56	3.4	13.8
	AT-100%	0.90	7.3	4.6	12.2	0.27	5.9	15.3
	CCAT	1.00	0.1	2.1	2.7	0.60	2.9	91.3
Worst-Case($L_2, \epsilon = 1$)	Normal	0.17	95.8	2.6	99.9	0.78	3.6	99.9
	AT-50%	0.26	88.4	2.5	92.0	0.56	3.4	92.4
	AT-100%	0.38	87.3	4.6	93.4	0.27	5.9	93.5
	CCAT	0.88	18.9	2.1	21.7	0.60	2.9	80.9
PGD Conf ($L_2, \epsilon = 1$)	Normal	0.22	95.4	2.6	99.5	0.78	3.6	99.6
	AT-50%	0.49	73.6	2.5	77.1	0.56	3.4	78.7
	AT-100%	0.48	75.5	4.6	81.4	0.27	5.9	81.7
	CCAT	0.88	18.6	2.1	21.4	0.60	2.9	74.6
PGD CE ($L_2, \epsilon = 1$)	Normal	0.17	95.8	2.6	99.9	0.78	3.6	99.9
	AT-50%	0.27	88.4	2.5	92.0	0.56	3.4	92.4
	AT-100%	0.39	87.3	4.6	93.4	0.27	5.9	93.5
	CCAT	0.99	2.1	2.1	4.8	0.60	2.9	100.0
Black-Box ($L_2, \epsilon = 1$)	Normal	0.42	88.3	2.6	92.3	0.78	3.6	94.4
	AT-50%	0.98	10.8	2.5	13.8	0.56	3.4	29.8
	AT-100%	0.85	22.5	4.6	27.7	0.27	5.9	30.1
	CCAT	1.00	0.1	2.1	2.7	0.60	2.9	96.5
Worst-Case ($L_2, \epsilon = 2$)	Normal	0.16	95.9	2.6	100.0	0.78	3.6	100.0
	AT-50%	0.11	95.7	2.5	99.4	0.56	3.4	99.4
	AT-100%	0.12	93.3	4.6	99.5	0.27	5.9	99.5
	CCAT	0.89	25.4	2.1	28.3	0.60	2.9	91.9
PGD Conf ($L_2, \epsilon = 2$)	Normal	0.21	95.4	2.6	99.5	0.78	3.6	99.8
	AT-50%	0.49	76.2	2.5	79.7	0.56	3.4	81.2
	AT-100%	0.45	78.1	4.6	84.0	0.27	5.9	84.3
	CCAT	0.89	19.1	2.1	21.9	0.60	2.9	88.0
PGD CE ($L_2, \epsilon = 2$)	Normal	0.16	95.9	2.6	100.0	0.78	3.6	100.0
	AT-50%	0.12	95.7	2.5	99.4	0.56	3.4	99.4
	AT-100%	0.12	93.3	4.6	99.5	0.27	5.9	99.5
	CCAT	0.98	5.0	2.1	7.7	0.60	2.9	100.0

Table 14: Per-Attack Results on SVHN, Part II (L_2). Per-attack results considering PGD-CE, as in (Madry et al., 2018), our PGD-Conf and the remaining black-box attacks for L_2 threat model. The used ϵ values are reported in the left-most column. For the black-box attacks, we report the per-example worst-case across all black-box attacks. In addition to FPR and RErr we include ROC AUC, Err as well as Err and RErr in the standard, non-thresholded setting, as reference.

Confidence-Calibrated Adversarial Training

SVHN: Supplementary Results for L_1 , L_0 Adversarial Examples and Adversarial Frames								
Attack	Training	Detection Setting $\tau@99\%TPR$					Standard Setting $\tau=0$	
		ROC AUC	FPR in %	Err in %	RErr in %	τ	Err in %	RErr in %
Worst-Case ($L_1, \epsilon = 18$)	Normal	0.17	95.9	2.6	100.0	0.78	3.6	100.0
	AT-50%	0.09	95.0	2.5	98.7	0.56	3.4	98.7
	AT-100%	0.14	93.1	4.6	99.3	0.27	5.9	99.3
	CCAT	0.82	24.3	2.1	27.2	0.60	2.9	72.8
PGD Conf ($L_1, \epsilon = 18$)	Normal	0.17	95.9	2.6	100.0	0.78	3.6	100.0
	AT-50%	0.11	94.8	2.5	98.5	0.56	3.4	98.5
	AT-100%	0.15	92.9	4.6	99.1	0.27	5.9	99.1
	CCAT	0.82	23.4	2.1	26.3	0.60	2.9	69.3
PGD CE ($L_1, \epsilon = 18$)	Normal	0.21	95.7	2.6	99.8	0.78	3.6	99.8
	AT-50%	0.29	92.8	2.5	96.5	0.56	3.4	96.6
	AT-100%	0.27	92.1	4.6	98.3	0.27	5.9	98.3
	CCAT	0.99	2.7	2.1	5.4	0.60	2.9	100.0
Black-Box ($L_1, \epsilon = 18$)	Normal	0.89	6.2	2.6	9.2	0.78	3.6	13.0
	AT-50%	0.97	3.7	2.5	6.6	0.56	3.4	10.9
	AT-100%	0.90	7.4	4.6	12.3	0.27	5.9	14.9
	CCAT	1.00	0.5	2.1	3.2	0.60	2.9	10.0
Worst-Case ($L_1, \epsilon = 24$)	Normal	0.16	95.9	2.6	100.0	0.78	3.6	100.0
	AT-50%	0.05	95.8	2.5	99.5	0.56	3.4	99.5
	AT-100%	0.09	93.6	4.6	99.8	0.27	5.9	99.8
	CCAT	0.80	28.1	2.1	31.0	0.60	2.9	77.0
PGD Conf ($L_1, \epsilon = 24$)	Normal	0.16	95.9	2.6	100.0	0.78	3.6	100.0
	AT-50%	0.06	95.7	2.5	99.4	0.56	3.4	99.4
	AT-100%	0.09	93.6	4.6	99.8	0.27	5.9	99.8
	CCAT	0.79	27.1	2.1	30.0	0.60	2.9	73.3
PGD CE ($L_1, \epsilon = 24$)	Normal	0.19	95.8	2.6	99.9	0.78	3.6	99.9
	AT-50%	0.25	94.0	2.5	97.7	0.56	3.4	98.0
	AT-100%	0.22	92.5	4.6	98.7	0.27	5.9	98.7
	CCAT	0.98	3.4	2.1	6.1	0.60	2.9	100.0
Black-Box ($L_1, \epsilon = 24$)	Normal	0.86	18.7	2.6	21.8	0.78	3.6	27.1
	AT-50%	0.96	11.2	2.5	14.2	0.56	3.4	22.2
	AT-100%	0.86	16.3	4.6	21.3	0.27	5.9	24.6
	CCAT	1.00	1.3	2.1	4.0	0.60	2.9	18.3
Worst-Case ($L_0, \epsilon = 10$)	Normal	0.60	79.6	2.6	83.5	0.78	3.6	98.0
	AT-50%	0.90	70.0	2.5	73.5	0.56	3.4	89.2
	AT-100%	0.65	83.1	4.6	89.2	0.27	5.9	89.9
	CCAT	1.00	0.4	2.1	3.0	0.60	2.9	75.3
PGD Conf ($L_0, \epsilon = 10$)	Normal	0.55	63.4	2.6	67.1	0.78	3.6	69.0
	AT-50%	0.90	48.0	2.5	51.3	0.56	3.4	59.7
	AT-100%	0.64	61.3	4.6	67.2	0.27	5.9	68.0
	CCAT	1.00	0.1	2.1	2.7	0.60	2.9	63.9
PGD CE ($L_0, \epsilon = 10$)	Normal	0.52	71.4	2.6	75.2	0.78	3.6	78.1
	AT-50%	0.89	57.4	2.5	60.8	0.56	3.4	68.9
	AT-100%	0.65	68.2	4.6	74.2	0.27	5.9	75.5
	CCAT	1.00	0.0	2.1	2.6	0.60	2.9	96.9
Black-Box ($L_0, \epsilon = 10$)	Normal	0.96	44.5	2.6	47.9	0.78	3.6	97.7
	AT-50%	0.98	34.4	2.5	37.7	0.56	3.4	86.6
	AT-100%	0.86	74.3	4.6	80.6	0.27	5.9	85.5
	CCAT	1.00	0.3	2.1	3.0	0.60	2.9	93.1
Adversarial Frames	Normal	0.47	74.6	2.6	78.4	0.78	3.6	80.1
	AT-50%	0.77	30.0	2.5	33.1	0.56	3.4	36.0
	AT-100%	0.78	19.9	4.6	25.1	0.27	5.9	27.4
	CCAT	1.00	1.0	2.1	3.7	0.60	2.9	97.3

Table 15: Per-Attack Results on SVHN, Part III (L_1 , L_0 , Adversarial Frames). Per-attack results considering PGD-CE, as in (Madry et al., 2018), our PGD-Conf and the remaining black-box attacks for L_1 , L_0 threat models and adversarial frames. The used ϵ values are reported in the left-most column. For the black-box attacks, we report the per-example worst-case across all black-box attacks. In addition to FPR and RErr we include ROC AUC, Err as well as Err and RErr in the standard, non-thresholded setting, as reference.

Confidence-Calibrated Adversarial Training

CIFAR10: Supplementary Results for L_∞ Adversarial Examples								
Attack	Training	Detection Setting $\tau @ 99\% \text{TPR}$					Standard Setting $\tau = 0$	
		ROC AUC	FPR in %	Err in %	RErr in %	τ	Err in %	RErr in %
Worst-Case ($L_\infty, \epsilon = 0.03$)	Normal	0.20	93.0	7.4	100.0	0.59	8.3	100.0
	AT-50%	0.64	47.6	15.1	62.3	0.35	16.6	62.7
	AT-100%	0.64	42.3	18.3	59.5	0.29	19.4	59.9
	CCAT	0.60	59.9	8.7	67.9	0.40	10.1	96.7
	MSD	0.66	35.3	17.6	53.0	0.24	18.4	53.2
	TRADES	0.73	28.9	13.2	41.9	0.30	15.2	43.5
	AT-Madry	0.73	33.8	11.7	44.4	0.29	13.0	45.1
PGD Conf ($L_\infty, \epsilon = 0.03$)	Normal	0.20	93.0	7.4	100.0	0.59	8.3	100.0
	AT-50%	0.65	46.2	15.1	60.9	0.35	16.6	61.3
	AT-100%	0.65	40.0	18.3	57.2	0.29	19.4	57.6
	CCAT	0.60	55.1	8.7	63.0	0.40	10.1	95.0
	MSD	0.66	33.0	17.6	50.7	0.24	18.4	50.9
	TRADES	0.73	28.2	13.2	41.2	0.30	15.2	42.8
	AT-Madry	0.73	31.9	11.7	42.5	0.29	13.0	43.2
PGD CE ($L_\infty, \epsilon = 0.03$)	Normal	0.20	93.0	7.4	100.0	0.59	8.3	100.0
	AT-50%	0.67	46.7	15.1	61.4	0.35	16.6	62.3
	AT-100%	0.69	40.5	18.3	57.7	0.29	19.4	59.3
	CCAT	0.99	2.5	8.7	9.8	0.40	10.1	100.0
	MSD	0.75	33.2	17.6	50.9	0.24	18.4	52.6
	TRADES	0.80	25.3	13.2	38.4	0.30	15.2	42.9
	AT-Madry	0.78	30.3	11.7	40.9	0.29	13.0	44.2
Black-Box ($L_\infty, \epsilon = 0.03$)	Normal	0.21	93.0	7.4	100.0	0.59	8.3	100.0
	AT-50%	0.70	42.2	15.1	56.9	0.35	16.6	57.3
	AT-100%	0.70	36.9	18.3	54.1	0.29	19.4	54.7
	CCAT	0.90	41.6	8.7	49.3	0.40	10.1	96.4
	MSD	0.73	30.2	17.6	47.9	0.24	18.4	48.4
	TRADES	0.78	25.1	13.2	38.0	0.30	15.2	40.0
	AT-Madry	0.78	29.2	11.7	39.7	0.29	13.0	41.2
Worst-Case ($L_\infty, \epsilon = 0.06$)	Normal	0.20	93.0	7.4	100.0	0.59	8.3	100.0
	AT-50%	0.35	78.6	15.1	93.6	0.35	16.6	93.7
	AT-100%	0.39	72.7	18.3	90.2	0.29	19.4	90.3
	CCAT	0.40	83.9	8.7	92.3	0.40	10.1	99.4
	MSD	0.43	71.5	17.6	89.4	0.24	18.4	89.4
	TRADES	0.53	66.4	13.2	80.5	0.30	15.2	81.0
	AT-Madry	0.46	73.2	11.7	84.3	0.29	13.0	84.5
PGD Conf ($L_\infty, \epsilon = 0.06$)	Normal	0.20	93.0	7.4	100.0	0.59	8.3	100.0
	AT-50%	0.37	77.1	15.1	92.1	0.35	16.6	92.2
	AT-100%	0.43	70.7	18.3	88.2	0.29	19.4	88.3
	CCAT	0.45	64.5	8.7	72.6	0.40	10.1	97.4
	MSD	0.46	68.7	17.6	86.5	0.24	18.4	86.6
	TRADES	0.54	63.9	13.2	77.9	0.30	15.2	78.5
	AT-Madry	0.51	69.4	11.7	80.4	0.29	13.0	80.7
PGD CE ($L_\infty, \epsilon = 0.06$)	Normal	0.20	93.0	7.4	100.0	0.59	8.3	100.0
	AT-50%	0.40	78.6	15.1	93.6	0.35	16.6	93.7
	AT-100%	0.45	72.7	18.3	90.2	0.29	19.4	90.3
	CCAT	0.98	3.7	8.7	11.0	0.40	10.1	100.0
	MSD	0.53	71.6	17.6	89.5	0.24	18.4	89.5
	TRADES	0.64	64.8	13.2	78.8	0.30	15.2	80.4
	AT-Madry	0.50	73.1	11.7	84.2	0.29	13.0	84.4
Black-Box ($L_\infty, \epsilon = 0.06$)	Normal	0.20	93.0	7.4	100.0	0.59	8.3	100.0
	AT-50%	0.50	72.1	15.1	87.1	0.35	16.6	87.2
	AT-100%	0.53	65.9	18.3	83.4	0.29	19.4	83.5
	CCAT	0.77	79.1	8.7	87.4	0.40	10.1	99.7
	MSD	0.58	60.5	17.6	78.3	0.24	18.4	78.5
	TRADES	0.65	57.6	13.2	71.4	0.30	15.2	72.2
	AT-Madry	0.62	63.5	11.7	74.5	0.29	13.0	75.2

Table 16: Per-Attack Results on Cifar10, Part I (L_∞). Per-attack results considering PGD-CE, as in (Madry et al., 2018), our PGD-Conf and the remaining black-box attacks for L_∞ and L_2 threat models. The used ϵ values are reported in the left-most column. For the black-box attacks, we report the per-example worst-case across all black-box attacks. In addition to FPR and RErr we include ROC AUC, Err as well as Err and RErr in the standard, non-thresholded setting, as reference.

Confidence-Calibrated Adversarial Training

CIFAR10: Supplementary Results for L_2 Adversarial Examples								
Attack	Training	Detection Setting					Standard Setting	
		ROC AUC	FPR in %	Err in %	RErr in %	τ	Err in %	RErr in %
Worst-Case ($L_2, \epsilon = 1$)	Normal	0.20	93.0	7.4	100.0	0.59	8.3	100.0
	AT-50%	0.59	59.1	15.1	73.9	0.35	16.6	74.4
	AT-100%	0.57	55.8	18.3	73.2	0.29	19.4	73.4
	CCAT	0.75	42.6	8.7	50.4	0.40	10.1	83.2
	MSD	0.68	34.3	17.6	52.0	0.24	18.4	52.2
	TRADES	0.64	56.3	13.2	70.1	0.30	15.2	71.3
	AT-Madry	0.59	62.4	11.7	73.4	0.29	13.0	73.8
PGD Conf ($L_2, \epsilon = 1$)	Normal	0.20	93.0	7.4	100.0	0.59	8.3	100.0
	AT-50%	0.63	50.2	15.1	64.9	0.35	16.6	65.3
	AT-100%	0.62	46.4	18.3	63.7	0.29	19.4	64.0
	CCAT	0.76	41.9	8.7	49.6	0.40	10.1	82.6
	MSD	0.68	30.4	17.6	48.1	0.24	18.4	48.3
	TRADES	0.67	43.1	13.2	56.5	0.30	15.2	57.7
	AT-Madry	0.68	44.8	11.7	55.5	0.29	13.0	56.1
PGD CE ($L_2, \epsilon = 1$)	Normal	0.20	93.0	7.4	100.0	0.59	8.3	100.0
	AT-50%	0.61	59.1	15.1	73.9	0.35	16.6	74.6
	AT-100%	0.60	55.1	18.3	72.5	0.29	19.4	73.7
	CCAT	0.93	13.8	8.7	21.2	0.40	10.1	100.0
	MSD	0.74	33.6	17.6	51.3	0.24	18.4	52.1
	TRADES	0.68	56.1	13.2	70.0	0.30	15.2	72.6
	AT-Madry	0.61	61.9	11.7	72.9	0.29	13.0	74.1
Black-Box ($L_2, \epsilon = 1$)	Normal	0.38	90.1	7.4	97.1	0.59	8.3	97.4
	AT-50%	0.81	21.3	15.1	35.8	0.35	16.6	36.9
	AT-100%	0.78	19.8	18.3	36.8	0.29	19.4	37.8
	CCAT	0.99	5.0	8.7	12.3	0.40	10.1	78.8
	MSD	0.80	16.5	17.6	34.2	0.24	18.4	34.6
	TRADES	0.84	15.2	13.2	27.9	0.30	15.2	31.0
	AT-Madry	0.83	16.3	11.7	26.7	0.29	13.0	28.8
Worst-Case ($L_2, \epsilon = 2$)	Normal	0.20	93.0	7.4	100.0	0.59	8.3	100.0
	AT-50%	0.28	83.3	15.1	98.4	0.35	16.6	98.4
	AT-100%	0.34	80.7	18.3	98.3	0.29	19.4	98.4
	CCAT	0.74	43.7	8.7	51.5	0.40	10.1	85.8
	MSD	0.53	70.6	17.6	88.5	0.24	18.4	88.8
	TRADES	0.64	56.3	13.2	70.1	0.30	15.2	71.3
	AT-Madry	0.26	87.4	11.7	98.7	0.29	13.0	98.7
PGD Conf ($L_2, \epsilon = 2$)	Normal	0.20	93.0	7.4	100.0	0.59	8.3	100.0
	AT-50%	0.62	52.4	15.1	67.2	0.35	16.6	67.5
	AT-100%	0.60	48.2	18.3	65.5	0.29	19.4	65.8
	CCAT	0.76	42.4	8.7	50.2	0.40	10.1	84.6
	MSD	0.67	31.9	17.6	49.6	0.24	18.4	49.8
	TRADES	0.67	43.1	13.2	56.5	0.30	15.2	57.7
	AT-Madry	0.67	48.6	11.7	59.4	0.29	13.0	59.9
PGD CE ($L_2, \epsilon = 2$)	Normal	0.20	93.0	7.4	100.0	0.59	8.3	100.0
	AT-50%	0.28	83.3	15.1	98.4	0.35	16.6	98.4
	AT-100%	0.34	80.7	18.3	98.3	0.29	19.4	98.4
	CCAT	0.92	15.9	8.7	23.3	0.40	10.1	100.0
	MSD	0.54	71.2	17.6	89.1	0.24	18.4	89.5
	TRADES	0.68	56.1	13.2	70.0	0.30	15.2	72.6
	AT-Madry	0.26	87.4	11.7	98.7	0.29	13.0	98.7
Black-Box ($L_2, \epsilon = 2$)	Normal	0.21	93.0	7.4	100.0	0.59	8.3	100.0
	AT-50%	0.67	47.5	15.1	62.2	0.35	16.6	62.6
	AT-100%	0.66	43.4	18.3	60.6	0.29	19.4	61.3
	CCAT	0.99	7.7	8.7	15.1	0.40	10.1	81.0
	MSD	0.71	33.7	17.6	51.5	0.24	18.4	51.8
	TRADES	0.84	15.2	13.2	27.9	0.30	15.2	31.0
	AT-Madry	0.73	42.2	11.7	52.9	0.29	13.0	53.9

Table 17: Per-Attack Results on Cifar10, Part II (L_2). Per-attack results considering PGD-CE, as in (Madry et al., 2018), our PGD-Conf and the remaining black-box attacks for the L_2 threat model. The used ϵ values are reported in the left-most column. For the black-box attacks, we report the per-example worst-case across all black-box attacks. In addition to FPR and RErr we include ROC AUC, Err as well as Err and RErr in the standard, non-thresholded setting, as reference.

Confidence-Calibrated Adversarial Training

CIFAR10: Supplementary Results for L_1 Adversarial Examples								
Attack	Training	Detection Setting					Standard Setting	
		ROC AUC	FPR in %	Err in %	RErr in %	τ	Err in %	RErr in %
		$\tau@99\%TPR$					$\tau=0$	
Worst-Case ($L_1, \epsilon = 18$)	Normal	0.20	93.0	7.4	100.0	0.59	8.3	100.0
	AT-50%	0.39	80.1	15.1	95.2	0.35	16.6	95.2
	AT-100%	0.39	76.8	18.3	94.3	0.29	19.4	94.4
	CCAT	0.67	47.6	8.7	55.4	0.40	10.1	85.4
	MSD	0.63	40.0	17.6	57.7	0.24	18.4	57.9
	TRADES	0.45	78.6	13.2	93.0	0.30	15.2	93.2
	AT-Madry	0.39	83.0	11.7	94.2	0.29	13.0	94.3
PGD Conf ($L_1, \epsilon = 18$)	Normal	0.20	93.0	7.4	100.0	0.59	8.3	100.0
	AT-50%	0.39	79.9	15.1	94.9	0.35	16.6	95.0
	AT-100%	0.40	76.5	18.3	94.0	0.29	19.4	94.1
	CCAT	0.67	47.3	8.7	55.1	0.40	10.1	85.4
	MSD	0.63	38.6	17.6	56.3	0.24	18.4	56.5
	TRADES	0.45	78.4	13.2	92.8	0.30	15.2	93.0
	AT-Madry	0.41	82.5	11.7	93.7	0.29	13.0	93.8
PGD CE ($L_1, \epsilon = 18$)	Normal	0.20	92.9	7.4	99.9	0.59	8.3	99.9
	AT-50%	0.57	69.0	15.1	83.9	0.35	16.6	85.0
	AT-100%	0.55	66.2	18.3	83.7	0.29	19.4	84.6
	CCAT	0.94	13.8	8.7	21.1	0.40	10.1	100.0
	MSD	0.75	32.2	17.6	49.9	0.24	18.4	51.1
	TRADES	0.63	69.4	13.2	83.6	0.30	15.2	85.5
	AT-Madry	0.55	74.6	11.7	85.8	0.29	13.0	87.0
Black-Box ($L_1, \epsilon = 18$)	Normal	0.94	3.6	7.4	9.9	0.59	8.3	11.6
	AT-50%	0.93	1.9	15.1	16.3	0.35	16.6	17.6
	AT-100%	0.93	1.0	18.3	17.9	0.29	19.4	19.1
	CCAT	0.99	0.8	8.7	8.1	0.40	10.1	18.7
	MSD	0.84	0.8	17.6	18.4	0.24	18.4	18.8
	TRADES	0.92	0.9	13.2	13.3	0.30	15.2	15.9
	AT-Madry	0.90	1.1	11.7	11.3	0.29	13.0	12.8
Worst-Case ($L_1, \epsilon = 24$)	Normal	0.20	93.0	7.4	100.0	0.59	8.3	100.0
	AT-50%	0.28	83.3	15.1	98.4	0.35	16.6	98.4
	AT-100%	0.31	80.4	18.3	98.0	0.29	19.4	98.0
	CCAT	0.62	50.3	8.7	58.2	0.40	10.1	87.0
	MSD	0.57	50.7	17.6	68.5	0.24	18.4	68.6
	TRADES	0.37	82.3	13.2	96.8	0.30	15.2	97.0
	AT-Madry	0.29	86.5	11.7	97.8	0.29	13.0	97.8
PGD Conf ($L_1, \epsilon = 24$)	Normal	0.20	93.0	7.4	100.0	0.59	8.3	100.0
	AT-50%	0.29	83.3	15.1	98.4	0.35	16.6	98.4
	AT-100%	0.32	80.1	18.3	97.7	0.29	19.4	97.7
	CCAT	0.63	50.2	8.7	58.1	0.40	10.1	86.9
	MSD	0.57	49.3	17.6	67.1	0.24	18.4	67.2
	TRADES	0.37	82.3	13.2	96.8	0.30	15.2	96.9
	AT-Madry	0.31	86.3	11.7	97.6	0.29	13.0	97.6
PGD CE ($L_1, \epsilon = 24$)	Normal	0.20	92.9	7.4	99.9	0.59	8.3	99.9
	AT-50%	0.52	76.3	15.1	91.3	0.35	16.6	92.5
	AT-100%	0.51	72.7	18.3	90.2	0.29	19.4	91.2
	CCAT	0.94	15.0	8.7	22.4	0.40	10.1	100.0
	MSD	0.72	38.7	17.6	56.4	0.24	18.4	57.9
	TRADES	0.59	75.6	13.2	89.9	0.30	15.2	91.2
	AT-Madry	0.49	80.5	11.7	91.7	0.29	13.0	92.4
Black-Box ($L_1, \epsilon = 24$)	Normal	0.93	8.6	7.4	14.9	0.59	8.3	17.4
	AT-50%	0.93	3.5	15.1	17.9	0.35	16.6	19.7
	AT-100%	0.90	3.8	18.3	20.7	0.29	19.4	21.8
	CCAT	0.99	1.6	8.7	8.9	0.40	10.1	26.8
	MSD	0.87	2.6	17.6	20.2	0.24	18.4	20.6
	TRADES	0.89	1.7	13.2	14.0	0.30	15.2	16.7
	AT-Madry	0.89	2.9	11.7	13.2	0.29	13.0	14.9

Table 18: Per-Attack Results on Cifar10, Part III (L_1). Per-attack results considering PGD-CE, as in (Madry et al., 2018), our PGD-Conf and the remaining black-box attacks for the L_1 threat model. The used ϵ values are reported in the left-most column. For the black-box attacks, we report the per-example worst-case across all black-box attacks. In addition to FPR and RErr we include ROC AUC, Err as well as Err and RErr in the standard, non-thresholded setting, as reference.

CIFAR10: Supplementary Results for L_0 Adversarial Examples and Adversarial Frames								
Attack	Training	Detection Setting					Standard Setting	
		ROC AUC	FPR in %	Err in %	RErr in %	τ	Err in %	RErr in %
Worst-Case ($L_0, \epsilon = 10$)	Normal	0.80	77.7	7.4	84.6	0.59	8.3	96.2
	AT-50%	0.80	59.3	15.1	74.1	0.35	16.6	75.9
	AT-100%	0.75	54.7	18.3	72.0	0.29	19.4	73.2
	CCAT	0.97	14.4	8.7	21.9	0.40	10.1	54.7
	MSD	0.84	21.4	17.6	39.1	0.24	18.4	39.8
	TRADES	0.78	22.3	13.2	35.2	0.30	15.2	37.8
	AT-Madry	0.73	31.0	11.7	41.5	0.29	13.0	42.8
PGD Conf ($L_0, \epsilon = 10$)	Normal	0.74	48.9	7.4	55.5	0.59	8.3	57.4
	AT-50%	0.74	29.7	15.1	44.3	0.35	16.6	45.1
	AT-100%	0.72	25.2	18.3	42.3	0.29	19.4	43.3
	CCAT	0.98	5.2	8.7	12.5	0.40	10.1	34.8
	MSD	0.81	5.2	17.6	22.8	0.24	18.4	23.1
	TRADES	0.80	18.0	13.2	30.8	0.30	15.2	33.2
	AT-Madry	0.77	21.8	11.7	32.3	0.29	13.0	33.5
PGD CE ($L_0, \epsilon = 10$)	Normal	0.73	56.3	7.4	63.0	0.59	8.3	65.4
	AT-50%	0.76	34.8	15.1	49.4	0.35	16.6	51.4
	AT-100%	0.72	30.3	18.3	47.5	0.29	19.4	48.9
	CCAT	1.00	0.3	8.7	7.6	0.40	10.1	79.3
	MSD	0.82	5.9	17.6	23.5	0.24	18.4	23.9
	TRADES	0.81	21.0	13.2	33.9	0.30	15.2	37.5
	AT-Madry	0.77	26.7	11.7	37.2	0.29	13.0	39.2
Black-Box ($L_0, \epsilon = 10$)	Normal	0.94	66.1	7.4	72.9	0.59	8.3	96.2
	AT-50%	0.91	54.2	15.1	69.6	0.35	16.6	75.7
	AT-100%	0.83	52.8	18.3	70.3	0.29	19.4	72.4
	CCAT	0.99	12.0	8.7	19.6	0.40	10.1	96.6
	MSD	0.86	22.1	17.6	39.8	0.24	18.4	41.0
	TRADES	0.84	8.4	13.2	20.9	0.30	15.2	24.3
	AT-Madry	0.79	15.7	11.7	26.1	0.29	13.0	27.6
Adversarial Frames	Normal	0.28	89.7	7.4	96.7	0.59	8.3	96.9
	AT-50%	0.40	63.6	15.1	78.5	0.35	16.6	78.7
	AT-100%	0.39	62.0	18.3	79.4	0.29	19.4	79.6
	CCAT	0.75	57.4	8.7	65.6	0.40	10.1	86.7
	MSD	0.38	64.7	17.6	82.5	0.24	18.4	82.6
	TRADES	0.45	57.5	13.2	71.3	0.30	15.2	72.1
	AT-Madry	0.48	62.0	11.7	72.9	0.29	13.0	73.3

Table 19: Per-Attack Results on Cifar10, Part IV (L_0 , Adversarial Frames). Per-attack results considering PGD-CE, as in (Madry et al., 2018), our PGD-Conf and the remaining black-box attacks for the L_0 threat model and adversarial frames. The used ϵ values are reported in the left-most column. For the black-box attacks, we report the per-example worst-case across all black-box attacks. In addition to FPR and RErr we include ROC AUC, Err as well as Err and RErr in the standard, non-thresholded setting, as reference.

Confidence-Calibrated Adversarial Training

MNIST-C: Supplementary Results for Corruption							
Corruption	Training	Detection Setting $\tau@99\%TPR$					Standard Setting $\tau=0$
		ROC AUC	FPR in %	TNR in %	Err in %	τ	Err in %
all	Normal	0.75	82.8	17.2	31.9	0.98	36.4
	AT-50%	0.80	59.0	41.0	4.0	1.00	26.9
	AT-100%	0.78	63.5	36.5	8.6	1.00	27.4
	CCAT	0.96	29.0	71.0	6.7	0.85	41.5
	MSD	0.75	75.0	25.0	5.4	0.51	14.0
	TRADES	0.79	74.1	25.9	5.5	0.92	16.1
mean	Normal	0.75	82.8	17.2	32.8	1.0	36.3
	AT-50%	0.80	59.0	41.0	12.6	1.0	26.9
	AT-100%	0.78	63.5	36.5	17.6	1.0	27.4
	CCAT	0.96	29.0	71.0	5.7	0.9	41.5
	MSD	0.75	75.0	25.0	6.0	0.5	14.0
	TRADES	0.79	74.1	25.9	7.9	0.9	16.1
brightness	Normal	0.36	100.0	0.0	90.2	0.98	90.2
	AT-50%	0.99	0.9	99.1	36.4	1.00	84.3
	AT-100%	0.97	35.4	64.6	82.2	1.00	90.9
	CCAT	1.00	0.0	100.0	0.0	0.85	90.5
	MSD	0.95	38.7	61.3	0.1	0.51	23.1
	TRADES	0.95	43.7	56.3	67.3	0.92	77.2
canny_edges	Normal	0.91	62.4	37.6	34.8	0.98	45.6
	AT-50%	0.96	28.8	71.2	33.4	1.00	53.2
	AT-100%	0.94	35.3	64.7	38.2	1.00	53.4
	CCAT	0.99	34.3	65.7	70.5	0.85	61.9
	MSD	0.87	63.4	36.6	5.5	0.51	17.8
	TRADES	0.92	53.2	46.8	21.5	0.92	36.3
dotted_line	Normal	0.76	85.4	14.6	2.4	0.98	7.6
	AT-50%	0.77	72.8	27.2	0.9	1.00	7.9
	AT-100%	0.75	74.5	25.5	0.9	1.00	6.4
	CCAT	0.98	53.4	46.6	2.5	0.85	10.1
	MSD	0.60	94.2	5.8	1.1	0.51	2.9
	TRADES	0.73	84.5	15.5	0.5	0.92	4.2
fog	Normal	0.38	99.9	0.1	90.2	0.98	90.2
	AT-50%	0.90	29.7	70.3	10.4	1.00	59.0
	AT-100%	0.88	46.3	53.7	37.7	1.00	62.0
	CCAT	1.00	0.0	100.0	0.0	0.85	90.3
	MSD	0.92	46.8	53.2	4.3	0.51	26.1
	TRADES	0.87	60.9	39.1	14.3	0.92	35.8
glass_blur	Normal	0.87	71.6	28.4	57.2	0.98	56.2
	AT-50%	0.82	67.4	32.6	1.2	1.00	11.0
	AT-100%	0.77	70.5	29.5	1.1	1.00	8.5
	CCAT	1.00	0.0	100.0	0.0	0.85	86.8
	MSD	0.69	89.1	10.9	1.7	0.51	4.9
	TRADES	0.81	80.9	19.1	0.6	0.92	6.0
impulse_noise	Normal	0.87	72.4	27.6	79.2	0.98	81.3
	AT-50%	0.98	13.9	86.1	18.8	1.00	61.4
	AT-100%	0.97	18.8	81.2	12.8	1.00	56.2
	CCAT	1.00	0.0	100.0	0.0	0.85	69.1
	MSD	0.83	69.4	30.6	0.7	0.51	8.2
	TRADES	0.91	57.3	42.7	2.2	0.92	17.2
motion_blur	Normal	0.86	73.9	26.1	29.5	0.98	37.2
	AT-50%	0.62	90.6	9.4	0.3	1.00	2.7
	AT-100%	0.58	91.3	8.7	0.3	1.00	2.4
	CCAT	1.00	0.0	100.0	0.0	0.85	75.6
	MSD	0.74	83.1	16.9	3.6	0.51	9.1
	TRADES	0.71	88.3	11.7	0.6	0.92	4.0
rotate	Normal	0.70	92.4	7.6	1.7	0.98	4.6
	AT-50%	0.64	87.9	12.1	0.8	1.00	4.1
	AT-100%	0.63	87.2	12.8	0.8	1.00	4.5
	CCAT	0.98	41.5	58.5	0.3	0.85	4.4
	MSD	0.64	90.7	9.3	5.7	0.51	9.7
	TRADES	0.66	87.7	12.3	1.4	0.92	4.8

Table 20: Per-Corruptions Results on MNIST-C, PART I. Results on MNIST-C, broken down by individual corruptions (first column); mean are the averaged results over all corruptions. We report ROC AUC, FPR and the true negative rate (TNR) in addition to the thresholded and unthresholded Err on the corrupted examples. The table is continued in Tab. 21.

Confidence-Calibrated Adversarial Training

MNIST-C: Supplementary Results for Corruption							
Corruption	Training	Detection Setting $\tau@99\%TPR$					Standard Setting $\tau=0$
		ROC AUC	FPR in %	TNR in %	Err in %	τ	Err in %
scale	Normal	0.84	89.5	10.5	0.7	0.98	3.1
	AT-50%	0.86	78.5	21.5	0.1	1.00	3.0
	AT-100%	0.80	82.1	17.9	0.4	1.00	3.0
	CCAT	0.75	96.7	3.3	0.8	0.85	2.0
	MSD	0.84	64.4	35.6	8.1	0.51	18.1
	TRADES	0.82	84.4	15.6	0.3	0.92	2.9
shear	Normal	0.60	97.6	2.4	0.2	0.98	0.8
	AT-50%	0.56	95.1	4.9	0.1	1.00	0.9
	AT-100%	0.55	94.8	5.2	0.1	1.00	0.9
	CCAT	0.98	27.4	72.6	0.0	0.85	1.1
	MSD	0.56	95.9	4.1	1.9	0.51	3.2
	TRADES	0.61	94.8	5.2	0.3	0.92	1.4
shot.noise	Normal	0.74	93.0	7.0	1.4	0.98	3.6
	AT-50%	0.62	91.3	8.7	0.2	1.00	1.9
	AT-100%	0.57	92.6	7.4	0.2	1.00	1.8
	CCAT	0.96	61.2	38.8	0.1	0.85	2.3
	MSD	0.59	95.2	4.8	0.9	0.51	2.4
	TRADES	0.65	94.9	5.1	0.2	0.92	1.4
spatter	Normal	0.85	72.8	27.2	18.9	0.98	28.1
	AT-50%	0.65	88.3	11.7	0.6	1.00	3.6
	AT-100%	0.61	90.3	9.7	0.4	1.00	2.7
	CCAT	1.00	0.0	100.0	0.0	0.85	29.7
	MSD	0.56	95.6	4.4	1.2	0.51	2.6
	TRADES	0.63	90.4	9.6	0.7	0.92	3.3
stripe	Normal	0.92	61.1	38.9	69.6	0.98	70.2
	AT-50%	0.98	12.2	87.8	83.8	1.00	81.3
	AT-100%	0.99	12.4	87.6	88.2	1.00	87.4
	CCAT	1.00	0.0	100.0	0.0	0.85	78.0
	MSD	0.90	55.8	44.2	1.1	0.51	10.4
	TRADES	0.88	72.9	27.1	0.6	0.92	5.9
translate	Normal	0.72	95.2	4.8	0.3	0.98	1.6
	AT-50%	0.80	74.6	25.4	0.2	1.00	4.0
	AT-100%	0.79	72.4	27.6	0.2	1.00	4.2
	CCAT	0.84	95.3	4.7	0.3	0.85	1.4
	MSD	0.88	59.3	40.7	44.7	0.51	55.2
	TRADES	0.94	42.3	57.7	6.3	0.92	28.1
zigzag	Normal	0.85	74.5	25.5	16.3	0.98	24.8
	AT-50%	0.87	53.6	46.4	10.9	1.00	24.9
	AT-100%	0.87	48.3	51.7	10.1	1.00	25.8
	CCAT	0.99	25.6	74.4	9.8	0.85	18.6
	MSD	0.70	83.5	16.5	9.7	0.51	15.8
	TRADES	0.76	75.2	24.8	4.9	0.92	13.8

Table 21: Per-Corruptions Results on MNIST-C, PART II. Continued results of Tab. 20 including results on MNIST-C focusing on individual corruptions. textttmean are the averaged results over all corruptions. We report ROC AUC, FPR and the true negative rate (TNR) in addition to the thresholded and unthresholded Err on the corrupted examples.

Confidence-Calibrated Adversarial Training

CIFAR10-C: Supplementary Results for Corruption							
Corruption	Training	Detection Setting $\tau@99\%TPR$					Standard Setting
		ROC AUC	FPR in %	TNR in %	Err in %	τ	Err in %
all	Normal	0.57	97.1	2.9	12.2	0.59	13.7
	AT-50%	0.53	96.2	3.8	16.2	0.35	18.1
	AT-100%	0.53	97.2	2.8	19.6	0.29	20.9
	CCAT	0.66	72.1	27.9	10.4	0.40	27.2
	MSD	0.53	98.2	1.8	19.2	0.24	20.2
	TRADES	0.53	95.8	4.2	15.0	0.30	17.3
	AT-Madry	0.53	96.3	3.7	12.8	0.29	14.7
mean	Normal	0.57	97.1	2.9	12.3	0.6	13.7
	AT-50%	0.53	96.2	3.8	16.2	0.3	18.1
	AT-100%	0.53	97.2	2.8	19.6	0.3	21.0
	CCAT	0.66	72.1	27.9	8.5	0.4	27.2
	MSD	0.53	98.2	1.8	19.3	0.2	20.2
	TRADES	0.53	95.8	4.2	15.0	0.3	17.3
	AT-Madry	0.53	96.3	3.7	12.9	0.3	14.7
brightness	Normal	0.50	98.1	1.9	7.5	0.59	8.4
	AT-50%	0.50	97.0	3.0	14.9	0.35	16.5
	AT-100%	0.50	97.9	2.1	18.2	0.29	19.2
	CCAT	0.54	94.8	5.2	8.2	0.40	10.4
	MSD	0.50	98.6	1.4	17.8	0.24	18.5
	TRADES	0.49	96.8	3.2	13.1	0.30	14.9
	AT-Madry	0.49	97.5	2.5	11.2	0.29	12.5
contrast	Normal	0.52	98.1	1.9	8.4	0.59	9.4
	AT-50%	0.60	94.1	5.9	17.1	0.35	20.0
	AT-100%	0.60	95.2	4.8	21.1	0.29	23.5
	CCAT	0.55	96.6	3.4	10.3	0.40	11.9
	MSD	0.60	97.3	2.7	22.2	0.24	23.5
	TRADES	0.58	94.4	5.6	17.2	0.30	20.2
	AT-Madry	0.58	94.6	5.4	13.5	0.29	16.3
defocus_blur	Normal	0.50	98.1	1.9	7.4	0.59	8.4
	AT-50%	0.51	96.8	3.2	15.5	0.35	17.2
	AT-100%	0.51	97.7	2.3	18.6	0.29	19.7
	CCAT	0.49	97.5	2.5	9.2	0.40	10.5
	MSD	0.51	98.5	1.5	18.2	0.24	19.0
	TRADES	0.51	96.3	3.7	13.7	0.30	15.7
	AT-Madry	0.51	96.9	3.1	12.0	0.29	13.6
elastic_transform	Normal	0.60	97.3	2.7	12.1	0.59	13.5
	AT-50%	0.57	95.8	4.2	19.0	0.35	21.1
	AT-100%	0.57	96.7	3.3	22.0	0.29	23.6
	CCAT	0.54	96.5	3.5	13.2	0.40	14.9
	MSD	0.57	98.0	2.0	21.0	0.24	22.2
	TRADES	0.56	95.0	5.0	17.5	0.30	20.0
	AT-Madry	0.58	96.0	4.0	15.5	0.29	17.6
fog	Normal	0.51	98.0	2.0	7.9	0.59	8.8
	AT-50%	0.57	94.7	5.3	15.7	0.35	18.3
	AT-100%	0.57	96.1	3.9	19.5	0.29	21.5
	CCAT	0.55	96.0	4.0	9.0	0.40	11.1
	MSD	0.57	97.5	2.5	19.7	0.24	21.0
	TRADES	0.55	95.2	4.8	15.0	0.30	17.5
	AT-Madry	0.55	95.3	4.7	12.2	0.29	14.7
frost	Normal	0.57	97.2	2.8	11.5	0.59	12.8
	AT-50%	0.53	95.9	4.1	16.0	0.35	18.0
	AT-100%	0.53	96.9	3.1	20.1	0.29	21.6
	CCAT	0.65	88.1	11.9	9.0	0.40	12.5
	MSD	0.52	98.2	1.8	20.6	0.24	21.4
	TRADES	0.51	96.0	4.0	14.7	0.30	16.8
	AT-Madry	0.51	96.7	3.3	12.1	0.29	13.6
gaussian_blur	Normal	0.50	98.0	2.0	7.4	0.59	8.4
	AT-50%	0.51	96.8	3.2	15.5	0.35	17.1
	AT-100%	0.51	97.7	2.3	18.6	0.29	19.7
	CCAT	0.49	97.4	2.6	9.2	0.40	10.4
	MSD	0.51	98.5	1.5	18.1	0.24	19.0
	TRADES	0.51	96.3	3.7	13.7	0.30	15.7
	AT-Madry	0.51	96.9	3.1	12.0	0.29	13.5
gaussian_noise	Normal	0.62	96.2	3.8	15.7	0.59	17.7
	AT-50%	0.51	96.8	3.2	15.5	0.35	17.0
	AT-100%	0.51	97.7	2.3	18.6	0.29	19.8
	CCAT	1.00	0.0	100.0	0.0	0.40	84.9
	MSD	0.51	98.5	1.5	18.6	0.24	19.3
	TRADES	0.52	96.0	4.0	14.3	0.30	16.5
	AT-Madry	0.52	96.7	3.3	12.2	0.29	13.9
glass_blur	Normal	0.76	92.5	7.5	40.8	0.59	43.1
	AT-50%	0.58	95.4	4.6	18.0	0.35	20.2
	AT-100%	0.56	97.2	2.8	21.1	0.29	22.4
	CCAT	0.93	31.1	68.9	14.7	0.40	31.8
	MSD	0.56	98.1	1.9	21.0	0.24	22.0
	TRADES	0.56	95.1	4.9	17.6	0.30	20.1
	AT-Madry	0.58	95.5	4.5	15.4	0.29	17.6

Table 22: Per-Corruptions Results on Cifar10-C, PART I. Results on Cifar10-C focusing on individual corruptions (first column); textttmean are the averaged results over all corruptions. We report ROC AUC, FPR and the true negative rate (TNR) in addition to the thresholded and unthresholded Err on the corrupted examples. The table is continued in Tab. 23.

Confidence-Calibrated Adversarial Training

CIFAR10-C: Supplementary Results for Corruption							
Corruption	Training	Detection Setting $\tau@99\%TPR$					Standard Setting $\tau=0$
		ROC AUC	FPR in %	TNR in %	Err in %	τ	Err in %
impulse_noise	Normal	0.59	97.0	3.0	13.1	0.59	14.5
	AT-50%	0.53	96.4	3.6	16.4	0.35	17.9
	AT-100%	0.52	97.6	2.4	19.8	0.29	21.1
	CCAT	1.00	0.1	99.9	0.0	0.40	61.0
	MSD	0.51	98.4	1.6	18.3	0.24	19.2
	TRADES	0.54	94.9	5.1	15.7	0.30	18.4
	AT-Madry	0.53	96.1	3.9	13.3	0.29	15.3
jpeg_compression	Normal	0.59	96.9	3.1	12.3	0.59	13.7
	AT-50%	0.51	96.8	3.2	15.5	0.35	17.0
	AT-100%	0.51	97.6	2.4	18.9	0.29	20.2
	CCAT	0.59	93.3	6.7	9.3	0.40	12.1
	MSD	0.51	98.3	1.7	18.3	0.24	19.3
	TRADES	0.51	96.3	3.7	14.4	0.30	16.6
	AT-Madry	0.52	96.5	3.5	12.6	0.29	14.4
motion_blur	Normal	0.58	97.3	2.7	10.9	0.59	12.2
	AT-50%	0.55	95.9	4.1	16.8	0.35	18.9
	AT-100%	0.54	97.1	2.9	19.9	0.29	21.3
	CCAT	0.52	96.5	3.5	11.9	0.40	13.6
	MSD	0.54	98.1	1.9	19.7	0.24	20.7
	TRADES	0.54	95.8	4.2	15.7	0.30	17.9
	AT-Madry	0.55	95.9	4.1	13.3	0.29	15.6
pixelate	Normal	0.54	97.6	2.4	9.7	0.59	10.9
	AT-50%	0.51	96.7	3.3	15.3	0.35	17.0
	AT-100%	0.51	97.8	2.2	18.6	0.29	19.7
	CCAT	0.52	97.0	3.0	9.2	0.40	10.8
	MSD	0.51	98.4	1.6	18.2	0.24	19.1
	TRADES	0.51	96.4	3.6	14.0	0.30	16.0
	AT-Madry	0.51	97.1	2.9	12.1	0.29	13.6
saturate	Normal	0.55	97.5	2.5	10.0	0.59	11.3
	AT-50%	0.55	95.3	4.7	18.2	0.35	20.5
	AT-100%	0.54	96.0	4.0	21.3	0.29	23.3
	CCAT	0.48	97.6	2.4	11.8	0.40	13.0
	MSD	0.55	97.3	2.7	20.9	0.24	22.1
	TRADES	0.53	95.0	5.0	15.6	0.30	18.2
	AT-Madry	0.54	95.2	4.8	14.2	0.29	16.4
shot_noise	Normal	0.58	97.0	3.0	12.1	0.59	13.7
	AT-50%	0.51	97.1	2.9	15.4	0.35	16.7
	AT-100%	0.50	97.7	2.3	18.5	0.29	19.6
	CCAT	1.00	0.0	100.0	0.0	0.40	84.5
	MSD	0.51	98.5	1.5	18.1	0.24	18.9
	TRADES	0.51	96.2	3.8	13.7	0.30	15.8
	AT-Madry	0.51	97.1	2.9	11.8	0.29	13.4
snow	Normal	0.57	97.3	2.7	12.1	0.59	13.5
	AT-50%	0.51	96.7	3.3	15.3	0.35	17.0
	AT-100%	0.51	97.5	2.5	18.8	0.29	20.1
	CCAT	0.58	95.6	4.4	11.2	0.40	13.3
	MSD	0.51	98.4	1.6	18.7	0.24	19.6
	TRADES	0.50	96.3	3.7	14.1	0.30	16.1
	AT-Madry	0.51	97.0	3.0	12.3	0.29	13.8
spatter	Normal	0.54	97.5	2.5	9.4	0.59	10.6
	AT-50%	0.51	96.8	3.2	15.5	0.35	17.2
	AT-100%	0.51	97.6	2.4	18.5	0.29	19.8
	CCAT	0.58	95.2	4.8	9.3	0.40	11.6
	MSD	0.51	98.3	1.7	18.0	0.24	18.8
	TRADES	0.51	96.0	4.0	14.2	0.30	16.4
	AT-Madry	0.51	96.7	3.3	12.3	0.29	13.9
speckle_noise	Normal	0.57	97.0	3.0	12.4	0.59	13.8
	AT-50%	0.51	97.1	2.9	15.2	0.35	16.7
	AT-100%	0.51	97.7	2.3	18.4	0.29	19.5
	CCAT	1.00	0.0	100.0	0.0	0.40	83.0
	MSD	0.51	98.4	1.6	17.9	0.24	18.8
	TRADES	0.51	96.4	3.6	13.8	0.30	15.9
	AT-Madry	0.51	96.9	3.1	12.0	0.29	13.4
zoom_blur	Normal	0.61	96.7	3.3	12.9	0.59	14.6
	AT-50%	0.56	95.7	4.3	17.2	0.35	19.2
	AT-100%	0.56	97.0	3.0	21.1	0.29	22.4
	CCAT	0.52	97.1	2.9	13.9	0.40	15.6
	MSD	0.56	98.0	2.0	20.5	0.24	21.5
	TRADES	0.55	95.4	4.6	17.0	0.30	19.2
	AT-Madry	0.56	95.7	4.3	14.3	0.29	16.4

Table 23: Per-Corruptions Results on Cifar10-C, PART II Continued results of Tab. 22 including results on Cifar10-C focusing on individual corruptions. textttmean are the averaged results over all corruptions. We report ROC AUC, FPR and the true negative rate (TNR) in addition to the thresholded and unthresholded Err on the corrupted examples.